

**DEVELOPMENT OF A NOVEL HYBRID STORAGE SYSTEM FOR  
AQUA-AMMONIA SOLAR ABSORPTION REFRIGERATION CYCLE**

BY

FAROOQ RIAZ SIDDIQUI

A Thesis Presented to the  
DEANSHIP OF GRADUATE STUDIES

**KING FAHD UNIVERSITY OF PETROLEUM & MINERALS**

DHAHRAN, SAUDI ARABIA

1963 ١٣٨٣

In Partial Fulfillment of the  
Requirements for the Degree of

**MASTER OF SCIENCE**


In

MECHANICAL ENGINEERING


JANUARY 2014


KING FAHD UNIVERSITY OF PETROLEUM & MINERALS  
DHAHRAN- 31261, SAUDI ARABIA  
**DEANSHIP OF GRADUATE STUDIES**


This thesis, written by **FAROOQ RIAZ SIDDIQUI** under the direction his thesis advisor and approved by his thesis committee, has been presented and accepted by the Dean of Graduate Studies, in partial fulfillment of the requirements for the degree of **MASTER OF SCIENCE IN MECHANICAL ENGINEERING.**

  
13/2/2014  
Dr. Maged A.I. El-Shaarawi  
(Advisor)

  
Dr. Zuhair M. A. Gasem  
Department Chairman

  
Dr. Salam A. Zummo  
Dean of Graduate Studies

  
Dr. S. A. M. Said  
(Member)

  
Dr. Amro Al-Qutub  
(Member)

23/2/14  
Date



© Farooq Riaz Siddiqui

2014

**DEDICATED TO MY BELOVED PARENTS, MY FIANCÉE, MY ONLY  
SISTER, ONLY BROTHER AND BROTHER IN LAW**

## **ACKNOWLEDGMENTS**

This research work would not have been possible without the help of Allah Almighty, who provided me with sound health and kept me focused and well composed towards the successful completion of my MS thesis. I am grateful to my parents who were like the beacon of light in most difficult times and who supported my decision to join KFUPM.

My special thanks to my advisor, Dr. Maged A.I. El-Shaarawi, for his valuable guidance and supervision. He always assisted me and was like a helping hand in my research work. I would also like to thank Dr. S. A. M. Said and Dr. Amro Al-Qutub for always encouraging my efforts towards my thesis work.

My deep gratitude and acknowledgement for Mr. Umar Siddiqui, a Phd student at KFUPM. I am extremely grateful for his extensive cooperation in my research work. I would also like to thank my distinguished friends in KFUPM, Muhammad Nauman Zafar, Ahmad Rafiq, Omer bin Sohail, Bilal Tanweer, Ossama Hassan, Haroon Ashraf, Amer Hamza, Hussain Ali, Azhar Mehmood, Najam and Shomaail Jafri for making my stay at KFUPM a memorable journey of my life. I also thank my sister, my brother in law, Yusuf Sharif Hassan, my little nephew and niece who filled my life with joy and happiness. I also acknowledge King Fahd University of Petroleum and Minerals for providing excellent research opportunities and a healthy academic environment.

# TABLE OF CONTENTS

<b>ACKNOWLEDGMENTS .....</b>	<b>V</b>
<b>LIST OF TABLES .....</b>	<b>IX</b>
<b>LIST OF FIGURES.....</b>	<b>XI</b>
<b>LIST OF ABBREVIATIONS .....</b>	<b>XV</b>
<b>ABSTRACT.....</b>	<b>XXII</b>
<b>ABSTRACT ARABIC.....</b>	<b>XXIV</b>
<b>CHAPTER 1 INTRODUCTION.....</b>	<b>1</b>
<b>1.1 Various designs of absorption refrigeration cycle .....</b>	<b>2</b>
1.1.1 Single-effect absorption system .....	2
1.1.2 Absorption heat transformer .....	4
1.1.3 Double effect absorption refrigeration cycle .....	6
1.1.4 Half effect absorption refrigeration cycle .....	8
1.1.5 Absorption refrigeration cycle with GAX .....	8
1.1.6 Absorption refrigeration cycle with absorber heat recovery .....	10
1.1.7 Dual Cycle absorption refrigeration .....	10
1.1.8 Continuous Absorption Refrigeration system .....	12
1.1.9 Intermittent Absorption Systems.....	14
<b>1.2 Thesis Objectives .....</b>	<b>16</b>
<b>1.3 Methodology of Proposed Work .....</b>	<b>16</b>
<b>CHAPTER 2 LITERATURE REVIEW .....</b>	<b>17</b>
<b>CHAPTER 3 ENERGY AND ECONOMIC ANALYSIS OF HSAR CYCLE .....</b>	<b>26</b>
<b>3.1 Flow Diagram.....</b>	<b>26</b>
<b>3.2 h-x diagram .....</b>	<b>29</b>
<b>3.3 Assumptions for Steady State Model.....</b>	<b>33</b>
<b>3.4 Steady-State Thermodynamic analysis .....</b>	<b>35</b>
3.4.1 Generator-double rectification column-dephlegmator .....	35
3.4.2 Condenser .....	37

3.4.3	Evaporator .....	37
3.4.4	Absorber .....	37
3.4.5	Refrigerant Heat Exchanger .....	38
3.4.6	Solution Heat Exchanger .....	38
<b>3.5</b>	<b>Area of Solar Collector Field .....</b>	<b>39</b>
<b>3.6</b>	<b>Economic Assessment .....</b>	<b>40</b>
<b>3.7</b>	<b>Effectiveness, area and cost of SHX and RHX .....</b>	<b>44</b>
 <b>CHAPTER 4 UNSTEADY THERMODYNAMIC ANALYSIS OF HSAR CYCLE</b>		<b>46</b>
<b>4.1</b>	<b>Assumptions for Unsteady State Analysis .....</b>	<b>47</b>
<b>4.2</b>	<b>h-x diagram .....</b>	<b>51</b>
<b>4.3</b>	<b>Unsteady Thermodynamic analysis .....</b>	<b>56</b>
<b>4.4</b>	<b>Governing Mass and Energy Equations .....</b>	<b>59</b>
4.4.1	Generator- Double Rectification Column-Dephlegmator Assembly .....	61
4.4.2	Evaporator .....	63
4.4.3	Absorber .....	67
4.4.4	Condenser .....	67
4.4.5	Refrigerant Heat Exchanger (RHX) .....	69
4.4.6	Solution Heat Exchanger (SHX) .....	69
<b>4.5</b>	<b>Determination of mass inside each component and the term <math>(m(u_f - u_i))</math> in the unsteady energy equation for each component of HSAR cycle .....</b>	<b>72</b>
 <b>CHAPTER 5 EXERGY ANALYSIS OF HSAR CYCLE .....</b>		<b>77</b>
<b>5.1</b>	<b>Generalized Mathematical Formulation .....</b>	<b>78</b>
5.1.1	Physical Exergy and Exergy Loss .....	78
5.1.2	Exergetic Efficiency .....	79
<b>5.2</b>	<b>Mathematical formulation of HSAR Cycle .....</b>	<b>80</b>
5.2.1	Generator- Double Rectification Column-Dephlegmator assembly .....	81
5.2.2	Condenser .....	81
5.2.3	Evaporator .....	81
5.2.4	Absorber .....	82
5.2.5	Liquid-Liquid Heat Exchanger/Solution Heat Exchanger (LLHX/SHX) .....	82
5.2.6	Vapor-Liquid Heat Exchanger/Refrigerant Heat Exchanger (VLHX/RHX) .....	83
5.2.7	COP, ECOP, Circulation Ratio (f) and Exergy Loss Ratio .....	83
 <b>CHAPTER 6 EXERGO-ECONOMIC EVALUATION OF HYBRID STORAGE ABSORPTION REFRIGERATION (HSAR) SYSTEM .....</b>		<b>84</b>

<b>6.1 Economic Evaluation .....</b>	<b>84</b>
<b>6.2 Assumptions.....</b>	<b>88</b>
<b>6.3 Exergy analysis of HSAR Cycle based on Fuel, Product and Loss (F-P-L) streams ...</b>	<b>89</b>
<b>6.4 Exergy Costing .....</b>	<b>92</b>
6.4.1 Generator.....	93
6.4.2 Condenser .....	94
6.4.3 Evaporator .....	95
6.4.4 Absorber .....	95
6.4.5 Refrigerant Heat Exchanger (RHX).....	96
6.4.6 Solution Heat Exchanger (SHX) .....	96
6.4.7 Pump.....	96
<b>6.5 Non-Exergy costs of storage tanks .....</b>	<b>98</b>
<b>6.6 Exergo-economic evaluation of HSAR cycle.....</b>	<b>99</b>
6.6.1 Generator.....	100
6.6.2 Evaporator Assembly.....	100
6.6.3 Refrigerant Heat Exchanger (RHX).....	101
6.6.4 Solution Heat Exchanger (SHX) .....	102
6.6.5 Pump.....	102
<b>6.7 Exergo-economic variables.....</b>	<b>103</b>
 <b>CHAPTER 7 RESULTS AND DISCUSSION.....</b>	 <b>105</b>
<b>7.1 Steady State Thermodynamic Analysis .....</b>	<b>105</b>
<b>7.2 Unsteady Thermodynamic Analysis .....</b>	<b>111</b>
<b>7.3 Exergy Analysis.....</b>	<b>124</b>
<b>7.4 Exergo-Economic Evaluation.....</b>	<b>131</b>
 <b>CHAPTER 8 VALIDATION .....</b>	 <b>142</b>
<b>8.1 Unsteady analysis .....</b>	<b>142</b>
<b>8.2 Energy and exergy analysis .....</b>	<b>149</b>
 <b>CHAPTER 9 CONCLUSION AND RECOMMENDATIONS .....</b>	 <b>151</b>
 <b>REFERENCES.....</b>	 <b>154</b>
 <b>VITAE.....</b>	 <b>159</b>



## LIST OF TABLES

Table 3-1 Thermodynamic analysis of HSAR cycle .....	39
Table 3-2 Cost Summary of AST and CST .....	41
Table 3-3 Cost and design specification of evaporator and condenser units .....	42
Table 3-4 Comparison of size of storage tanks for different storage designs.....	43
Table 3-5 Specification details and cost of flat plate solar collectors.....	43
Table 4-1 The given cooling energy outputs of HSAR cycle during the effective sunlight hours .....	64
Table 6-1 Cost estimation of HSAR cycle.....	85
Table 6-2 Fuel-Product-Loss streams for HSAR cycle .....	90
Table 6-3 Cost rates of Capital Investment of HSAR cycle components [40] .....	93
Table 6-4 Exergo-economic data for HSAR cycle .....	98
Table 7-1 Comparison of size of storage tanks for different storage designs.....	105
Table 7-2 Comparison of thermodynamic energy analysis of HSAR Cycle, RSAR Cycle and CSAR Cycle .....	108
Table 7-3 Average daily and night COP of HSAR Cycle for representative days of summer and winter .....	115
Table 7-4 Required solar collector field area per kW of cooling power for different cycles .....	119
Table 7-5 Size of storage tanks used in HSAR cycle .....	120
Table 7-6 Exergy analysis results for HSAR cycle .....	135
Table 7-7 Exergo-economic variables of HSAR cycle.....	136

Table 8-1 Comparison between unsteady and steady software results of HSAR Cycle for same given input non-variable with time (average values) data and 5 kW cooling power ..... 143

Table 8-2 Comparison of heat capacities and COP between basic solar absorption chiller model (without storage tank) and a DACM chiller # 3 [46] ..... 144

## LIST OF FIGURES

Figure 1-1 Single effect absorption system .....	3
Figure 1-2 Absorption heat transformer .....	5
Figure 1-3 LiBr absorption Refrigeration Cycle.....	7
Figure 1-4 Aqua ammonia absorption refrigeration cycle .....	7
Figure 1-5 Half effect absorption refrigeration cycle .....	9
Figure 1-6 Absorption refrigeration cycle with GAX.....	9
Figure 1-7 Absorption refrigeration cycle with absorber heat recovery .....	11
Figure 1-8 Dual Cycle absorption refrigeration cycle .....	11
Figure 1-9 Continuous absorption Refrigeration System .....	13
Figure 1-10 Aqua ammonia absorption refrigeration cycle .....	13
Figure 1-11 T-x Diagram of intermittent absorption refrigeration cycle.....	15
Figure 3-1 Schematics of HSAR Cycle .....	31
Figure 3-2 h-x diagram of HSAR Cycle .....	32
Figure 3-3 Plots of heat exchanger area versus effectiveness for SHX and RHX.....	45
Figure 4-1 Plots of solar radiation and ambient temperature for a representative summer and winter day .....	50
Figure 4-2 h-x diagram of HSAR Cycle .....	55
Figure 4-3 Efficiency curves for solar collectors [49] .....	58
Figure 4-4 Flow across a generator-double rectification column-dephlegmator unit.....	66
Figure 4-5 Flow across an evaporator unit and cold storage tank (CST) .....	66
Figure 4-6 Flow across an absorber unit.....	68
Figure 4-7 Flow across a condenser unit .....	68

Figure 4-8 Flow across a RHX .....	71
Figure 4-9 Flow across a SHX.....	71
Figure 4-10 Specific heat capacity of ammonia solution [51].....	76
Figure 6-1 Flow path of refrigerant, weak solution and strong solution in HSAR cycle .	87
Figure 7-1 (a) COP and ECOP versus $T_{gen}$ at different condenser temperatures (b) COP versus generator temperature for different values of SHX effectiveness ( $\epsilon_{SHX}$ ) (c) Circulation ratio (f) versus generator temperature ( $T_{gen}$ ) at different condenser temperatures.....	110
Figure 7-2 Plots of instantaneous solar radiation, ambient temperature, condenser pressure, weak solution concentration at exit of generator ( $x_{ws} = x_4$ ) and COP day versus time for summer.....	114
Figure 7-3 Plots of instantaneous solar radiation (I), ambient temperature ( $T_{amb}$ ), condenser pressure ( $P_{cond}$ ), weak solution concentration at generator exit ( $x_{ws}$ ) and COP day versus time for winter.....	114
Figure 7-4 Plot of hourly energy versus time for HSAR components for representative days of summer .....	117
Figure 7-5 Plot of hourly energy versus time for HSAR components for representative days of winter.....	117
Figure 7-6 Plots of absorber temperature ( $T_{abs}$ ) and strong solution (aqua-ammonia) concentration ( $X_{abs}$ ) inside absorber for representative days of summer.....	123
Figure 7-7 Generator temperature ( $T_4$ ), mass of ammonia vapor at exit of dephlagmator ( $m_7$ ) and mass of weak solution at exit of generator ( $m_4$ ) versus time for representative days of summer.....	123

Figure 7-8 Generator exergy loss ratio versus generator temperature at different condenser temperatures. ....	126
Figure 7-9 Evaporator exergy loss ratio versus generator temperature at different condenser temperatures. ....	126
Figure 7-10 (a) Absorber exergy loss ratio versus generator temperature at different condenser temperatures (b) Condenser exergy loss ratio versus generator temperature at different condenser temperatures.....	127
Figure 7-11 (a) SHX exergy loss ratio versus generator temperature at different condenser temperatures (b) RHX exergy loss ratio versus generator temperature at different condenser temperatures.....	129
Figure 7-12 Exergy loss ratio of pump ( $y_{L,pump}$ ) versus generator temperature at different condenser temperatures.....	130
Figure 7-13 Total exergy loss ratio ( $y_{L,tot}$ ) versus generator temperature at different condenser temperatures .....	130
Figure 7-14 Cost rates associated to Capital Investment for HSAR components .....	132
Figure 7-15 Exergetic efficiency of overall system versus generator temperature at different condenser temperatures.....	139
Figure 7-16 Exergetic efficiency of overall system versus evaporator temperature at different condenser temperatures.....	139
Figure 7-17 Exergetic efficiency of overall system versus generator temperature at different effectiveness values of solution heat exchanger (SHX) .....	140
Figure 7-18 Plots of total cost rate ( $CD + CL + Z$ ) and cost of the product ( $c_{p,os}$ ) of overall system versus generator temperature.....	140

Figure 7-19 Plots of solar radiation ( $I$ ), ambient temperature ( $T_{amb}$ ), exergo-economic factor of overall system ( $f_{os}$ ) and the exergetic efficiency of overall system ( $\epsilon_{os}$ ) versus time (hours) for June 16, 2013.....	141
Figure 8-1 Plots of heating capacity and COP for basic solar absorption chiller model (without storage tanks) and a DACM chiller#1 (experimental setup) [54], the quantities with superscript * are from the results of Jakob and Eicker, 2002 .....	146
Figure 8-2 Plots of solar radiation, temperatures and heat fluxes for basic solar absorption chiller model (without storage tanks) and a small scale absorption chiller (experimental setup) [55], the quantities with superscript ** are obtained from Zetsche et al. 2008.....	146
Figure 8-3 Plots of solar radiation, temperatures and heat fluxes for basic solar absorption chiller model (without storage tanks) and a small scale absorption chiller (experimental setup) [55], the quantities with superscript ** are from the results of Zetsche et al. 2008.....	148
Figure 8-4 Plot of exergy loss ratio ( $y_L$ ), COP and ECOP versus generator temperature used for validation of basic solar absorption refrigeration (HSAR) system, the plots of HSAR system are shown by lines (————) without legend symbols .....	150

## LIST OF ABBREVIATIONS

AST	:	Ammonia Storage Tank
A	:	Heat transfer area, m <sup>2</sup>
A <sub>c</sub>	:	Total solar collector field area required for both storage and refrigeration in DSAR cycle = A <sub>c1</sub> + A <sub>c2</sub> , m <sup>2</sup>
A <sub>c1</sub>	:	Solar collector field area required for daytime refrigeration only (without any storage), m <sup>2</sup>
A <sub>c2</sub>	:	Part of total solar collector field area of DSAR cycle used for storage of ammonia and cold for nighttime refrigeration only, m <sup>2</sup>
c	:	Constant, kJ.kg <sup>-1</sup>
COP <sub>day</sub>	:	Coefficient of Performance (day)
COP <sub>night</sub>	:	Coefficient of Performance (night)
CSAR	:	Cold Storage Absorption Refrigeration
CST	:	Cold Storage Tank
$\dot{C}$	:	Thermal capacitance rate (product of mass flow rate times specific heat capacity), $\dot{C} = \dot{m}c_p$ , kJ.K <sup>-1</sup> .s <sup>-1</sup>
$\dot{C}_{min}$	:	Minimum thermal capacitance rate, kJ.K <sup>-1</sup> .s <sup>-1</sup>

$c_p$	:	Specific heat capacity at constant pressure, $\text{kJ.kg}^{-1} \cdot \text{K}^{-1}$
$\dot{C}_{D,k}$	:	Cost rate of exergy destruction for kth component, $\text{\$yr}^{-1}$
$\dot{C}_{L,k}$	:	Cost rate of exergy loss for kth component, $\text{\$yr}^{-1}$
$\dot{C}_{P,k}$	:	Cost rate of exergy of the product for kth component, $\text{\$yr}^{-1}$
$\dot{C}_{F,k}$	:	Cost rate of exergy of fuel for kth component, $\text{\$yr}^{-1}$
$E_{\text{final}}$	:	Final total energy within boundaries of a system, kJ
$E_{\text{in}}$	:	Total energy of fluid at system inlet, kJ
$E_{\text{initial}}$	:	Total energy within boundaries of a system, kJ
$E_{\text{out}}$	:	Total energy of fluid at system outlet, kJ
EV1	:	Liquid Expansion Valve
EV2	:	Refrigerant expansion valve
$f_k$	:	Exergoeconomic factor
HSAR	:	Hybrid Storage Absorption Refrigeration
$h$	:	Enthalpy, $\text{kJ.kg}^{-1}$
$h_{\text{pd}}$	:	Enthalpy at pole of dephlagmator, $\text{kJ.kg}^{-1}$
$h_{\text{pg}}$	:	Enthalpy at pole of generator, $\text{kJ.kg}^{-1}$



$I$	:	Solar Intensity, $\text{W.m}^{-2}$
$I_T$	:	Monthly average hourly solar energy per unit area, $\text{MJ.m}^{-2}$
$ke$	:	Kinetic energy per unit mass, $\text{kJ.kg}^{-1}$
$l$	:	Length of tube in heat exchanger, m
$m$	:	Mass, kg
$m_{in}$	:	Mass of fluid entering a system, kg
$m_i$	:	Initial mass within boundaries of a system at start of a time interval ( $\Delta t$ ), kg
$m_f$	:	Final mass within boundaries of a system at end of a time interval $\Delta t$
$m_{out}$	:	Mass of fluid exiting a system, kg
$M_{ice}$	:	Mass of ice in CST, kg
$M_{ref}$	:	Mass of refrigerant in AST, kg
$M_{ss}$	:	Mass of strong solution in SST, kg
$M_{ws}$	:	Mass of weak solution in WST, kg
$\dot{m}$	:	Mass flow rate, $\text{kg.s}^{-1}$
$n$	:	Number of tubes in heat exchanger

NTU	:	Number of transfer units
P	:	Pressure, kPa
$P_{\text{cond}}$	:	Condenser pressure, kPa
POL	:	Principal operating line
$Q_a$	:	Thermal energy lost in exothermic process in absorber during a period of time $\Delta t$ , MJ
$Q_{AST}$	:	Energy of ammonia in AST, MJ
$Q_c$	:	Thermal energy rejected by ammonia to coolant in condenser during a period of time $\Delta t$ , MJ
$Q_{AST}$	:	Energy of ammonia in AST, MJ
$Q_{CST}$	:	Energy of ice in CST, MJ
$Q_{e, \text{day}}$	:	Evaporator energy during the day (effective sunlight hours) or during a period of time $\Delta t$ during the day, MJ
$Q_{e, \text{night}}$	:	Evaporator energy during the night (24 - effective sunlight hours) or during a period of time $\Delta t$ in the night, MJ
$Q_g$	:	Energy gained by generator during effective sunlight hours or during a period of time $\Delta t$ during the day, MJ
$Q_{\text{ref},d}$	:	Energy for refrigeration effect during the day (effective

		sunlight hours), MJ
$Q_{ref,n}$	:	Energy for refrigeration effect during the night (24 - effective sunlight hours), MJ
$Q_{g,CST+AST}$	:	Part of generator energy ( $Q_g$ ) required to produce ammonia in AST and ice in CST, MJ
$\dot{Q}_{max}$	:	Maximum heat duty, kW
$q_c$	:	Average energy gain per unit area of the collector during effective sunlight hours, MJ.m <sup>-2</sup>
RHX	:	Refrigerant Heat Exchanger
RSAR	:	Refrigerant Storage Absorption Refrigeration
r	:	Radius of tube in heat exchanger, m
SHX	:	Solution Heat Exchanger
SST	:	Strong Solution Tank
t	:	Time, s
T	:	Temperature, °C
$T_{abs}$	:	Absorber temperature, °C
$T_{amb}$	:	Ambient temperature, °C

$T_{\text{cond}}$	:	Condenser temperature, °C
$T_{\text{evap}}$	:	Evaporator temperature, °C
$T_f$	:	Exit temperature of the working fluid of solar collectors field
$T_{\text{gen}}$	:	Weak solution temperature at exit of generator, °C
$T_{\text{gen,min}}$	:	Minimum required weak solution temperature at exit of generator, °C
$T_{\text{drybulb}}$	:	Dry Bulb temperature, °C
$T_{\text{wetbulb}}$	:	Wet Bulb temperature, °C
$u_i$	:	Initial internal energy per unit mass within boundaries of a system at start of a time interval ( $\Delta t$ ), $\text{kJ.kg}^{-1}$
$u_f$	:	Final internal energy per unit mass within boundaries of a system at end of a time interval ( $\Delta t$ ), $\text{kJ.kg}^{-1}$
$U$	:	Overall heat transfer coefficient, $\text{kW.m}^{-2}.\text{K}^{-1}$
$V$	:	Heat transfer volume, $\text{m}^3$
$W_p$	:	Pump mechanical energy, MJ
WST	:	Weak Solution Tank
$x_{\text{ss}}$	:	Concentration of strong solution
$x_{\text{ws}}$	:	Concentration of weak solution

$\dot{X}_i$	:	Exergy rate at inlet, kW
$\dot{X}_o$	:	Exergy rate at outlet, kW
$\dot{X}_L$	:	Rate of exergy loss, kW
$\dot{X}_D$	:	Rate of exergy destruction, kW
$\dot{X}_P$	:	Exergy rate of product, kW
$\dot{X}_F$	:	Exergy rate of fuel, kW
$Y_D$	:	Exergy destruction ratio
$Y_L$	:	Exergy loss ratio
$\dot{Z}$	:	Cost of Capital Investment, $\text{\$yr}^{-1}$

### **Greek Symbols**

$\eta$	:	Efficiency
$\rho$	:	Density, $\text{kg.m}^{-3}$
$\varepsilon$	:	Effectiveness

## ABSTRACT

**Full Name : Farooq Riaz Siddiqui**

**Thesis Title : Development of a novel hybrid storage system for aqua-ammonia solar absorption refrigeration cycle**

**Major Field : Mechanical Engineering - ThermoFluids**

**Date of Degree : January, 2014**

This research work proposes the development of a novel hybrid storage absorption refrigeration (HSAR) cycle using aqua-ammonia mixture, capable of providing continuous refrigeration and is powered by solar energy. The cycle integrates a cold storage tank with two aqua ammonia storage tanks and one ammonia storage tank to accommodate a 24-hour uninterrupted daily cooling load. During the daytime, solar energy is used to provide the refrigeration that suffices both the daily cooling load and the production of both ammonia and ice for the night cooling load. The cold storage tank together with the ammonia and aqua-ammonia tanks share the night cooling load. The proposed absorption cycle reduces the size of the storage tanks by 50 % or even more for the same cooling capacity compared to the currently available storage designs. The proposed cycle continues the refrigeration even if one of the storage tanks ceases to operate or need maintenance.

The study also explores the impact of unsteady solar intensity and ambient conditions on the operation and performance parameters of an aqua-ammonia absorption chiller of 5kW cooling power. It presents an unsteady analysis for five representative days of summer and winter in Dhahran, Saudi Arabia. The unsteady analysis gives the variation of the absorption-chiller parameters every one hour. Capacity of these tanks and

the required solar collectors area are computed for 24-hour operation per day at 5kW cooling power. The results show that, for the given cooling load in Dhahran, the coefficient of performance is better in winter than in summer (0.68 as compared to 0.39) but the required solar collector field area is more in winter than in summer.

This research work applies energy and exergy analysis for comparing a solar-powered absorption refrigeration system with different storages. These storages include refrigerant, cold/ice and a combination of refrigerant and cold/ice storage systems (hybrid storage) to ensure meeting the night time cooling demand. The results indicated a slight drop in coefficient of performance (COP) and exergetic coefficient of performance (ECOP) in HSAR system compared to that of the refrigerant storage system while the cold storage system achieves the least COP/ECOP. An exergo-economic analysis is implemented on HSAR cycle to compare the components based on the costs of initial capital investment and the costs of irreversibilities. The components of the refrigeration cycle are also evaluated and compared using exergo-economic variables such as the relative cost difference, exergy destruction cost rate and exergo-economic factor. The effect of generator temperature, condenser temperature and evaporator temperature on the exergetic efficiency of the system is also studied. Finally, this research work presents a quasi-steady exergy and exergo-economic analysis for a representative summer day of Dhahran region. This study can be further used in the optimization of design variables of the studied refrigeration cycle.

## **MASTER OF SCIENCE DEGREE**

**KING FAHD UNIVERSITY OF PETROLEUM AND MINERALS**

Dhahran, Saudi Arabia

## ملخص الرسالة

الاسم الكامل: فاروق رياض صديقي

عنوان الرسالة: تطوير نظام تخزين هجينة جديدة لأكوا-الأمونيا الشمسية امتصاص دورة التبريد

التخصص: الهندسة الميكانيكية

تاريخ الدرجة العلمية: ربيع الأول ١٤٣٥

تهدف هذه الرسالة إلى تطوير نظام تبريد شمسي مستمر. يقوم النظام الجديد على دورة الامتصاص عن طريق استخدام خليط الماء مع الأمونيا (أكوا - أمونيا). يدمج خزان التبريد في الدورة مع خزاني أكوا-أمونيا إضافة إلى خزان واحد من الأمونيا لضمان إستمرارية التبريد طوال اليوم دون انقطاع. خلال وقت اليوم تستغل الطاقة الشمسية في انتاج التبريد اللازم لتغطية حمل التبريد خلال فترة النهار إضافة إلى انتاج الأمونيا و الجليد اللازمان لتغطية حمل التبريد خلال فترة الليل. خزان التبريد الأصلي مع خزان الأكوا-أمونيا و خزان الأمونيا يشتركان في تغطية حمل التبريد الليلي. استخدام دورة الامتصاص المقترحة في هذا الرسالة يقلص حجم التخزين إلى ما يقارب 50% أو أكثر مقارنة بالتصاميم الحالية. أيضا دورة الامتصاص تضمن عملية تبريد مستمرة حتى في حالة أي انقطاع أو توقف لأي واحد من الخزانات لأسباب الصيانة أو غيرها. هذه الرسالة درست أثر تغير كثافة أشعة الشمس و بعض الظروف الجوية على أداء مبرد دورة امتصاص أكوا-أمونيا ذو قدرة تبريد تصل 5كيلووات. الدراسة شملت تحليل عدم الثبات (التغير) لخمس أيام من فصول الصيف و الشتاء لمنطقة الظهران-السعودية. الدراسة التحليلية أظهرت التغيرات في أداء مبرد الامتصاص في كل ساعة. سعة الخزانات و مساحة المجمعات الشمسية المطلوبة حسبت ل 24 ساعة تشغيل ل 5كيلووات قدرة تبريد. النتائج أظهرت أن معامل الأداء للدورة في الشتاء أفضل و أعلى منه في الصيف و لكن مساحة المجمعات الشمسية المطلوبة بالشتاء أكبر منها في الصيف. أيضا هذه الرسالة قارنت بين عدة أنظمة تخزين في مبرد الامتصاص الشمسي للتأكد من إمكانية تغطية حمل التبريد الليلي عن طريق دراسة تحليل الطاقة لمنظومة دورة الامتصاص. منظومات التخزين المقترحة شملت تخزين الأمونيا، الجليد، نظام هجين من الأمونيا و الجليد. النتائج أظهرت تناقض ضئيل في معامل أداء النظام الهجين مقارنة بنظام تخزين الأمونيا، أو نظام تخزين الجليد الذي أظهر أقل معامل أداء. أيضا في هذه الرسالة تمت عمل دراسة اقتصادية على دورة مبرد الامتصاص .

شهادة ماجستير علوم

جامعة الملك فهد للبترول والمعادن

الظهران ، المملكة العربية السعودية



# CHAPTER 1

## INTRODUCTION

Depletion of fossil fuels is the result of excessive energy demands in the last few decades. Dependency on fossil fuel has also resulted in global warming and pollution. Solar energy is an alternative cheap energy source which has attracted the attention of the researchers in the last few decades. More than 60 % of the electricity used in the building sector in KSA is consumed in air conditioning and refrigeration [1]. KSA is one of the few countries with abundant solar energy available all along the year. This cheap energy can be used effectively for refrigeration cooling to reduce the fossil fuel dependency. Therefore some recent research [1] has been carried out to develop a 24-h operating aqua ammonia absorption refrigeration cycle using different storage options to overcome the intermittency caused by the absence of solar energy at night. Research has shown that chillers with ice storage system are less efficient than heat storage and refrigerant storage systems. Also if any of the storage tanks ceases to work, refrigeration cannot be produced for 24 hours. The present study considers the development of a hybrid storage absorption refrigeration (HSAR) system (combined cold and refrigerant storage) with downsized storage tanks for the same cooling capacity. HSAR provides uninterrupted refrigeration if any storage tank ceases to work or needs maintenance.

## **1.1 Various designs of absorption refrigeration cycle**

### **1.1.1 Single-effect absorption system**

A single effect absorption refrigeration system is composed of a generator, absorber, condenser and evaporator. Figure 1-1 shows the H<sub>2</sub>O-LiBr absorption refrigeration system. In a single effect system, low-grade thermal energy is used as a heat input to the generator. The energy released in the absorber and condenser results in irreversibility because a large portion of the heat input at the generator is wasted in the condenser and absorber. In order to reduce irreversibility, a solution heat exchanger is used in between the absorber and the generator. The weak solution from the generator at high temperature transfers heat to the cold concentrated solution coming from the absorber in the solution heat exchanger.

In the absorber, the refrigerant vapors are absorbed by the absorbent and hence an exothermic process results in the dissipation of energy. Solution heat exchanger has a significant effect on the system COP. Refrigerant heat exchanger may also be employed between the condenser and the evaporator but it has a little effect on the COP of the absorption system.

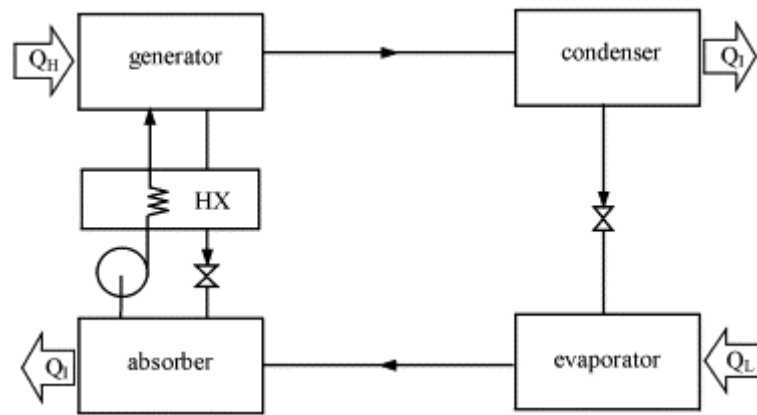


**Figure 1-1 Single effect absorption system**

### **1.1.2 Absorption heat transformer**

Absorption refrigeration cycles are composed of three temperature levels, high temperature, intermediate temperature and low temperature levels. In case of absorption refrigerators or air conditioners, heat is supplied to the high temperature level (generator) while refrigeration or cooling effect is obtained at low temperature level (evaporator). Heat is rejected to the atmosphere at intermediate temperature level (condenser).

In absorption heat transformer, heat is supplied to the intermediate temperature level while heat is rejected to the low temperature level. The useful output is obtained at the high temperature level. Hence in absorption heat transformer, low graded thermal energy is converted to high temperature level. The expansion valve between the condenser and the evaporator in absorption refrigeration system is replaced by a pump in absorption heat transformer. The low grade thermal energy is absorbed by the generator. The refrigerant in liquid phase is pumped to the evaporator where it absorbs the low grade thermal energy which is used as a heat input to the generator. The refrigerant vapor is absorbed in the absorber where the heat is released at the high temperature level.

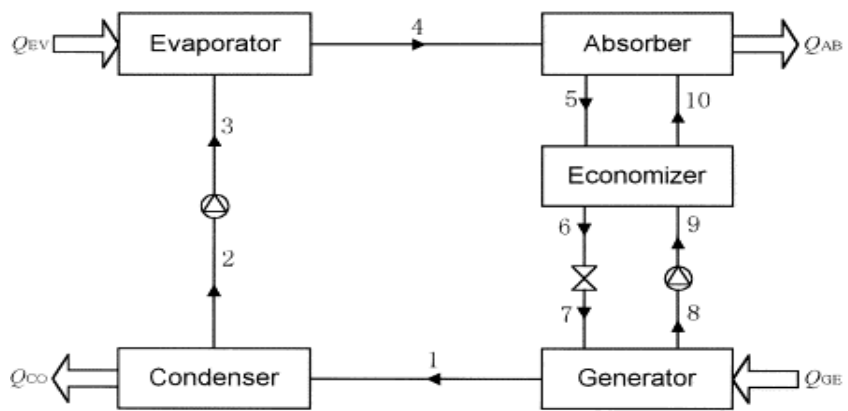


**Figure 1-2 Absorption heat transformer**

### **1.1.3 Double effect absorption refrigeration cycle**

#### **1.1.3.1 For LiBR system**

The purpose of multi effect absorption refrigeration cycle is to obtain higher efficiency than single effect systems. The heat of vapor condensation in stage 1 is used as a heat input in the generator of stage 2. The weak solution from stage 1 is introduced into the generator of stage 2 to further extract ammonia vapors. The system shown in Figure 1-3 is a three-pressure system, i.e. high pressure, intermediate pressure and low pressure. A double effect absorption refrigeration system is considered as a combination of two single effect systems. The COP for double effect system is calculated as:

$$\text{COP}_{\text{double}} = \text{COP}_{\text{single}} + (\text{COP}_{\text{single}})^2 \quad (1.1)$$

#### **1.1.3.2 For Aqua Ammonia system**

For aqua ammonia double effect system, a two pressure system was developed. The heat from an external source is supplied to generator II while the heat of absorption from absorber II is used as a heat source for generator I. hence absorber is operated at higher temperatures to generate enough heat for generator I.

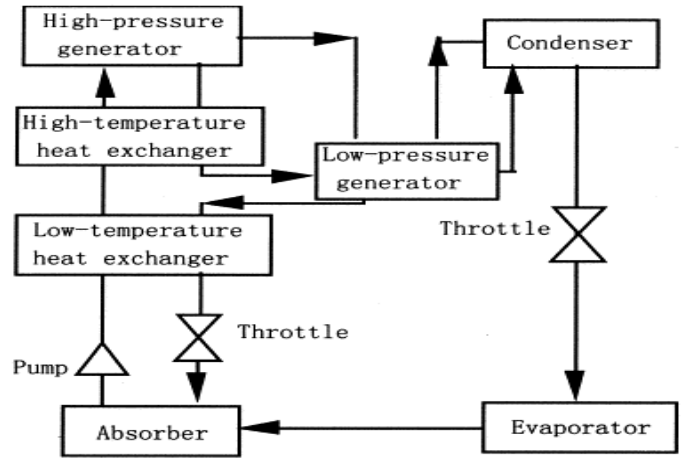


Figure 1-3 LiBr absorption Refrigeration Cycle

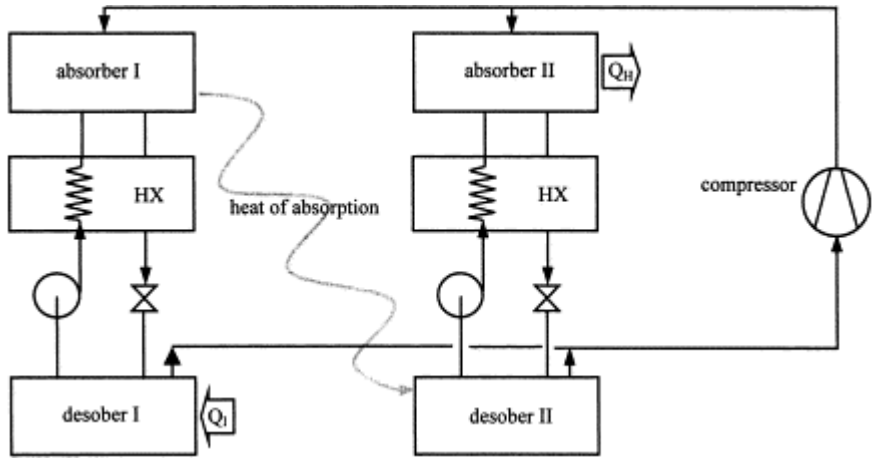


Figure 1-4 Aqua ammonia absorption refrigeration cycle

### **1.1.4 Half effect absorption refrigeration cycle**

Half effect absorption refrigeration cycle can be considered as a combination of two single effect systems in which a low-grade thermal energy is supplied to both generators. Its configuration is exactly the same as a double effect absorption refrigeration system for aqua ammonia solution except the difference in heat input processes. In half effect systems, both absorbers reject heat and hence the COP of half effect absorption refrigeration systems is relatively less.

### **1.1.5 Absorption refrigeration cycle with GAX**

GAX stands for generator absorber heat exchanger. The COP of the single stage absorption cycle becomes equal to the double stage system by using GAX. The cycle consists of two single-stage systems in parallel with the use of GAX which simplifies the cycle. In GAX cycle, the heat of absorber is utilized by the generator thus results in an increase of system COP.



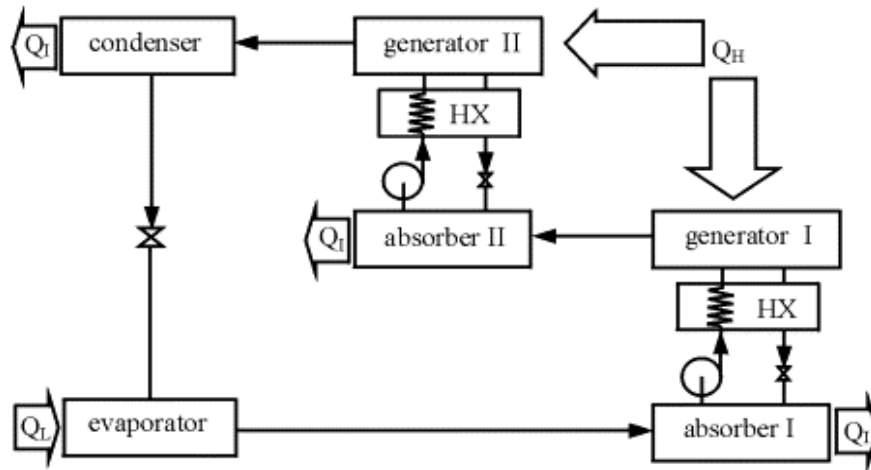


**Figure 1-5 Half effect absorption refrigeration cycle**

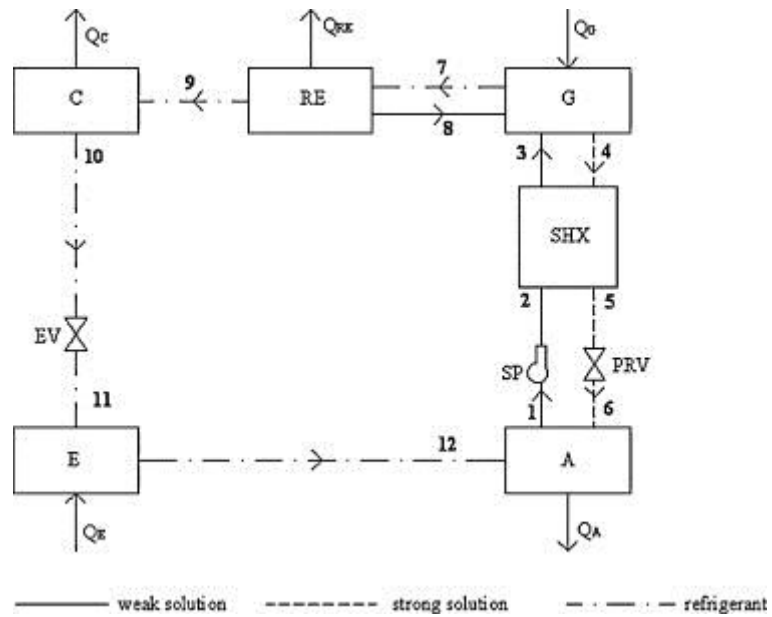


**Figure 1-6 Absorption refrigeration cycle with GAX**

### **1.1.6 Absorption refrigeration cycle with absorber heat recovery**

In the absorber, the absorbent absorbs the refrigerant which results in heat dissipation by an exothermic process. A secondary fluid takes the heat from the high temperature section of the absorber to the low temperature section of the generator. Hence, the heat input in the generator is decreased and the COP of the system increases.

### **1.1.7 Dual Cycle absorption refrigeration**

This cycle is somewhat similar to double effect absorption cycle. In this cycle, two single effect absorption cycles work in parallel with two different fluids. The heat rejected by the absorber and condenser of aqua ammonia system is used as a heat input in the generator of LiBr cycle. The heat of absorber and condenser of LiBr cycle are usual dissipated to the atmosphere.

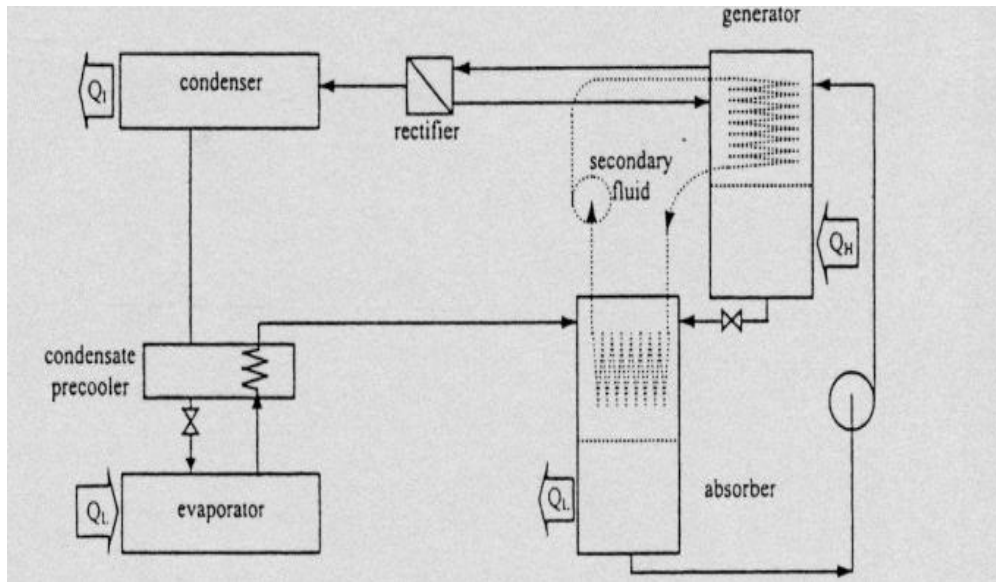


**Figure 1-7 Absorption refrigeration cycle with absorber heat recovery**

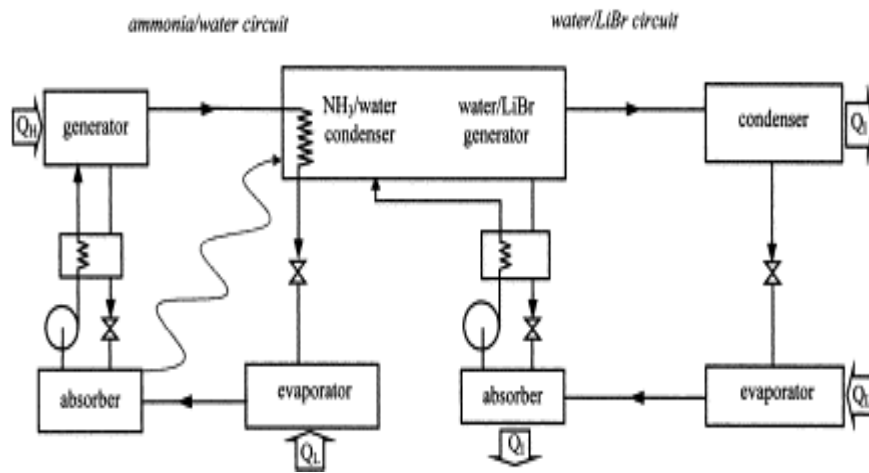


**Figure 1-8 Dual Cycle absorption refrigeration cycle**

### **1.1.8 Continuous Absorption Refrigeration system**

Absorption refrigeration systems are different from conventional vapor compression systems in a way that the compressor unit is replaced by the absorber unit. The absorber unit is composed of an absorber, a pump and a generator. The refrigerant vapors formed by the generator are sent to the condenser. In condenser, the vapors are converted into saturated liquid and passed on to the evaporator via expansion valve. The refrigerant takes the heat of the cooling space and is converted to saturated vapors. The refrigerant vapors are absorbed by the absorbent in the absorber and hence, heat of this exothermic process is dissipated to the environment. The strong solution thus formed in the absorber is allowed to pass through a pump and enters into the generator. In generator, the refrigerant evaporates and a weak solution enters into the absorber through a valve.

In aqua ammonia absorption cycle, two additional components namely, rectifier and dephlegmator, are used to ensure that pure ammonia enters into the condenser. Rectifier is composed of series of baffles which separates water from ammonia. In order to ensure 99.9 % pure ammonia going into the condenser, dephlegmator unit is used after the rectifier. Dephlegmator is a heat exchanger in which external fluid is used to condense water present in ammonia vapors. The main advantage of aqua ammonia absorption system over the LiBr absorption system is its ability to provide cooling at subzero temperatures. LiBr system cannot reach below 0 C as water is the refrigerant and it blocks the refrigerant piping with ice.

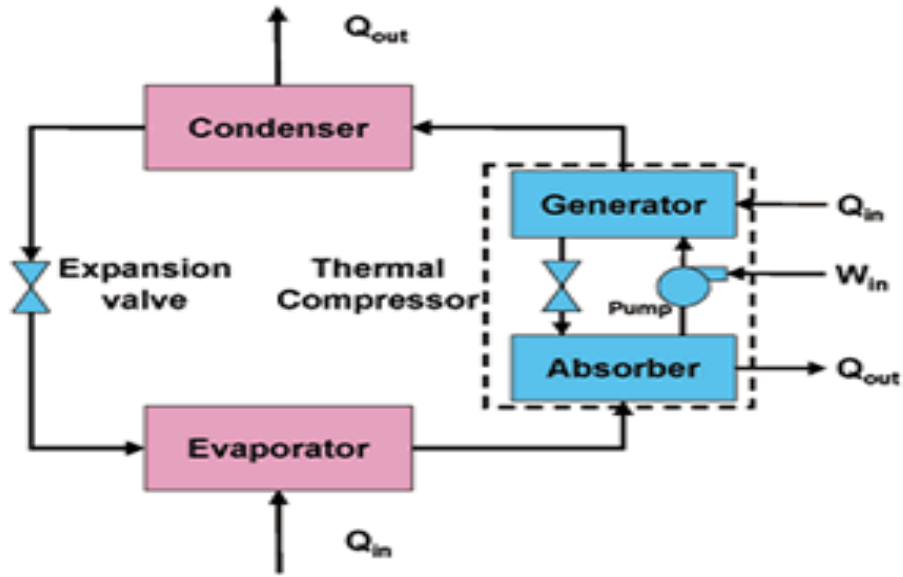


Figure 1-9 Continuous absorption Refrigeration System

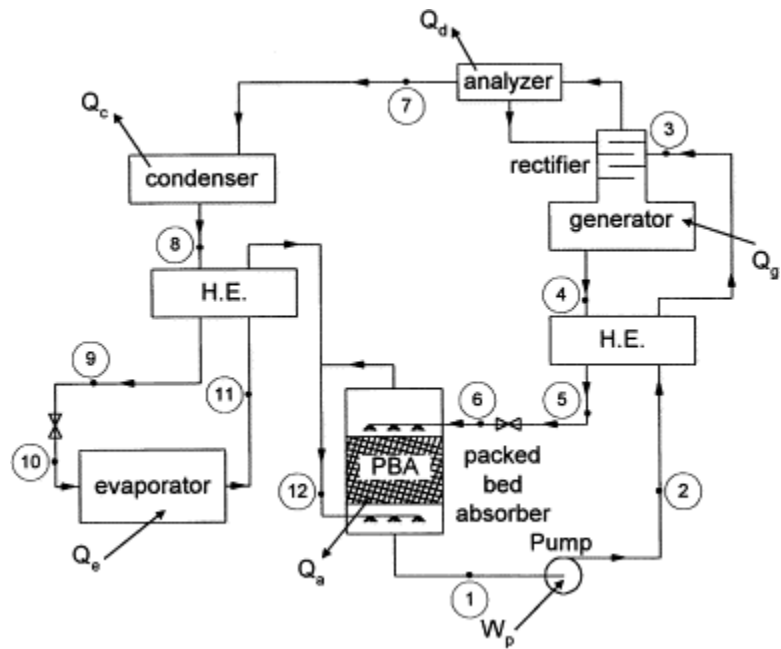


Figure 1-10 Aqua ammonia absorption refrigeration cycle

### **1.1.9 Intermittent Absorption Systems**

An Intermittent absorption refrigeration system is composed of generator – absorber unit and a condenser – evaporator unit. Intermittent systems are composed of two processes, regeneration and refrigeration. Regeneration means the separation of refrigerant vapors from absorbent by means of thermal energy. The vapors thus formed are allowed to enter into the condenser. When the entire refrigerant enters into the condenser, the valve is closed. The generator is allowed to cool and now behaves as an absorber. The absorber is at low pressure than condenser. As the valve is opened again, the condenser behaves as an evaporator and refrigerant vapors hence formed are sent into the absorber. The process continues until all the refrigerant enters into the absorber.

For Solar intermittent systems, regeneration takes place during the day time whereas the refrigeration occurs at night. When the heat is supplied to the generator at daytime, the temperature of the generator rises from 1 to 2 as shown in Figure 1-11. When the solution in generator reaches a saturation state, refrigerant vapors are formed and the concentration of solution becomes weak in refrigerant. The liquid in generator is allowed to cool so that its state becomes 4 as shown in Figure 1-11. When the valve is opened and the refrigerant is allowed to enter into the absorber during the night time, the solution concentration increases and the cycle is completed.

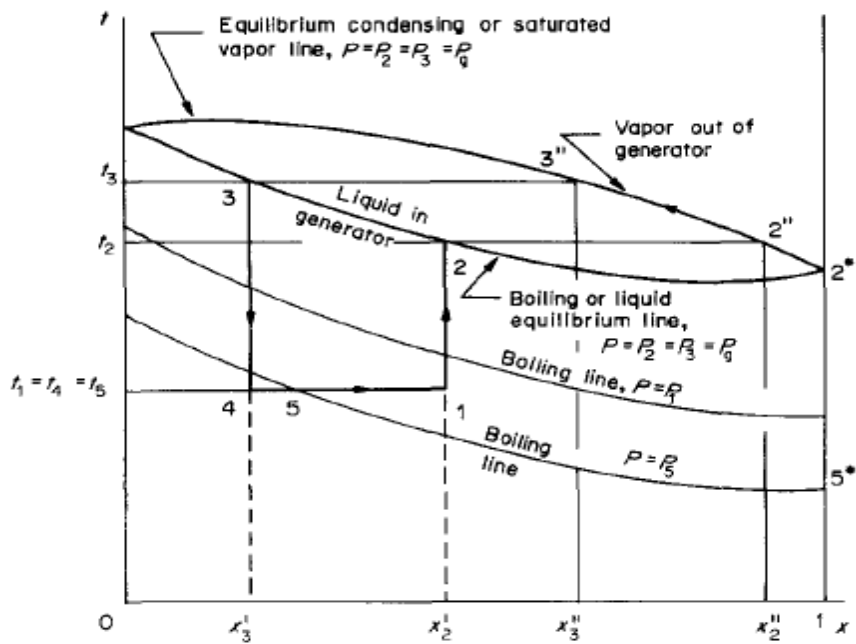


Figure 1-11 T-x Diagram of intermittent absorption refrigeration cycle

## 1.2 Thesis Objectives

The salient objectives of this research work are as follows:

- Development of hybrid storage absorption refrigeration (HSAR) cycle.
- Thermodynamic analysis of HSAR cycle on EES Software Package.
- Unsteady analysis of HSAR cycle for both summer and winter using Dhahran ambient conditions.
- Economic study of HSAR cycle.
- Study the impact of different design cases on size of storage tanks.
- Exergy analysis to investigate the exergy losses associated with major components of HSAR cycle.
- Exergo-economic evaluation of HSAR cycle.

## 1.3 Methodology of Proposed Work

The following methodology was adopted for this research work:

- A detailed literature review of aqua ammonia absorption refrigeration systems.
- Development of a novel HSAR cycle.
- Thermodynamic analysis of HSAR cycle (mass and energy balance equations) using *EES Software*.
- Study the impact of different designs of HSAR cycle on size of storage tanks.
- Cost breakdown assessment of HSAR cycle with the assistance of Chinese manufacturers for aqua-ammonia chillers.
- Unsteady analysis of HSAR cycle using Dhahran ambient conditions for year 2011.
- Implementation of exergy analysis of HSAR cycle on *EES Software*.
- Exergo-economic evaluation of HSAR cycle on *EES Software*.



## CHAPTER 2

### LITERATURE REVIEW

Said et al. [1] studied the 24 hour operating cycle of solar powered aqua ammonia absorption refrigeration system. Three different storage systems were considered to ensure 24 hour operation, cold storage, refrigerant storage and heat storage tanks. The three storage systems were used in the analysis of continuous based operation cycle while only the cold storage tank was considered in intermittent system. It was found that the system with hot storage tank produced maximum COP followed by the cold storage tank. El Shaarawi et al. [2] developed new set of correlations for estimating the design parameters of intermittent solar powered absorption refrigeration systems. These design parameters were the functions of four operating temperatures. The developed correlations were found easy to use and can be used effectively with a percentage error of less than 3%. Brendel et al. [3] developed a small scale ammonia absorption chiller with cooling capacity of 10 kW. Ice storage tank was integrated in the system along with the absorption chiller to enhance the overall system performance. TRANSYS simulations were performed to access the feasibility of using this system as a heat pump in winter.

Cerezo et al. [4] performed an experimental study using a plate heat exchanger for absorber in absorption refrigeration systems. It was suggested that relatively low COP of such machines could be compensated by increasing the heat and mass transfer properties in critical components like absorber. They also studied the effects of absorber operating conditions on system performance. Abdulateef et al. [5, 6] investigated the performance of solar absorption refrigeration system in Malaysia. They studied the effects of

generator, condenser and absorber temperatures on the COP of the system. It was observed that a high generator temperature was required if a high cooling load and low evaporator temperature were desired. The results showed that with increase in condenser and decrease in evaporator temperatures, COP decreases. They also performed thermodynamic analysis of solar absorption refrigeration system using different solution pairs. It was found that ammonia lithium nitrate and ammonia sodium thio-cyanate give better performance than aqua ammonia solution. It was also investigated that ammonia sodium thio-cyanate had chances of crystallization and hence cannot be used at evaporator temperature below -10 C.

Chidambaram et al. [7] presented a review on different solar cooling technologies and storage systems. It was found that latent heat storage systems which involve phase change material (PCM) has more dense energy storage with a narrow temperature range as compared to the sensible heat storage (SHS). Half and single effect chillers required less temperature at generator as compared to the multi effect systems. Cheap flat plate or evacuated tube solar collectors were found appropriate for single effect systems as these systems do not require very high generator temperature. Koca et al. [8] performed analysis of a latent heat storage of a phase change material ( $\text{CaCl}_2 \cdot 6\text{H}_2\text{O}$ ) for solar collectors. A special heat transfer fluid was used to carry the heat energy obtained from the solar collectors to phase change material (PCM). The average energy and exergy efficiencies were found to be 45 % and 2.2 % respectively.

Mokhtar et al. [9] investigated economics and performance of 25 different solar cooling technologies. It was found that flat plate and evacuated tube solar collectors are affected by the ambient conditions and hence these needed to be modeled on hourly

basis. It was found that absorption chillers are degraded severely by hot climate and hence efficient cooling methods should be used for heat rejection in condenser and absorber.

Pongsid et al. [10] provided the detailed literature review of different types of absorption systems. Different absorption cycles are compared to invent new efficient cycles. Multi effect systems with increased COP have shown a great potential to be used for large scale industries. The paper also discussed the ways by which the increased COP of the system can be achieved without increasing the complexities. A combined ejector-absorption system can provide the COP as high as a double effect system and it can be used for domestic refrigeration.

El Shaarawi et al. [11] investigated the effect of a condenser temperature on the performance of an intermittent system. The paper concluded that for a certain maximum generator temperature, decreasing the condenser temperature increases the COP of the system. The paper suggested the use of well water for heat exchange in condensers in areas where the water temperature is less than ambient temperature. Francisco et al. [12] discussed the prototype setup of aqua ammonia solar absorption system. The 2kW refrigeration test system harnessed the concentrated solar energy. Galvanized steel piping was used in the heat exchangers and transfer tank instead of the conventional pump to carry the ammonia solution. A single unit containing the collector - generator and the heat exchanger was invented to reduce heat losses. The solar collector was designed such that it performed the operation of heat exchange between the rich and the weak solution in two different concentric tubes. Kim et al. [13] performed dynamic modeling of a small scale aqua ammonia absorption chiller. The model showed that chiller was very sensitive

to some design and operation parameters. System performance was also found to be strongly dependent on initial charging of the solution and the concentration of the refrigerant.

Alizadeh et al. [14] performed a technical and economic study of multi pressure absorption cooling systems. The study showed that double effect absorption refrigeration has almost twice the COP at the optimum generator temperature as compared to the single effect refrigeration system. The effective electrical COP for different chiller configurations was also compared. The paper concluded that the maximum effective electrical COP for ideal single effect refrigeration system was achieved. Bulgan et al. [15] performed a sensitivity analysis for an aqua ammonia absorption refrigeration system. The objective of sensitivity analysis was the reduction of total annual costs. It was found that the strong solution ammonia concentration and the generator temperature have the greatest effect on the total annual cost.

Alvares et al. [16] simulated the aqua ammonia absorption refrigeration system. They performed a detailed thermodynamic analysis of the ammonia absorption refrigeration system. Thirteen different cycles were compared to get the maximum COP. The paper also investigated the exergetic performance of the aqua-ammonia refrigeration system. It was found that the maximum COP achieved was for aqua-ammonia refrigeration system integrated with both solution heat exchanger and refrigerant heat exchanger along with external and internal cooled rectifier. Karamangil et al. [17] performed a simulation study of single stage absorption refrigeration using different working fluids like water-lithium bromide, aqua ammonia and ammonia lithium nitrate solution. A thermodynamic analysis of the absorption refrigeration system was carried

out and the effects of different heat exchangers, operating temperatures and the effectiveness of the solution are also studied. The simulation showed that the COP of the system was increased by increasing the generator and evaporator temperature while it was decreased with the increase of condenser and absorber temperatures.

Darwish et al. [18] investigated the performance of a commercial absorption refrigeration water ammonia (ARWA) system. The simulation was performed using Aspen Plus software and a very good compromise in results was found between the simulation and experiments. Different strategies for COP enhancement have been discussed in detail and it was found that the extent of separation obtained in the generator was extremely important. The COP increased from 0.39 to 0.45 in going from poor separator performance to the best separator performance. The paper also investigated the increase in COP as the number of stages was increased from 1 to 6. Sozen [19] studied the effect of heat exchangers on the performance of absorption refrigeration systems. Three different configurations of heat exchangers were used in the analysis, one with refrigerant heat exchanger (RHE), other with mixing heat exchanger (MHE) and third one with using both heat exchangers. COP, ECOP and recirculation ratio were calculated for different operating conditions at a constant cooling load of 1kW. High COP was obtained for high evaporator and low generator temperatures. It was found that the effect of MHE was very prominent as compared to the RHE.

Khaled [20] performed experiments on the use of aqua ammonia absorption system in automobile air conditioning by using the exhaust gas as an energy source for generator. The purpose of this study is to analyze the feasibility of using the exhaust gas as a generator energy source in order to replace CFCs used in automobile air

conditioning. The COP of the system was found to be varying between 0.85 – 1.04 and the estimated cooling load was about 1.37 ton. Ercan et al. [21] performed second law analysis to determine the irreversibilities in the components of aqua ammonia absorption refrigeration system. Pressure losses between the components are considered and a constant ammonia concentration of 0.999 is used at the exit of generator. It was observed that the maximum exergy losses occur in absorber and evaporator. It was concluded that for each condenser, absorber and evaporator temperature, there is a certain generator temperature at which the dimensionless exergy loss was minimum. This was the point of maximum COP and ECOP.

Bulgan [22, 23] presented the optimization of an aqua ammonia absorption refrigeration model using two degrees of freedom, generator temperature ( $T_g$ ) and the mole ratio of ammonia ( $X_3$ ) in refrigerant. The objective of this optimization study was to maximize the COP by changing condenser, absorber and evaporator temperatures. It was concluded that maximum COP depends on condenser and absorber temperatures, as these temperatures decrease, COP increases. He also investigated the use of low temperature energy sources for generator in aqua ammonia absorption refrigeration system. He concluded that COP increases as the heating source temperature was increased. The circulation ratio also decreased with increasing generator temperatures. Misra et al. [24] presented the thermo economic evaluation and optimization of an aqua ammonia absorption refrigeration system. The exergy analysis was performed and the fuel, product and loss definition was used for each subsystem. The iterative procedure was used for system optimization which further enhanced the system performance without any additional resources. Sulaiman et al. [25] used isotropic sky model for monthly average

daily and hourly solar radiation for Dhahran region. The radiation values are theoretically estimated for sloped surfaces because of their vast applications. The values have been estimated for the entire year but these could not be verified because of unavailability of the measured data for Dhahran region.

Cai et al. [26, 27] developed a dynamic model of an absorption refrigeration system using ionic liquids as absorbents. The parameters affecting the system performance were also identified. They found that COP increases as the generator and absorber temperatures decrease. Friction factors were assumed for pressure losses in pipes. Kong et al. [28] performed experimental analysis of aqua ammonia absorption chiller. Thermodynamic energy and exergy analysis was also carried out the results of which were compared with the experimental outputs. The COP of experimental setup was found to be between 0.32 and 0.36. It was found that generator and evaporator had larger irreversibilities as compared to other components. Clerx et al. [29] studied the performance of an aqua ammonia absorption refrigerator. They performed analysis using both flat plate collectors (FPC) and concentrated parabolic collectors (CPC). They found that for generator temperature beyond 120 C, FPC is not suitable and hence CPC should be used for optimum performance.

Sun [30] presented a thermodynamic design data and design maps for aqua ammonia and water lithium Bromide absorption refrigeration systems. The design data can be used for developing cycles using new refrigerant absorbent pairs. The data can also be used for existing refrigeration cycles. Zalba et al. [31] presented a review on energy storage using phase change materials (PCM). The review also covered heat transfer analysis and its applications. The paper discussed 150 materials used as PCMs in

research and 45 materials commercially available in markets. Kim et al. [32] presented a review on different solar refrigeration options like solar electric, solar thermal etc. It was found that solar electric systems are more expensive than sorption systems. Adsorption chillers were found to be more expensive and bulkier than absorption systems. Boer et al. [33] modified the irreversibility in each component of the absorption refrigeration system which improved the efficiency of the whole cycle. They investigated how the selection of efficiency parameters affects the coefficients of structural bonds of heat exchangers. They proposed that these results could be used in thermodynamic analysis and economic optimization.

Rosen [34] preferred the economic analysis based on exergy rather than energy analysis of the system components. He reviewed different relations based on exergoeconomics, thermodynamics, capital cost and thermodynamic loss and EXCEM analysis. Kizilkan et al. [35] performed thermoeconomic optimization of a LiBr absorption refrigeration system. They optimized different components like condenser, absorber, generator and evaporator. This study also investigated optimum heat exchanger areas with optimum operating temperatures. Massimo and Filippo [36] applied Theory of Exergetic Cost on a refrigeration plant. This methodology reduced the global problem into a locally optimized system in which costs of all internal flows were evaluated. The results showed acceptable accuracy when compared with the conventional optimization methodology. Berhane et al. [37-39] considered the exergy destruction of single, double, triple and half effect H<sub>2</sub>O-LiBr absorption cycles. They investigated an increase in COP from double to triple effect absorption cycles. Largest energy destruction was obtained at generator and absorber components. They considered the effect of coefficient of



structural bonds on the heat exchanger area. They also studied the design of eco-friendly absorption cooling systems which caters cost minimization and environmental impact. This proposed approach could be used for alternative design cycles rather than a single design. Varela et al. [40] developed a thermodynamic design of the solar refrigerator of 2 kW cooling capacity to preserve the sea products. They presented the cost breakdown of each component of the refrigerator with heat duties. The refrigerator had the capacity to store 200 kg fish at -10 °C.

## CHAPTER 3

### ENERGY AND ECONOMIC ANALYSIS OF HSAR CYCLE

#### 3.1 Flow Diagram

The developed HSAR cycle integrates two storage systems, namely, the refrigerant storage system and the cold storage system. The refrigerant storage system is composed of three storage tanks, Ammonia Storage Tank (AST), Weak Solution Tank (WST) and the Strong Solution Tank (SST) whereas the cold storage system comprises of only one storage tank, the Cold Storage Tank (CST). Figure 1-1 shows the detailed layout of a HSAR cycle. During the daytime, solar collectors receive heat from the sun which is used to generate aqua-ammonia vapors from the strong aqua-ammonia liquid solution inside the generator.

The water vapors present in the ascending generated aqua-ammonia vapors are partly condensed in the exhausting column and returned back to the generator, leaving vapors richer in ammonia (13) go to the rectifying-column and then the dephlegmator. In order to ensure very high concentration of ammonia (say 99.6%) in the vapors going into the condenser (7), heat is further removed from the generated vapors that leaves the exhausting column (13) in both the rectifying column (by direct contact with the cold descending liquid) and the dephlegmator (by an external coolant). The condensed weak liquid solution from the dephlegmator is sent back to the top of the rectifying column. Ammonia vapors (7) dissipate heat to the cooling water in the condenser and are

converted into saturated liquid (8 and 14). The temperature of the cooling water should be 3-5 °C less than the condenser temperature [16]. Part of the liquid ammonia produced by the condenser (14) is continuously sent into the ammonia storage tank (AST) for use in producing cooling effect during night time; the rest of the produced liquid ammonia (8) is used in the cycle during the day time. The temperature of the liquid ammonia (9) that is cooled down as it passed through the Vapor liquid heat exchanger (VLHX) is further decreased as it is throttled (10) in the refrigerant expansion valve (EV2).

After the expansion valve, the throttled ammonia refrigerant splits between the evaporator and the cold storage tank (CST). The throttled ammonia flow rate to the CST (10) is controlled such that the required amount of ice and/or cold non-frozen liquid is produced inside the CST during daytime. Ammonia absorbs heat in the evaporator and the refrigerating coil of the CST and comes out as saturated vapors (11). Saturated vapors (11) absorb further heat in the VLHX and become superheated vapors (12). In the absorber, the ammonia vapors (12) are absorbed back by the weak solution (6) and hence a strong aqua-ammonia solution (1) is formed in an exothermic process.

The strong solution (1) is pumped into the LLHX (2) where it is preheated to a saturated liquid state (3). The saturated strong liquid solution (3) enters into the mid of the double rectifying column where it is further heated (while descending in the exhausting column) by the ascending hot vapors coming from the generator. The generator is heated by an external liquid coming from the solar collectors' field, aqua-ammonia vapors are formed in the generator and enter the exhausting column for purification (i.e. increase its concentration). The saturated weak solution from the generator (4) enters the LLHX where it rejects heat to the strong solution (2) until the

latter becomes saturated strong solution (3). Part of the weak solution (16) is continuously entered into the weak solution tank (WST) throughout the day so that it can be used during the night to absorb ammonia vapors in the absorber. The other part of the weak solution (17) flows into the absorber through liquid expansion valve (EV1). The cycle continues as such throughout the day as long as the effective solar energy is available. However, the cooling effect is continued as well during the night as explained here under.

When the night starts, AST filled with ammonia enters into the refrigeration cycle by opening valve  $V_1$  and feeding the evaporator with ammonia while valve  $V_5$  will be closed. Also the ice and/or the cold non-frozen liquid stored in CST are used in carrying part (half in the present work) of the cooling load. In other words, the cooling capacity of the CST ( $\dot{Q}_{CST}$ ) will now be used to cool part of the cooling load during the night, instead of being utilized during the day for forming ice in the CST. Thus the night cooling load is shared between the liquid ammonia refrigerant stored in AST and the ice and/or the cold non-frozen liquid in CST. In this work both these storage tanks (AST and CST) share equally the night cooling load (that is deliberately chosen equal to the daytime cooling load) to achieve the 5 kW cooling power by the chiller. Ammonia vapor from the evaporator enters the absorber where it is absorbed by the weak solution coming from the WST after opening valves  $V_4$  and  $V_2$  and closing valve  $V_6$ . Exothermic process in absorber results in the formation of a strong solution which enters into the SST. Both AST and the WST are gradually unfilled during the night and the SST is filled by the end of the night. The concentration of the strong solution produced at night is greater than the concentration during the daytime because the ambient temperature is lower at night. The

strong solution from SST is continuously mixed with the strong solution produced in the absorber during the daytime until the SST is unfilled by the end of the day. Valves V1, V2 and V4 are closed (CD) while valve V3, V5 and V6 are opened (OD) during the daytime.

The authors would like to point out that an invention disclosure entitled “Design of a Novel Hybrid Storage System for Aqua-Ammonia Absorption Cycle” based on the idea discussed in this paper with reference Docket No. 419760US is filed by the authors.

### **3.2 h-x diagram**

On the h-x diagram, the state points 1-13 represent the steady state HSAR cycle as shown in Figure 3-2. Notice that point 1 has the low (evaporator) pressure value ( $P_{low}$ ), which is constant in this investigation. However, point 2 is after the pump and has the high (condenser) pressure value, even though it lies on top of point 1. Thus the point 2 is in sub-cooled liquid state but absorbing heat inside the liquid liquid heat exchanger (LLHX) from the weak solution that comes out of the generator at state 4, it reaches the saturated liquid state 3. Thus, the heating process is initiated by the heat exchange between the weak solution and the strong aqua-ammonia solution in the liquid liquid heat exchanger (LLHX) then it continues in the generator by the direct solar heating. The heating in the LLHX is represented in Fig. 2 by the processes 2-3 and the direct solar heating is represented by the processes 3-4.

Due to the simultaneous effects of the rectifier and the dephlegmator, the concentration of the generated refrigerant ammonia vapors after the dephlegmator ( $x_7$ ) remains fixed at the assumed constant value of 0.996. Accordingly, the concentration of the ammonia after the condenser ( $x_8$ ), after the Vapor liquid heat exchanger VLHX on the

liquid side ( $x_9$ ), after the expansion valve EV ( $x_{10}$ ) and before/after the Vapor liquid heat exchanger VLHX ( $x_{11}$ )/ ( $x_{12}$ ) on the vapor side remain fixed at the same value (i.e.  $x_7 = x_8 = x_9 = x_{10} = x_{11} = x_{12} = 0.996$ ).

Since the throttling process is a constant enthalpy process, point 10 lie in the h-x diagram on top of point 9. However, point 9 is at the higher (condenser) pressure ( $P_{\text{high}}$ ) while point 10 (as well as points 11, 12) is at the lower (evaporator) pressure ( $P_{\text{low}}$ ). Since the state of the saturated aqua-ammonia vapor that leaves the exhausting column and enters the rectifying column is assumed to lie on the principal operating line for the combined generator-rectifier-dephlegmator units, it is represented on the h-x diagram by points 13.

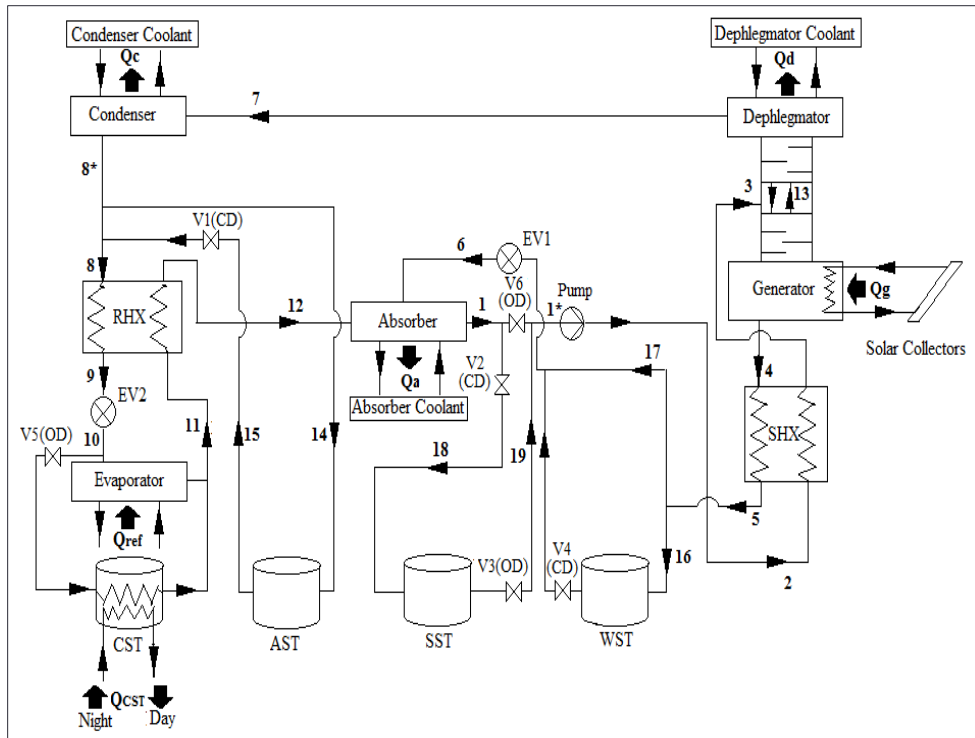


Figure 3-1 – Schematics of HSAR Cycle

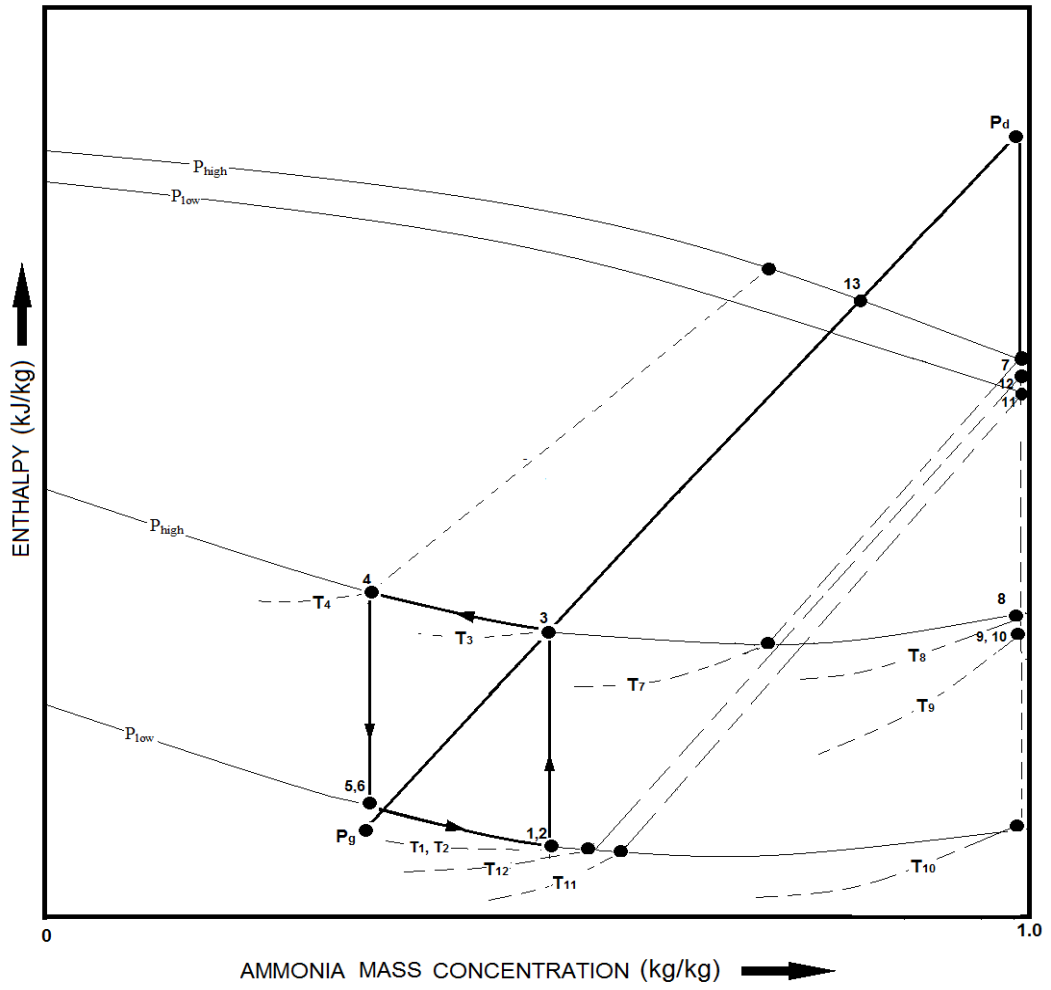


Figure 3-2 - h-x diagram of HSAR Cycle



### 3.3 Assumptions for Steady State Model

1. Almost pure refrigerant of ammonia concentration  $x = 0.996$  is assumed at the exit of the dephlegmator.
2. Refrigerant ammonia vapors at the exit of evaporator (state 11), liquid ammonia at the exit of condenser (state 8), strong solution at the inlet of generator (state 3), weak solution at the exit of generator (state 4) and the strong solution at the exit of the absorber (state 1) and SST (state 1\*) are in saturated states.
3. Concentrated solution is referred to as rich in ammonia and weak solution is referred to as weak in ammonia.
4. No energy loss is assumed between the solar collector and the generator.
5. The total sunlight hours in Dhahran region (Saudi Arabia) in summer (June 15) are 14 (from 5 AM in the morning to 7 PM in evening). But the solar intensity from 5-6 AM in the morning and 6-7 PM in the evening is insufficient to provide the minimum generator temperature ( $T_{\text{gen,min}}$ ) required to run the HSAR cycle. Hence the effective sunlight hours in summer are assumed as 12 (6 AM-6 PM) instead of 14.
6. The aqua-ammonia vapor that leaves the exhausting column and enters the rectifying column is saturated vapor with a temperature 10 °C higher than that of the strong solution entering the column at state 3 [47]. Moreover, it is assumed that this saturated vapor state lies on the principal operating line for the combined generator-rectifier-dephlegmator units [47].
7. The average daytime summer temperature in Dhahran region (Saudi Arabia) is assumed as 40 °C and the generator is assumed to operate at  $(T_{\text{ambient}} + 80)$  °C, i.e., 120 °C [1].

8. The daytime condenser and absorber temperatures are at  $(T_{\text{ambient, day}} + 5) \text{ }^\circ\text{C}$ , i.e.,  $T_c=T_a=45 \text{ }^\circ\text{C}$  [1].
9. The cooling load is equally shared between the ice in cold storage tank (CST) and ammonia in ammonia storage tank (AST) overnight.
10. The temperature drop of  $8 \text{ }^\circ\text{C}$  is considered at night as compared to daytime temperature, i.e., the average night temperature ( $T_{\text{ambient, night}}$ ) is  $32 \text{ }^\circ\text{C}$  [1].
11. The absorber temperature during night is assumed as  $(T_{\text{ambient, night}} + 5) \text{ }^\circ\text{C}$ , i.e.,  $T_a=37 \text{ }^\circ\text{C}$ .
12. The evaporator temperature is assumed constant at  $-5 \text{ }^\circ\text{C}$  and the cooling capacity at  $5 \text{ kW}$ .
13. Thermal inertia of the storage tanks and the heat exchangers has been neglected in this research work.
14. Non-tracking selective-coated flat plate solar collector with the tilt angle =  $26.26^\circ$  is used to provide the thermal energy to the generator with a stagnation temperature  $180\text{-}210 \text{ }^\circ\text{C}$  (the highest obtainable collector's absorber temperature (no output withdrawn) when the solar intensity is  $1000 \text{ W/m}^2$  on the outmost transparent cover) [49]. The efficiency of such selective flat plate solar collectors ranges between  $20\%$  and  $75\%$  depending on the ambient conditions [49].
15. Since almost all the components of the HSAR cycle are non-mechanical/non-moving (except the pump), the life expectancy of the HSAR cycle is  $15\text{-}20$  years [57-59].

These assumptions imply that the model has been simplified by assuming a fixed constant daytime temperature ( $= T_{\text{av, day}}$ ) and a constant nighttime temperature ( $= T_{\text{av, night}}$ ).

night) with constant solar insolation ( $= I_{av}$ ). Hence the system can be modeled on steady-state conditions during daytime and nighttime.

### 3.4 Steady-State Thermodynamic analysis

Steady thermodynamic analysis of hybrid storage aqua-ammonia absorption (HSAR) system is performed using Engineering Equation Solver (EES). The following input parameters were used for the thermodynamic analysis of HSAR cycle: ambient temperature ( $T_{amb}$ ), °C; weak solution temperature at the exit of generator ( $T_4 = T_{gen}$ ), °C; absorber exit temperature ( $T_1 = T_{amb} + 5$ ), °C; condenser exit temperature ( $T_{g*} = T_{amb} + 5$ ), °C; evaporator exit temperature ( $T_e = T_{11} = -5$  °C); cooling power (5kW); effectiveness of VLHX (0.75); effectiveness of LLHX (0.75).

#### 3.4.1 Generator-double rectification column-dephlegmator

The two columns (exhausting and rectifying columns) along with the generator and dephlegmator units are analyzed together. The generator and dephlegmator heat capacities ( $q_g$  and  $q_d$ ) are given by the following relations:

$$\dot{Q}_g = \dot{m}_4 (h_4 - h_{pg}) \quad (3.1)$$

$$\dot{Q}_d = \dot{m}_7 (h_{pd} - h_7) \quad (3.2)$$

$\dot{Q}_g$ ,  $\dot{Q}_d$ ,  $h_{pg}$  and  $h_{pd}$  are unknowns in equations (3.1) and (3.2). However, the poles  $P_g$  and  $P_d$  of the generator and dephlegmator are located on the principal operating line (shown in Figure 3-2) and their enthalpies ( $h_{pd}$  and  $h_{pg}$ ) can be determined by using the straight line equation of the principal operating line (POL), which has the following general form:

$$h = (\text{slope} \times x) + c \quad (3.3)$$

Where  $h$  is the enthalpy at any concentration  $x$  on the principal operating line. The slope of the POL is given by [47]:

$$\text{slope} = (h_{13} - h_3)/(x_{13} - x_3) \quad (3.4)$$

$h_{13}$  and  $x_{13}$  are determined using the EES Software by means of the three known properties for the state point 13 [Pressure = condenser pressure (obtained from the three given properties at the exit (state 8\*) of the condenser, i.e., condenser temperature ( $T_c = T_{8^*}$ ); ammonia concentration (say 0.996)); quality=saturated liquid); temperature  $T_{13} = (T_3+10)$  °C (assumption 6); and quality of aqua-ammonia vapors at state 13 is saturated vapor]. With  $h_{13}$  and  $x_{13}$  known, the slope of the principal operating line (POL) is determined by equation (3.4) and the constant  $c$  in the equation of a straight line (3) is determined using the following relation:

$$c = h_{13} - (\text{slope} \times x_{13}) \quad (3.5)$$

With the *slope* and constant the  $c$  known, the two unknowns  $h_{pg}$  and  $h_{pd}$  in equations (3.1) and (3.2) respectively can be determined as follows:

$$h_{pg} = (\text{slope} \times x_4) + c \quad (3.6)$$

where

$$h_{pd} = (\text{slope} \times x_7) + c \quad (3.7)$$

Enthalpy values for  $h_{pg}$  and  $h_{pd}$  are used in equation (3.1) and equation (3.2) to determine the generator heat capacity and the dephlegmator heat capacity.

### 3.4.2 Condenser

The heat capacity of the condenser is written as:

$$\dot{Q}_c = \dot{m}_7 (h_7 - h_8) \quad (3.8)$$

### 3.4.3 Evaporator

The evaporator cooling capacity during the daytime ( $\dot{Q}_{e,day}$ ) is 7.5 kW (for 12 hours of effective sunlight hours (assumption 5)) which is equal to the sum of constant refrigeration capacity ( $\dot{Q}_{ref,day} = 5$  kW) and the cooling capacity ( $\dot{Q}_{CST} = 2.5$  kW) required to produce ice in CST to share the nighttime refrigeration load.

$$\dot{Q}_{e,day} = \dot{Q}_{ref,day} + \dot{Q}_{CST} \quad (3.9)$$

$$\dot{Q}_{e,day} = \dot{m}_{10} (h_{11} - h_{10}) \quad (3.10)$$

The evaporator cooling capacity during the nighttime ( $\dot{Q}_{e,night}$ ) is equal to the cooling capacity of the ammonia stored in the ammonia storage tank ( $\dot{Q}_{AST}$ ) which is equal to 2.5 kW for 12 hours of nighttime refrigeration in summer for Dhahran region (assumption 5).

$$\dot{Q}_{e,night} = \dot{Q}_{AST} = \dot{m}_{15} (h_{11} - h_{10}) \quad (3.11)$$

### 3.4.4 Absorber

The heat capacity of the absorber for day and night is written as:

$$\dot{Q}_{a,day} = \dot{m}_6 h_6 + \dot{m}_{12} h_{12} - \dot{m}_1 h_1 \quad (3.12)$$

$$\dot{Q}_{a,night} = \dot{m}_{16} h_6 + \dot{m}_{15} h_{12} - \dot{m}_{18} h_1 \quad (3.13)$$

### 3.4.5 Refrigerant Heat Exchanger

The heat capacity of the RHX is written as:

$$\dot{Q}_{RHX,1} = \dot{m}_8 (h_8 - h_9) \quad (3.14)$$

$$\dot{Q}_{RHX,2} = \dot{m}_{11} (h_{12} - h_{11}) \quad (3.15)$$

Assuming negligible heat losses to the surroundings,

$$\dot{Q}_{RHX,1} = \dot{Q}_{RHX,2} \quad (3.16)$$

### 3.4.6 Solution Heat Exchanger

The heat capacity of the SHX is written as:

$$\dot{Q}_{SHX,1} = \dot{m}_8 (h_8 - h_9) \quad (3.17)$$

$$\dot{Q}_{SHX,2} = \dot{m}_{11} (h_{12} - h_{11}) \quad (3.18)$$

Assuming negligible heat losses to the surroundings,

$$\dot{Q}_{SHX,1} = \dot{Q}_{SHX,2} \quad (3.18)$$

Table 3-1 shows the values of heat capacity for the components of HSAR cycle for average summer ambient conditions of Dhahran (assumption 7), Saudi Arabia. Generator has the maximum value of heat capacity among all the components. Absorber and evaporator have more values of heat capacity during the day than that during the night. The net values of heat energy (in kWh) gained by the system is equal to the net value of heat energy (in kWh) lost by the system.

**Table 3-1– Thermodynamic analysis of HSAR cycle**

Components	Energy	Time	kWh	Energy	Time	kWh
	In (kW)	(hr)		Out (kW)	(hr)	
<b>Generator</b>	20.94	12	251.2			
<b>Absorber (DAY)</b>				14.23	12	170.76
<b>Absorber (NIGHT)</b>				4.52	12	54.24
<b>Condenser</b>				10.43	12	125.16
<b>Evaporator (DAY)</b>	7.5	12	90			
<b>Evaporator (Night)</b>	2.5	12	30			
<b>Dephlegmator</b>				1.826	12	21.912
<b>Pump</b>	0.1541	12	1.85			
<b>Total</b>			373.05			372.17

### 3.5 Area of Solar Collector Field

Size of solar collector field is one of the most important parameters in solar refrigeration systems [14]. The operation of refrigeration cycle is dependent on the energy received by the collectors from the sun. If collectors do not receive enough energy

needed by the generator, the system COP will be adversely affected. Flat plate solar collectors (FSC) are considered a feasible option for HSAR cycles as these are relatively inexpensive in the market and operate for generator temperature upto  $(T_{amb}+100)$  °C. Collector area is calculated using the method proposed by Duffie and Beckman in Solar Engineering of Thermal Sciences [45]. The area of solar collector depends on the average heat capacity of the generator. The greater the generator heat capacity, greater will be the required collector area. With 49.6 % efficiency ( $\eta$ ) of the collectors [9], the calculated area of FSC is 64.8 m<sup>2</sup>. The monthly average hourly solar radiation ( $I_T$ ) for Dhahran region is obtained from technical note presented by Al – Sulaiman and B. Ismail [25]. The useful energy gain per unit collector area ( $q_u$ ) is calculated as follows:

$$q_u = \eta * I_T \quad (3.18)$$

The collector area is calculated from the following equation:

$$A_c = \frac{Q_g}{q_u} \quad (3.19)$$

### 3.6 Economic Assessment

The present economic study is based on storage tanks, solar collectors and evaporator and condenser units. Based on storage capacities, operating temperature and pressure, the design of each storage tank is obtained from Chinese manufacturers. The ammonia tanks are much expensive in the market as compared to other components of the absorption system. Both AST and WST operate at a high pressure of 17 bars in this 5kW HSAR cycle. In order to sustain such a high pressure, thick walled stainless steel pressure vessels are used for ammonia storage which results in high initial cost of ammonia storage tanks. Despite having less storage capacity of AST than CST, the cost



of AST is around 5 times the cost of CST as shown in Table 3-2. As the storage capacity of WST is around 7 times the storage capacity of AST, the cost of WST is also expected to increase by the same proportion.

**Table 3-2 – Cost Summary of AST and CST**

<b>Manufacturer</b>	<b>Storage Type</b>	<b>Material</b>	<b>Storage Capacity (kg)</b>	<b>Cost FOB China (USD)</b>
<b>China National Air Separation Plant</b>	AST	Stainless Steel	113.5	4000
<b>Weigeli Factory</b>	CST	Galvanized Steel	377.7	850

Evaporator and condenser heat exchangers are cheaply available in the Chinese market as shown in Table 3-3. The cost of generator, absorber, rectifier and dephlegmator units could not be obtained from the market. It is expected that total commercial cost of these heat exchangers is less than the total cost of all the storage tanks. This means that storage tanks and solar collectors are more detrimental in the economic assessment than heat exchanger components. So the size of solar field and storage tanks need to be optimized to get an optimum balance between performance and cost.

**Table 3-3 – Cost and design specification of evaporator and condenser units**

<b>Manufacturer</b>	<b>Heat Exchanger Type</b>	<b>Diameter (mm)</b>	<b>Hole (mm)</b>	<b>Row (mm)</b>	<b>Cost FOB China (USD)</b>
<b>Shanghai</b>	Evaporator	9.52	25	21.65	262
<b>Shenglin M &amp; E Technology</b>	Condenser	9.52	25	21.65	454.1

In HSAR cycle, the nighttime refrigeration load (5kW) is equally shared between the CST and the AST (2.5 kW each). The total size of the required storage tanks is therefore reduced to 62 % the total size of storage tanks required in refrigerant-storage absorption refrigeration (RSAR) cycle as shown in Table 3-4.

The cost of flat plate solar collectors with technical specifications is shown in Table 3-5. The cost of collectors TTFC-B-2.0/1 with copper header and riser tubes is 97 USD/m<sup>2</sup> while the cost of collectors TTFC-B-2.0/2 with aluminum header and riser tubes is 74 USD/m<sup>2</sup>. The total cost of solar collector field TTFC-B-2.0/1 for this hybrid storage refrigeration system is 6200 USD.

**Table 3-4 – Comparison of size of storage tanks for different storage designs**

Storage Tank	Pressure (bar)	Temperature (°C)	NH <sub>3</sub> mass concentration, x	ρ (kg/m <sup>3</sup> )	Size for	Size for	Size for
					5 kW cooling power in HSAR Cycle (m <sup>3</sup> )	5 kW cooling power in RSAR Cycle (m <sup>3</sup> )	5 kW cooling power in CSAR Cycle (m <sup>3</sup> )
<b>CST</b>	1.01	-5	-	917.4	0.35	-	0.70
<b>AST</b>	17.69	43.86	0.996	573.2	0.17	0.34	-
<b>WST</b>	17.69	60	0.342	789.9	0.63	1.26	-
<b>SST</b>	3.53	45	0.404	846.7	0.70	1.40	-
<b>Total</b>					1.85	3.00	0.70

**Table 3-5 – Specification details and cost of flat plate solar collectors**

Manufacturer	Collector Dimension	Gross Area	Cover Thickness	Riser Tube Dimension	Insulation Back with thickness	Working Pressure	FOB price
	mm <sup>3</sup>	m <sup>2</sup>	mm	ODxT mm <sup>2</sup>	mm	MPa	USD
<b>TTFC-B-2.0/1</b>	2000*1000 *90	2	3.2	Φ10.5 * 0.8, Cu	Polytherene , 40	0.6	193
<b>TTFC-B-2.0/2</b>	2000*1000 *90	2	3.2	Φ10.5 * 0.8, Al	Polytherene , 40	0.6	148

### 3.7 Effectiveness, area and cost of SHX and RHX

The effectiveness value of heat exchanger affects the heat exchange area which in turn affects the cost of heat exchanger. The following equations were used to determine the heat exchange area:

$$\varepsilon = \dot{Q}/\dot{Q}_{max} \quad (3.20)$$

$$\dot{Q} = C_h(T_{hi} - T_{ho}) = C_c(T_{co} - T_{ci}) \quad (3.21)$$

$$\dot{Q}_{max} = C_{min}(T_{hi} - T_{ci}) \quad (3.22)$$

Effectiveness-NTU relation for counter-flow heat exchanger is given as:

$$\varepsilon = [1 - \exp\{-NTU(1 - C_r)\}]/[1 - C_r \exp\{-NTU(1 - C_r)\}] \quad (3.23)$$

$$C_r = C_{min}/C_{max} \quad (3.24)$$

$$A = (NTU \times C_{min})/U \quad (3.25)$$

The cost of the SHX and the RHX can be estimated using the following correlation [41]:

$$C_x = C_y \left(\frac{A_x}{A_y}\right)^{0.6} \quad (3.26)$$

Figure 3-3 shows the effect of heat exchanger effectiveness on the heat exchange area. The area of SHX is 10-15 times the heat exchange area of the RHX. The area of SHX/RHX at effectiveness = 0.8 is 13/10 times the heat exchange area at effectiveness = 0.2. Since the cost of the heat exchanger is proportional to its heat exchange area as shown in equation (3.26), the cost of the SHX and RHX is expected to rise in a similar fashion as shown in Figure 3-3.

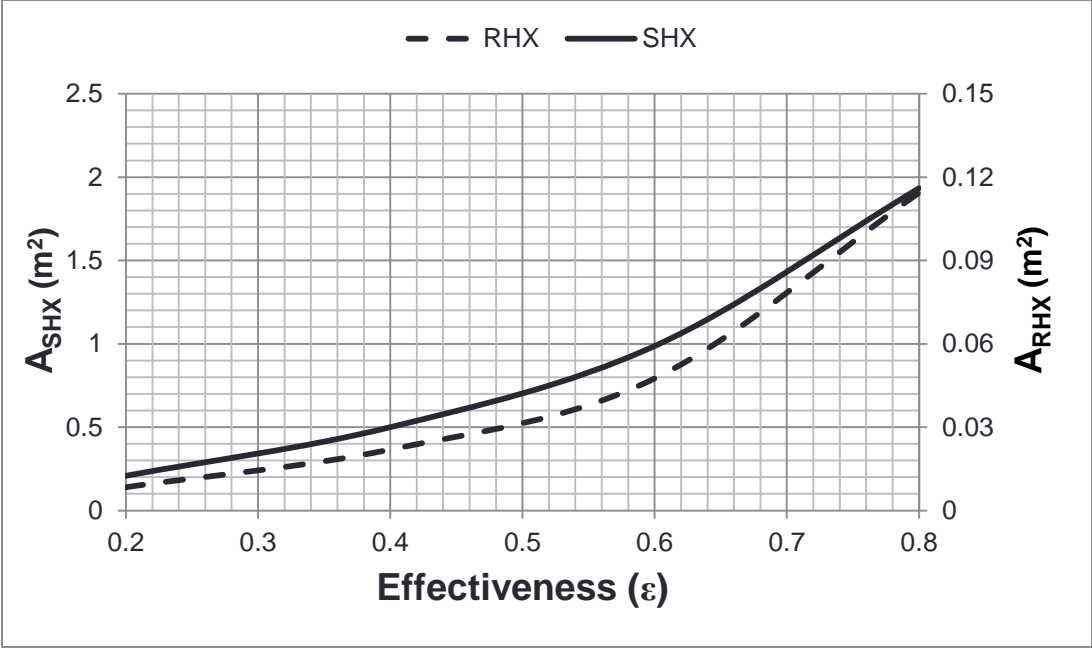


**Figure 3-3 Plots of heat exchanger area versus effectiveness for SHX and RHX**

# CHAPTER 4

## UNSTEADY THERMODYNAMIC ANALYSIS OF HSAR CYCLE

In steady state analysis, no changes occur either within the control volume or at the boundaries of the control volume. In the previous chapter, a steady state model for HSAR cycle has been developed which greatly simplified the thermodynamic analysis. However, in reality, HSAR cycle is unsteady and changes within the control volume occur with time. Hence, an unsteady thermodynamic model has been developed to comprehend the actual processes that occur in the control volume of each component of HSAR cycle. Unsteady processes occur over a finite period of time  $\Delta t$  and therefore, the mass as well as the energy content of the control volume change with time [42]. Unsteady thermodynamic model for HSAR cycle has been idealized as a *uniform flow process*. This implies that the flow properties do not change with time or position at the inlet or exit of each system component [42].

The ambient temperature data for Dhahran region was obtained for May/June and Nov/Dec for year 2011 from the Research Institute, KFUPM. The COP of HSAR cycle varies throughout the day with the change in ambient temperature. The parameters like generator temperature, absorber and condenser temperatures, condenser pressure, enthalpies and mass flow rates of different components are dependent on ambient conditions. The plots for unsteady energy analysis were developed on EES Software at every one hour interval.

## 4.1 Assumptions for Unsteady State Analysis

1. The total sunlight hours in summer/winter are about 14/10 (from 5 AM in the morning to 7 PM in the evening) / (from 7 AM in the morning till 5 PM in the evening). But the solar intensity in summer from 5-6 AM in the morning and 6-7 PM in the evening is too low to run the HSAR cycle (solar collectors do not gain enough solar energy to drive the HSAR cycle). Hence the effective sunlight hours in summer/winter are considered 12/8 instead of 14/10 as shown in Fig. 3, which shows the plots of the hourly variations of the solar intensity and ambient temperature for the representative days of summer and winter. Thus the HSAR cycle is in a complete running state from 6 AM in morning till 6 PM in the evening / from 8 AM in the morning till 4 PM in the evening for representative days of summer / winter. In other words, there is a warming-up period that starts at sun rise and ends at 6 AM in summer and at 8 AM in winter. Similarly, the generator and the condenser of the cycle have a run-down period that starts before sun set (at 6 PM in summer and 4 PM in winter) while the other components such as the evaporator; AST; CST; etc continue or start operation during this run-down period.
2. June 15, 2011 was selected as a representative day for summer as this day received the maximum peak solar radiation whereas Dec. 21, 2011 was chosen as a representative day for winter as it received the minimum peak solar radiation.
3. Unsteady thermodynamic analysis for HSAR cycle, assuming negligible changes in kinetic and potential energies from inlet to exit and uniform fluid properties at inlet or exit of each component of the cycle (uniform flow process [42]), was carried out on an hourly basis in a stepwise manner, i.e. using a time interval ( $\Delta t$ ) of 1 hour.

4. The weak solution temperature at exit from the generator ( $T_4$ ) is assumed at  $(T_f - 3)$  °C, where  $T_f$  is the exit temperature of the working fluid from the solar collectors field. This working fluid transports the thermal solar energy gained by the collectors to the generator.
5. Selective-coated flat plate solar collector is used to provide the thermal energy to the generator with a stagnation temperature 180-210 °C (the highest obtainable collector's absorber temperature (no output withdrawn) when the solar intensity is 1000 W/m<sup>2</sup> on the outmost transparent cover) [49]. The efficiency of such selective flat plate solar collectors ranges between 20% and 75% depending on the ambient conditions [49]. In the present analysis, this efficiency is assumed equal 42 % to determine the corresponding collectors' exit fluid temperature ( $T_f$ ).
6. The aqua-ammonia liquid leaves the solution heat exchanger (SHX) and enters the generator as saturated liquid.
7. The aqua-ammonia vapor that leaves the exhausting column and enters the rectifying column is saturated vapor with a temperature 10 °C higher than that of the strong solution entering the column at state 3 [47]. Moreover, it is assumed that this saturated vapor state lies on the principal operating line for the combined generator-rectifier-dephlegmator units [47].
8. The condenser and absorber exit temperatures are assumed equal to each other at  $(T_{amb} + 5)$  °C. The evaporator temperature is constant at -5 °C and the evaporator pressure with ammonia concentration ( $x=0.996$ ) is assumed constant at the corresponding pure ammonia ( $x=1$ ) saturation value (3.529 bar). The cooling power is constant over the 24



hours of the day at 5 kW and is equally shared between the CST and AST during the night.

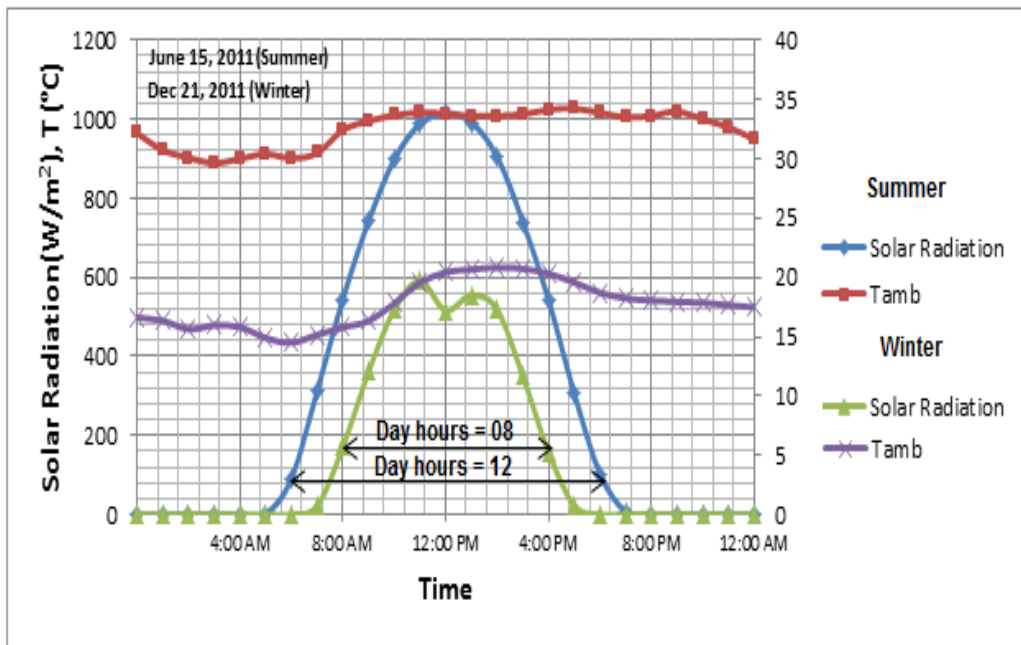


Figure 4-1 Plots of solar radiation and ambient temperature for a representative summer and winter day

## 4.2 h-x diagram

The h-x diagram for three different time intervals ( $\Delta t$ ) is shown in Figure 4-2. In this study the evaporator temperature as well as the net cooling power is assumed to be constant throughout the day and night in both summer and winter at 5 kW and a constant temperature of  $-5^{\circ}\text{C}$ . Accordingly, the low (evaporator) pressure ( $P_{\text{low}}$ ) in HSAR cycle does not vary with time; it equals the saturation pressure corresponding to the fixed evaporator operating temperature. On the other hand, the high (condenser) pressure in HSAR cycle is not constant and depends on the ambient conditions that vary with time.

On the h-x diagram, the state points 1-13 represent the cycle after a time interval  $\Delta t_0$  that starts after the warming-up period, the state points 1'-13' show the cycle after the time interval  $\Delta t_1$  (that starts just after the end of  $\Delta t_0$ ) and the state points 1''-13'' show the cycle after the time interval  $\Delta t_2$  (that starts just after the end of  $\Delta t_1$ ). Notice that points 1, 1', and 1'' are all having the low (evaporator) pressure value ( $P_{\text{low}}$ ), which is constant in this investigation. However, points 2, 2', and 2'' are all after the pump and have the high (condenser) pressure values, even though they lie on top of points 1, 1', and 1'', respectively. The high pressure values of points 2, 2', and 2'' ( $P_{\text{high}}$ ,  $P_{\text{high}} + \Delta P_1$ , and  $P_{\text{high}} + \Delta P_2$ , respectively) increase with time due to the increase in solar intensity and also the ambient temperature after the sunshine (hence the condenser temperature, which is assumed equal  $T_{\text{ambient}} + 5$ ). Thus, all the points 2, 2', and 2'' are in sub-cooled liquid states but absorbing heat inside the solution heat exchanger (SHX) from the weak solution that comes out of the generator at states 4, 4', and 4'', respectively, they become in the saturated liquid states 3, 3', and 3'', respectively. Thus, the heating process is initiated by the heat exchange between the weak solution and the strong aqua-ammonia

solution in the solution heat exchanger (SHX) then it continues in the generator by the direct solar heating. The heating in the SHX is represented in Figure 4-2 by the processes 2-3, 2'-3', or 2''-3'', and the direct solar heating is represented by the processes 3-4, 3'-4', or 3''-4''.

At the beginning of  $\Delta t_0$  the cycle starts to be in a complete working state and the saturated liquid solution in the generator is at temperature  $T_3$ . This temperature is the minimum generator temperature ( $T_{\text{gen, min}}$ ) required to start the complete operation of the HSAR cycle. However, the heating process starts at constant concentration ( $x_3$ ) during the morning warming-up period (say 5-6 AM/7-8 AM in summer/winter before the effective sunlight hours). During this period simultaneous increase in the generator temperature and pressure (due to the simultaneous increase in solar intensity and ambient temperature) occurs until the minimum generator temperature ( $T_{\text{gen, min}}$ ) required to start the HSAR cycle is reached. Then the ammonia vapor starts to leave the generator and goes to the dephlegmator, condenser, etc to complete the cycle. Similarly, the generator stops producing the aqua-ammonia vapor due to insufficient solar energy and low ambient temperature during the run-down period (say 6/ 4 PM onwards in summer/winter after the effective sunlight hours). During this period, simultaneous decrease in the generator temperature and pressure (due to the decrease in / absence of solar intensity and decrease in ambient temperature) occurs at constant concentration (say  $x_4^*$ ) until the minimum late-night generator temperature is reached. During the warming-up and run-down periods, the ammonia in AST and the ice in CST cope with the cooling load. The warming-up and run-down periods are not shown in the h-x diagram of HSAR cycle as the h-x diagram only represents the state points of the cycle in a complete working state.

However, the warming-up and run-down processes are similar to processes 1-3 and 4''-5'' shown on the h-x diagram.

The time step ( $\Delta t$ ) in the analysis using the EES software is chosen to be one hour. During the time interval  $\Delta t_1$ , the solar radiation is more intense than that during the time interval  $\Delta t_0$ . The strong solution formed inside the absorber during  $\Delta t_1$  has a relatively lower concentration than the strong solution formed during  $\Delta t_0$  as shown by state points 1', 2' on the h-x diagram. The isotherms shown on the h-x diagram of HSAR cycle in Fig. 2 are only for the time interval  $\Delta t_0$ .

As the time proceeds from morning to noon (from the beginning of  $\Delta t_0$  till the end of say six time-intervals ( $6 \Delta t = 6 \text{ hrs}$ ) in summer), the concentration of the strong solution liquid entering the generator ( $x_3, x_{3'}, x_{3''}$ ) as well as that of the weak solution liquid exiting the generator ( $x_4, x_{4'}, x_{4''}$ ) decrease. Similarly, the concentration of the saturated solution vapors exiting the rectifier/exhausting column ( $x_{13}, x_{13'}, x_{13''}$ ) decrease. The poles of the generator ( $P_g, P'_g, \text{ and } P''_g$ ) and those of the dephlegmator ( $P_d, P'_d, \text{ and } P''_d$ ) are also shifted on the h-x diagram with time throughout the day as shown in Fig. 2. Accordingly, the principal operating straight lines that link the pole of the generator, the pole of the dephlegmator and the assumed saturated vapor state exiting the exhausting column [18] also vary with time and move on the h-x diagram upward from left to right. However, due to the simultaneous effects of the rectifier and the dephlegmator, the concentration of the generated refrigerant ammonia vapors after the dephlegmator ( $x_7, x_{7'}, x_{7''}$ ) remains fixed at the assumed constant value of 0.996. Accordingly, the concentrations of the ammonia after the condenser ( $x_8, x_{8'}, x_{8''}$ ), after the refrigerant heat exchanger RHX on the liquid side ( $x_9, x_{9'}, x_{9''}$ ), after the expansion valve EV ( $x_{10}, x_{10'},$

$x_{10''}$ ) and before/after the refrigerant heat exchanger RHX ( $x_{11}, x_{11'}, x_{11''}$ )/ ( $x_{12}, x_{12'}, x_{12''}$ ) on the vapor side remain fixed at the same value (i.e.  $x_7 = x_{7'} = x_{7''} = x_8 = x_{8'} = x_{8''} = x_9 = x_{9'} = x_{9''} = x_{10} = x_{10'} = x_{10''} = x_{11} = x_{11'} = x_{11''} = x_{12} = x_{12'} = x_{12''} = 0.996$ ).

Since the throttling process is a constant enthalpy process [17-18], points 10, 10' and 10'' lie in the h-x diagram on top of points 9, 9' and 9'', respectively. However, points 9, 9' and 9'' are at the higher (condenser) pressures ( $P_{\text{high}}, P_{\text{high}} + \Delta P_1$ , and  $P_{\text{high}} + \Delta P_2$ ) while points 10, 10' and 10'' (as well as points 11, 11', 11'', 12, 12' and 12'') are all at the lower (evaporator) pressure ( $P_{\text{low}}$ ). Since the state of the saturated aqua-ammonia vapor that leaves the exhausting column and enters the rectifying column is assumed to lie on the principal operating line for the combined generator-rectifier-dephlegmator units [18], it is represented on the h-x diagram by points 13, 13' and 13''.

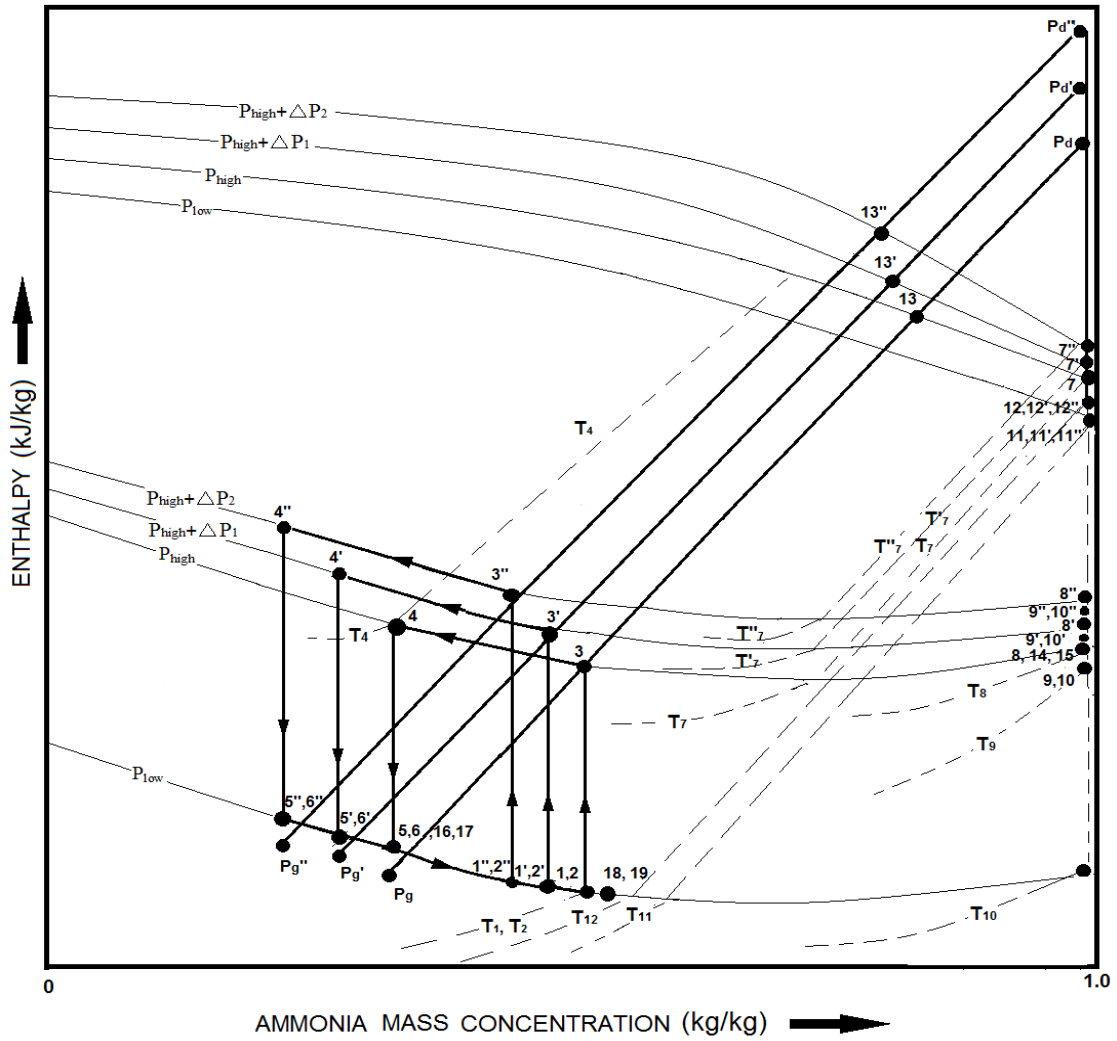


Figure 4-2 h-x diagram of HSAR Cycle

### 4.3 Unsteady Thermodynamic analysis

In any solar refrigeration cycle changes with time occur. Hence, an unsteady model has to be developed to comprehend the actual processes that occur within each component of HSAR cycle. Unsteady processes occur over finite time periods and mass as well as energy content of a control volume change with time. The present unsteady thermodynamic analysis for each component of the HSAR cycle has been idealized as a “uniform flow process” [42]; which implies that during each time step period  $\Delta t$ , the flow properties at the inlet and/or exit of each system component do not change with time or position. However, the mass and/or energy content of a control volume change with time and the flow properties at the inlet and/or exit change from a time step to another.

The ambient temperature and solar intensity data for year 2011 in Dhahran city, Saudi Arabia have been used in this study. The operating parameters like generator, absorber and condenser temperatures, condenser pressure, enthalpies, etc of different components are dependent on ambient conditions. Accordingly the performance parameters such as COP of HSAR cycle vary throughout the day with the changes in ambient temperature and solar intensity. The plots for unsteady energy analysis were developed by EES Software at every one hour time-step interval. The input parameters used for the present unsteady analysis of HSAR cycle are the following: hourly ambient temperature ( $T_{amb}$ ), °C; hourly solar intensity ( $I$ ),  $W/m^2$ ; initial weak solution temperature at exit of the generator ( $T_4 = T_f - 3$ ), °C; initial absorber exit temperature ( $T_1 = T_{amb} + 5$ ), °C; initial condenser exit temperature ( $T_{8*} = T_8 = T_{amb} + 5$ ), °C; evaporator exit temperature ( $T_{evap} = T_{11} = T_{11}' = T_{11}'' = -5$  °C); cooling power (5kW); effectiveness of RHX (0.75); effectiveness of SHX (0.75).



The operating temperature of the generator and hence the weak-solution temperature at exit from the generator ( $T_4$ ) depend on the temperature of the solar collectors' working fluid ( $T_f$ ), which depends on the efficiency of the collector, ambient temperature ( $T_{amb}$ ) and the solar intensity ( $I$ ). On the other hand, the area of the solar collector field depends on the thermal energy needed by the generator ( $Q_g$ ) to operate the HSAR cycle for the given input conditions. The efficiency curve of a selective flat plate solar collector (assumption 5) is shown in Figure 4-3[49] and the following correlation is developed for such an efficiency curve:

$$\eta = -3.6 \times (T_f - T_{amb}) / I + 0.776 \quad (a)$$

Using assumption (5), equation (a) can be rewritten as:

$$T_f = 0.098 \times I + T_{amb} \quad (b)$$

Equation (b) shows that the fluid temperature at the exit of the solar collector tubes ( $T_f$ ) depends on the ambient temperature as well as the solar intensity. Based on assumption (4), the instantaneous weak-solution temperature at the exit from the generator can be determined for HSAR cycle at any time  $t$  by means of equation (b).

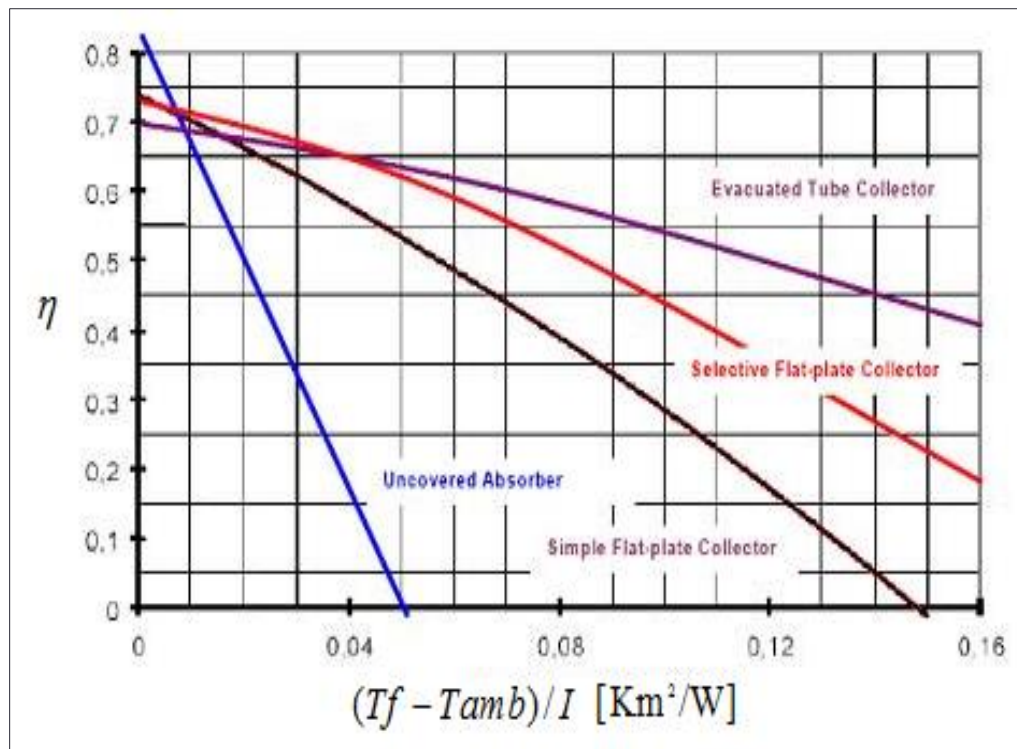


Figure 4-3 Efficiency curves for solar collectors [49]

#### 4.4 Governing Mass and Energy Equations

In unsteady flow processes, changes are analyzed over some finite time duration  $\Delta t$  instead of changes per unit time [42]. Therefore, in unsteady analysis, the heat energy ( $Q$ ) of HSAR components is determined instead of the heat duty ( $\dot{Q}$ ). The mass and energy of the uniform flow process change within the system boundaries.

$$m_{in} - m_{out} = \Delta m_{system} \quad (4.1)$$

where

$$\Delta m_{system} = m_{final} - m_{initial} \quad (4.2)$$

$$E_{in} - E_{out} = \Delta E_{system} \quad (4.3)$$

where

$$\Delta E_{system} = E_{final} - E_{initial} \quad (4.4)$$

The energy balance for a uniform flow process can be shown as

$$Q_{in} + W_{in} + \sum_{in} m\theta = Q_{out} + W_{out} + \sum_{out} m\theta = (m_f e_f - m_i e_i)_{system} \quad (4.5)$$

Where  $\theta = h + ke + pe$  is the energy of the fluid stream per unit mass at inlet or outlet and  $e = u + ke + pe$  is the energy of the non-flowing fluid per unit mass within the control volume [42]. As the kinetic and potential energies are assumed negligible in HSAR cycle, the above equation reduces to:

$$Q - W = \sum_{out} mh - \sum_{in} mh + (m_f u_f - m_i u_i)_{system} \quad (4.6)$$

Where  $Q = Q_{in} - Q_{out}$  is the net heat input and  $W = W_{out} - W_{in}$  is the net work output [42].

For each time interval  $\Delta t$ , after the cycle becomes in a complete working state (after the warming-up period mentioned in assumption (1)), the HSAR cycle can be

regarded as a quasi-steady closed cycle in which the mass leaving a component is filled immediately by the mass preceding it. The mass inside any component (control volume) of the completely operating HSAR cycle at the start of the time interval  $\Delta t$  is the same as the mass inside the same component (control volume) at the end of that time interval  $\Delta t$ . Hence, there is no change in mass inside the control volume as long as the cycle is in a complete working state (assumption 1), i.e.,

$$m_f = m_i = m \quad (4.7)$$

$$\sum m_{in} = \sum m_{out} \quad (4.8)$$

Note that equations (4.7) and (4.8) will not hold true during the periods of warming-up (when the generator starts from rest after sunrise) and run-down (when the cycle comes to rest from a complete working state by the end of the day).

Based on the above discussion, for each component in a HSAR cycle, under complete working conditions, the generalized unsteady energy equation over each finite time duration ( $\Delta t$ ) assuming uniform flow processes can be written as [42]:

$$Q - W = \sum_{out} mh - \sum_{in} mh + m(u_f - u_i)_{system} \quad (4.9)$$

Where  $Q$  and  $W$  are the net thermal and mechanical energies,  $m$  is the mass inside the control volume and  $(u_f - u_i)_{system}$  is the change in internal energy per unit mass inside the control volume during time  $\Delta t$ .

Referring to the flow diagram given in Figure 3-1 and the corresponding h-x diagram of Figure 3-2, the above 3 equations (4.7, 4.8 and 4.9) are used in the unsteady analysis of each component of the completely working HSAR cycle.

#### 4.4.1 Generator- Double Rectification Column-Dephlegmator Assembly

The generator in HSAR cycle works only during the daytime as long as solar energy is available. The net heat input to the generator remains unsteady throughout the day as the intensity of solar energy varies with time. The two columns (exhausting and rectifying columns) along with the generator and dephlegmator units are analyzed together [47]. Based on the generalized equations (1-3), the mass and energy balance for the generator-double rectification column-dephlegmator assembly for a finite time interval  $\Delta t$  are:

$$m_3 = m_4 + m_7 \quad (4.10)$$

$$m_3 x_3 = m_4 x_4 + m_7 x_7 \quad (4.11)$$

$$Q_g - Q_d = m_4 h_4 + m_7 h_7 - m_3 h_3 + [m(u_f - u_i)]_g + [m(u_f - u_i)]_d \quad (4.12)$$

Referring to the h-x diagram shown in Figure 3.2, the ratio of the generator heat ( $Q_g$ ) to the mass of weak solution ( $m_4$ ) at the exit of generator (state 4) is given [47] by:

$$Q_g / m_4 = h_4 - h_{pg} \quad (4.13)$$

Similarly, the ratio of the dephlegmator heat ( $Q_d$ ) to the mass of the ammonia vapor at the exit of dephlegmator ( $m_7$ ) is given by the following relation [47]:

$$Q_d / m_7 = h_{pd} - h_7 \quad (4.14)$$

$Q_g$ ,  $Q_d$ ,  $h_{pd}$  and  $h_{pg}$  in equations (4.13) and (4.14) are unknowns. However, the poles  $P_g$  and  $P_d$  of the generator and dephlegmator are located on the principal operating line (shown in Figure 3-2) and their enthalpies ( $h_{pd}$  and  $h_{pg}$ ) can be determined by using the straight line equation of the principal operating line (POL), which has the following general form:

$$h = slope \times x + c \quad (4.15)$$

Where  $h$  is the enthalpy at any concentration  $x$  on the principal operating line. The slope of the POL is given [47] by:

$$slope = (h_{13} - h_3)/(x_{13} - x_3) \quad (4.16)$$

$h_{13}$  and  $x_{13}$  are determined using the EES Software by means of the three known properties for the state point 13 [Pressure = condenser pressure (obtained from the three given properties at the exit of the condenser (state 8<sup>\*</sup>), i.e., condenser temperature ( $T_{cond} = T_{8^*} = T_{amb} + 5, \text{ }^\circ\text{C}$  (assumption 8)); ammonia concentration (say 0.996); and state 8<sup>\*</sup> is saturated liquid); temperature  $T_{13} = (T_3+10) \text{ }^\circ\text{C}$  (assumption 7); and state 13 is saturated aqua-ammonia vapors]. With  $h_{13}$  and  $x_{13}$  known, the slope of the principal operating line (POL) is determined by equation (4.16) and the constant  $c$  in the straight line equation (4.15) is determined by the relation:

$$c = h_{13} - (slope \times x_{13}) \quad (4.17)$$

With both the *slope* and the constant the  $c$  known, the two unknowns,  $h_{pg}$  and  $h_{pd}$ , in equations (4.13) and (4.14) can be determined respectively as follows:

$$h_{pg} = slope \times x_4 + c \quad (4.18)$$

$$h_{pd} = slope \times x_7 + c \quad (4.19)$$

Note that  $h_4$  and  $x_4$  are determined by EES at the 3 known properties of the weak solution at exit from the generator (Pressure = condenser pressure, generator temperature ( $T_4 = T_f - 3$ ) and quality = saturated liquid). Use  $h_{pg}$  and  $h_{pd}$  in equations (4.13) and (4.14) to determine the generator heat ( $Q_g$ ) and the dephlegmator heat ( $Q_d$ ) which will be used in equation (4.12).

Part of the computed generator energy ( $Q_g$ ) gained during the day is used to produce the desired daytime cooling effect ( $Q_{ref,d} = 5\text{kW} \times \text{time of the effective sunlight hours in seconds}$ ) and the other part of it ( $Q_{g,CST+AST}$ ) is used to produce ice/cold non-

frozen liquid in CST ( $Q_{CST} = 2.5 \text{ kW} \times \text{time of cooling hours of night in seconds}$ ) in addition to the extra ammonia in AST ( $Q_{AST} = 2.5 \text{ kW} \times \text{time of cooling hours of night in seconds}$ ).  $Q_{g,CST+AST}$  is obtained as follows. The program is run with a total cooling output equal to only the 5kW needed during the daytime and hence the required generator energy ( $Q_{g, \text{without storages}}$ ) to produce only the daytime cooling load without storages is obtained; the difference between the generator energy ( $Q_g$ ) and  $Q_{g, \text{without storages}}$  is  $Q_{g,CST+AST}$  (the part  $Q_g$  used to produce ice in CST and the extra ammonia in AST).

#### 4.4.2 Evaporator

The overall cooling output of the system ( $Q_{ref,d} + Q_{CST} + Q_{AST}$ ) during the effective sunlight hours in winter is assumed to remain the same as in summer as shown in Table 4-1. Part of the evaporator cooling energy during the daytime ( $Q_{e,day}$ ) is used to produce the desired cooling effect during the daytime ( $Q_{ref,d} = 5\text{kW} \times \text{time of the effective sunlight hours in seconds}$ ) and the other part is used to produce ice/non-frozen cold liquid in CST ( $Q_{CST} = 2.5 \text{ kW} \times \text{time of cooling hours of night in seconds}$ ). Mathematically,

$$Q_{e,day} = Q_{ref,d} + Q_{CST} \quad (4.20)$$

The evaporator mass and energy equations for a finite time interval  $\Delta t$  during the daytime are:

$$m_{10,day} = m_{11,day} \quad (4.21)$$

$$Q_{e,day} = m_{11,day}h_{11} - m_{10,day}h_{10} + [m(u_f - u_i)]_{e,day} \quad (4.22)$$

Where  $Q_{e,day} = Q_{ref,d} + Q_{CST} = 5 \text{ kW} \times \text{working cooling hours during day in seconds} + 2.5 \text{ kW} \times \text{working cooling hours during night in seconds}$ .

**Table 4-1– The given cooling energy outputs of HSAR cycle during the effective sunlight hours**

	Winter	Summer
<b>Effective sunlight hours</b>	8 h	12 h
<b>Nighttime cooling hours</b>	16 h	12 h
$Q_{ref,d}$	5kW x 8 = 40 kWh (144 MJ)	5kW x 12 = 60 kWh (216 MJ)
$Q_{CST}$	2.5 kW x 16 = 40 kWh	2.5 kW x 12 = 30 kWh
$Q_{AST}$	2.5 kW x 16 = 40 kWh	2.5 kW x 12 = 30 kWh
$Q_{ref,d} + Q_{CST} + Q_{AST}$	120 kWh (432 MJ)	120 kWh (432 MJ)
$Q_{e,day} = Q_{ref,d} + Q_{CST}$	80 kWh (288 MJ)	90 kWh (324 MJ)
<b>Hourly <math>Q_{e, day}</math></b>	10 kWh (36 MJ)	7.5 kWh (27 MJ)
$Q_{e, night} = Q_{ref, night}$ <b>=2.5 kW x night cooling hours</b>	40 kWh (144 MJ)	30 kWh (108 MJ)
<b>Hourly <math>Q_{e, night}</math></b>	2.5 kWh (9 MJ)	2.5 kWh (9 MJ)
<b>Given constant cooling energy output per hour</b>	5kWh = 18 MJ	5kWh = 18 MJ

During the night, valve V5 is closed and the mass of the ammonia coming from the AST does not split between the evaporator and the CST rather all the ammonia enters



into the evaporator. Furthermore, the mass of ammonia at state 10 during the day ( $m_{10, day}$ ) is not equal to the mass of ammonia at state 10 during the night ( $m_{10, night}$ ).

$$m_{10,night} = m_{11,night} \quad (4.23)$$

$$Q_{e,night} = m_{11,night} h_{11} - m_{10,night} h_{10} + [m(u_f - u_i)]_{e,night} \quad (4.24)$$

$$Q_{e,night} = Q_{ref,n} = 2.5kW \times \text{time of cooling hours of night in secs} \quad (4.25)$$

As long as the effective solar radiation is available, the instantaneous coefficient of performance ( $COP_{day}$ ) at any instant of time t for a given time interval ( $\Delta t$ ) is given by:

$$COP_{day} = (Q_{e,day} + Q_{AST}) / Q_g \quad (4.26)$$

All  $Q_s$  in the above equation are during the time interval ( $\Delta t$ ), the pump energy ( $W_p$ ) is negligible and thus not incorporated in equation (4.26). By extending  $\Delta t$  to be the whole cooling hours of the daytime, the same equation (4.26) gives the COP for the whole day (overall/average day COP).

The ammonia in AST and the ice and/or cold non-frozen liquid in cold storage tank (CST) share equally the cooling load during the cooling hours of the night, therefore:

$$Q_{AST} = Q_{CST} = 2.5kW \times \text{time of cooling hours of night in secs} \quad (4.27)$$

The COP of HSAR cycle at night can be defined by the following equation:

$$COP_{night} = (Q_{AST} + Q_{CST}) / Q_{g,CST+AST} \quad (4.28)$$

$Q_{g,CST+AST}$  is the part of the total generator energy ( $Q_g$ ) required during the day to produce ammonia in the AST and ice/non-frozen liquid in the CST to suffice the nighttime cooling load. Note that  $COP_{night}$  is for the whole night period (i.e., for a period = 24 – effective sunlight hours); even though  $Q_{g,CST+AST}$  has an hourly value but an hourly value for  $COP_{night}$  is meaningless.

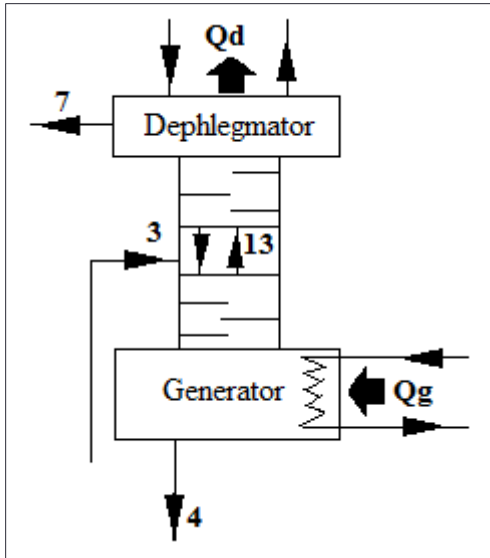


Figure 4-4 Flow across a generator-double rectification column-dephlegmator unit

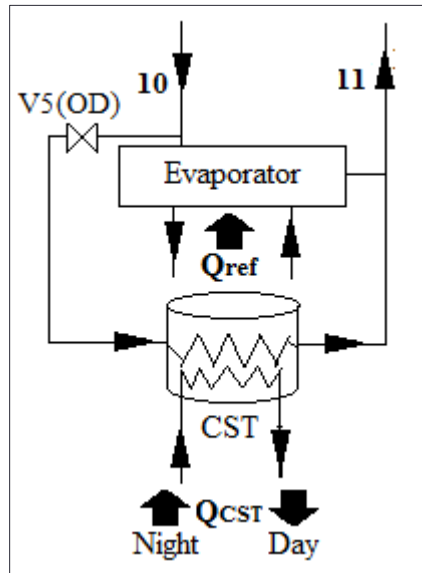


Figure 4-5 Flow across an evaporator unit and cold storage tank (CST)

### 4.4.3 Absorber

Like the evaporator, the absorber in HSAR cycle also operates continuously 24 hours a day. During the daytime, the strong solution produced at the exit of the absorber (state 1) enters the pump as the valve V6 is opened (OD) and the valve V2 is closed (CD). At night, the strong solution produced at the exit of the absorber (state 1) enters the strong solution tank (SST) as valve V6 is closed and valve V2 is opened. Based on the generalized equations (1-3), the mass and energy balance equations for the absorber over a finite time interval  $\Delta t$  are:

$$m_{12,day} + m_{6,day} = m_{1,day} \quad (4.29)$$

$$m_{12,day}x_{12} + m_{6,day}x_6 = m_{1,day}x_1 \quad (4.30)$$

$$Q_{a,day} = m_{12,day}h_{12} + m_{6,day}h_6 - m_{1,day}h_1 - [m(u_f - u_i)]_{a,day} \quad (4.31)$$

$$m_{12,night} + m_{6,night} = m_{1,night} \quad (4.32)$$

$$m_{12,night}x_{12} + m_{6,night}x_6 = m_{1,night}x_1 \quad (4.33)$$

$$Q_{a,night} = m_{12,night}h_{12} + m_{6,night}h_6 - m_{1,night}h_1 - [m(u_f - u_i)]_{a,night} \quad (4.34)$$

### 4.4.4 Condenser

The condenser continuously rejects heat from ammonia vapors to the coolant during the daytime. Based on the generalized equation (4.7), (4.8) and (4.9), the mass and energy balance equations for the condenser for a finite time interval  $\Delta t$  are written as:

$$m_7 = m_{8^*} \quad (4.35)$$

$$Q_c = m_7h_7 - m_{8^*}h_8 - [m(u_f - u_i)]_c \quad (4.36)$$

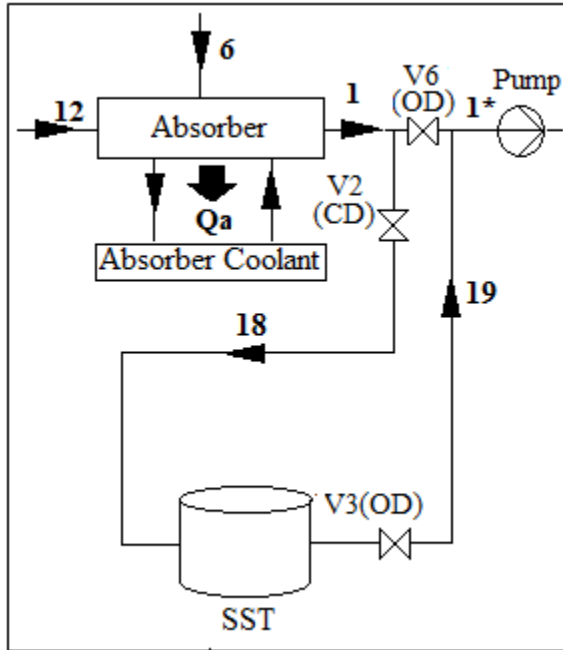


Figure 4-6 Flow across an absorber unit

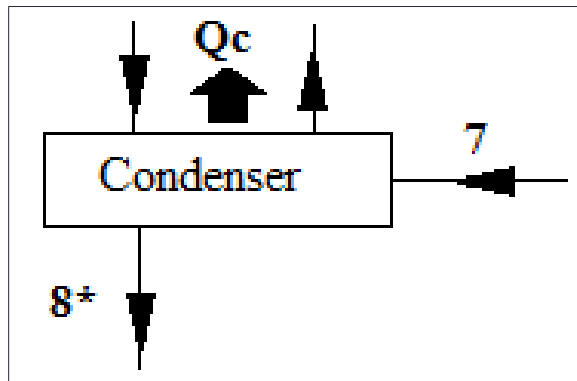


Figure 4-7 Flow across a condenser unit

#### 4.4.5 Refrigerant Heat Exchanger (RHX)

Refrigerant heat exchanger (RHX) involves heat transfer between the vapor ammonia leaving the evaporator and the liquid ammonia leaving the condenser. Based on the generalized equation (4.7), (4.8) and (4.9), the mass and energy balance equations for refrigerant heat exchanger (RHX) for finite time interval  $\Delta t$  are written as:

$$m_8 = m_9 \quad (4.37)$$

$$Q_{RHX,1} = m_8 h_8 - m_9 h_9 - [m(u_f - u_i)]_{RHX,8-9} \quad (4.38)$$

$$m_{11} = m_{12} \quad (4.39)$$

$$Q_{RHX,2} = m_{12} h_{12} - m_{11} h_{11} + [m(u_f - u_i)]_{RHX,11-12} \quad (4.40)$$

$$Q_{RHX,1} = Q_{RHX,2} \quad (4.41)$$

#### 4.4.6 Solution Heat Exchanger (SHX)

Solution heat exchanger operates only during the effective sunlight hours. Based on the generalized equation (4.7), (4.8) and (4.9), the mass and energy balance equations for refrigerant heat exchanger (RHX) for finite time interval  $\Delta t$  are written as:

$$m_4 = m_5 \quad (4.42)$$

$$Q_{SHX,1} = m_4 h_4 - m_5 h_5 - [m(u_f - u_i)]_{SHX,4-5} \quad (4.43)$$

$$m_2 = m_3 \quad (4.44)$$

$$Q_{SHX,2} = m_3 h_3 - m_2 h_2 + [m(u_f - u_i)]_{SHX,2-3} \quad (4.45)$$

$$Q_{SHX,1} = Q_{SHX,2} \quad (4.46)$$

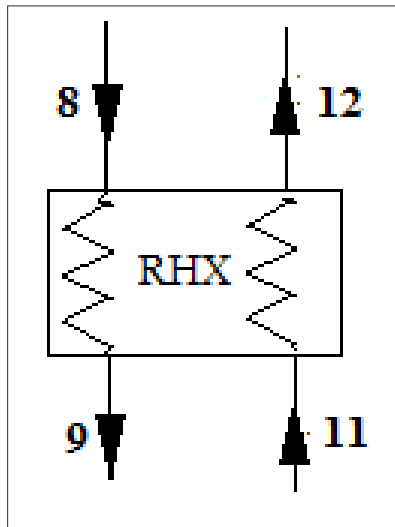


**Figure 4-8 Flow across a RHX**

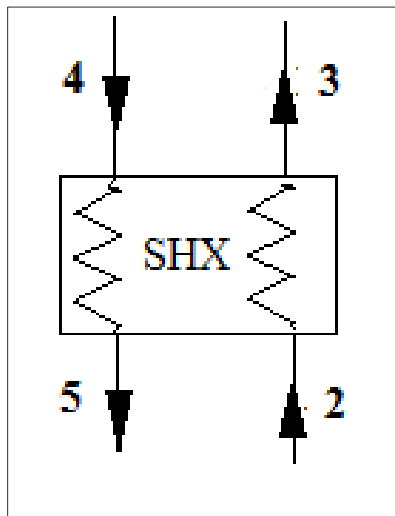


**Figure 4-9 Flow across a SHX**

#### 4.5 Determination of mass inside each component and the term ( $m (u_f - u_i)$ ) in the unsteady energy equation for each component of HSAR cycle

During the effective sunlight hours the mass inside each component is assumed constant for each time interval ( $\Delta t$ ). Hence, the unsteady behavior of HSAR cycle under the complete working conditions is mainly due to the time variations of: the internal energy per unit mass inside the system ( $u_i$  and  $u_f$ ) and the flowing masses in and out ( $m_{in}$  and  $m_{out}$ ) of each component (control volume) and their enthalpies ( $h_{in}$  and  $h_{out}$ ), not due to the mass ( $m$ ) inside each control volume (component).

The determination of the mass ( $m$ ) inside each component (control volume) of HSAR cycle develops the need to design the component as a heat exchanger. NTU (Number of transfer units) method [50] is used for the design of such heat exchangers using EES Software. For the sake of simplification, each of these heat exchangers in HSAR cycle is assumed to be of the counter-flow concentric annulus type with an effectiveness of 0.75. NTU for each counter-flow heat exchanger is determined from the known effectiveness ( $\epsilon$ ) and the capacitance rates  $\dot{C}$  ( $\dot{C} = \dot{m} c_p$ ) for the hot and cold fluids flowing in the heat exchanger. The mass flow rate ( $\dot{m}$ ) for each component is determined from the steady-state model using mass and energy balance equations of HSAR cycle (using average values for representative days of both summer and winter for Dhahran, 2011). The specific heat of pure ammonia / water (coolant) inside the heat exchanger is determined by EES using the average of two known properties at inlet and exit, e.g., pressure (P) and temperature (T). For heat exchangers which use aqua-ammonia solutions such as absorber and generator, the chart shown in Fig. (i) [51] is used to determine the



specific heat. Due to insufficient data and unknown coolant (water) temperatures at inlet or exit of heat exchanger, the mass flow rate of the coolant (water) used in condenser, absorber and dephlegmator is assumed equal the mass flow rate of ammonia inside these heat exchangers. Brine, due to its ability to decrease the freezing point of water up to -21 °C (at 23.3 % of NaCl by weight in water) [52], is used as a medium to transport heat from the cold space to the evaporator ( $T_{\text{evap}} = -5$  °C). Pressurized hot water at 5 bars (boiling point = 152 °C) is used as the medium to transport heat energy from the solar collectors ( $T_f = 123$  °C at  $T_{\text{amb}} = 40$  °C) to the generator. High pressure hot water in the collector-generator loop should have a saturation temperature greater than  $T_f$  to prevent evaporation and reduce the possibility of cavitation and degradation of pump used in collector-generator loop. From the known effectiveness and capacitance rates, NTU is determined using the following EES command:

$$\text{NTU}=\text{HX}(\text{'counterflow'}, \text{effectiveness}, \text{C\_dot\_fluid1}, \text{C\_dot\_fluid2}, \text{'NTU'})$$

Where C\_dot\_fluid1 and C\_dot\_fluid2 are the capacitance rates of the two fluids used in heat exchanger.

Having obtained the value of NTU, the total heat transfer area ( $A$ ) can be found by:  $A = (NTU \times \dot{C}_{\min}) / U$ ;  $\dot{C}_{\min}$  is the minimum of the values of capacitance rates of the two fluids used in the heat exchanger.  $U$  is the overall heat transfer coefficient which is obtained using the method proposed by Lavanya and Murthy [53]. Assuming tube length ( $l$ ) equal 0.5m, neglecting the thickness ( $t$ ) of the tube as compared to its length ( $t \ll l$ ) and thus inner radius  $\approx$  outer radius  $\approx$  radius ( $r$ ), the radius ( $r$ ) of each tube is determined as:  $r = A / (2\pi l)$  and the total volume of fluid inside the tube is determined as:  $V = \pi \times r^2 \times l$ .

The density ( $\rho$ ) of the fluid inside the tubes of the heat exchanger is determined by EES using the average of three/two known properties from any of the six properties (pressure, temperature, mass concentration, internal energy, specific volume, enthalpy, specific entropy and quality) for aqua-ammonia/pure ammonia at the inlet and exit. Thus the mass of the fluid inside the tubes of heat exchanger is:  $m = \rho \times V$ .

In condenser, evaporator, generator, absorber and dephlegmator heat exchangers, ammonia/ ammonia solution is assumed inside the tube whereas coolant (water)/pressurized hot water (in a loop between the collector and generator)/brine solution (in a loop between the evaporator and the cooling space) is assumed in the annular space between the tube and the shell of the concentric heat exchanger. In SHX, the strong solution is assumed inside the tube whereas the weak solution is assumed in the annular space between the tube and the shell of the heat exchanger. In RHX, the vapor ammonia (coming from the evaporator) is assumed inside the tube of the heat exchanger whereas the liquid ammonia (coming from the condenser) is assumed in the annular space. The volume of the fluid in the annular region in RHX and SHX is determined by:  $V = \pi(r_s^2 - r^2)l$  where  $r_s$  is the radius of the shell (inside diameter of the annulus outer tube) of the concentric counter-flow heat exchanger,  $r$  is the radius of the tube and the radius of the shell is assumed double the radius of the tube, i.e.,  $r_s = 2r$ . From the volume and density of the fluid in the annular region, the mass of the fluid in the annular region is determined.

The internal energy ( $u$ ) inside each control volume (component) of HSAR cycle is determined at the start ( $u_i$ ) and the end ( $u_f$ ) of each time interval  $\Delta t$  by EES software using three/two known properties of the substance inside the control volume. The very

initial internal energy value inside each control volume (component) of HSAR cycle is assigned zero at the beginning of the warming-up period ( $u_i = 0$  at sunrise, 5 AM/7 AM in summer/winter). At the end of the warming-up period (6 AM/8AM in summer/winter), the final internal energy ( $u_f$ ) is determined by EES Software using any three known properties for each control volume; this is the initial internal energy for the first time step in the unsteady analysis inside each component of HSAR cycle under the complete working conditions. As the properties inside the control volume are unknown, therefore, an iterative procedure is needed with initial values of these properties assumed to be the average of the known properties at the inlet and exit of each control volume.

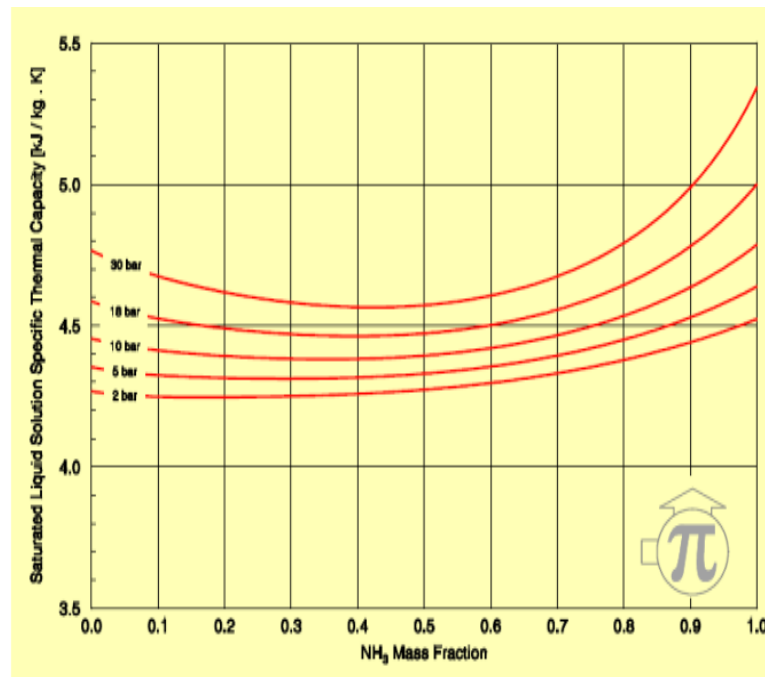


Figure 4-10 Specific heat capacity of ammonia solution [51]

## CHAPTER 5

### EXERGY ANALYSIS OF HSAR CYCLE

Chapter 3 discussed about the thermodynamic and economic assessment of HSAR cycle. Thermodynamic analysis using mass and energy balance equations present the quantitative aspect of any system. However, for comparison purposes, a more detailed qualitative analysis needs to be carried out. Exergy analysis based on second law of thermodynamics presents the quality of a system. The fact that exergy is not conserved and part of it is destroyed is of more significance than energy analysis in the design of thermal systems. Exergy analysis can be used to identify the components with high exergy losses. Once such components are identified, they can be modified to increase the overall efficiency of the system. As energy is conserved and does not reveal any information on energy losses of the system, it is inappropriate to design a thermal system based solely on energy analysis.

Exergy is defined as *the minimum theoretical useful work required to form a quantity of matter from substances present in the environment and to bring the matter to a specified state* [41]. While discussing exergy, it is important to consider the difference between the surrounding and the environment. Surrounding is everything outside the system where as environment is *a part of the surrounding, the intensive properties of which are uniform and do not change significantly as a result of any process* [41]. Exergy destruction which is mainly due to friction and other resistances will not be considered in the exergy analysis of HSAR cycle. However irreversibilities due to finite temperature heat transfer processes produce exergy losses that will be considered in each component

of the HSAR cycle. Exergy analysis for HSAR cycle is performed keeping in view the same assumptions as used in chapter 3.

## 5.1 Generalized Mathematical Formulation

The total exergy of a system is composed of four components namely, physical exergy  $X^{PH}$ , kinetic exergy  $X^{KT}$ , potential exergy  $X^{PT}$  and chemical exergy  $X^{CH}$ .

$$X^{tot} = X^{PH} + X^{KT} + X^{PT} + X^{CH} \quad (5.1)$$

The kinetic and potential exergies can be converted to work if the system is brought to rest relative to the environment. In HSAR cycle, the kinetic and potential exergies are considered zero for all the components. As no chemical reaction occurs in any component of HSAR cycle, the value of chemical exergy remains the same at inlet and outlet of all the components. Thus chemical exergy can be neglected for HSAR cycle as the difference between the exergy values at inlet and outlet for each component will eventually make it zero. Thus for HSAR cycle, the total exergy is equal to physical exergy for all the system components.

$$X^{tot} = X^{PH} \quad (5.2)$$

### 5.1.1 Physical Exergy and Exergy Loss

The physical exergy per unit mass of a closed system is given as [41]

$$X^{PH} = (u - u_o) + p_o(v - v_o) - T_o(s - s_o) \quad (5.3)$$

$$h - h_o = (u - u_o) + p_o(v - v_o) \quad (5.4)$$

$$X^{PH} = (h - h_o) - T_o(s - s_o) \quad (5.5)$$

Where  $T_o$  is the reference temperature which is assumed as the ambient temperature in the exergy analysis of HSAR cycle.

The exergy per unit mass of a mixture is given as [21]

$$X = \sum_{n=1}^m x_n h_n - T_o \sum_{n=1}^m x_n s_n \quad (5.6)$$

The exergy rate of a mixture is given by

$$\dot{X} = \dot{m} \left( \sum_{n=1}^m x_n h_n - T_o \sum_{n=1}^m x_n s_n \right) \quad (5.7)$$

The rate of exergy loss for a system component is governed by

$$\dot{X}_L = \sum \dot{X}_i - \sum \dot{X}_o + \dot{Q}(1 - T_o/T) + \dot{W} \quad (5.8)$$

The third term on right hand side of equation (5.8) is the exergy of heat.

### 5.1.2 Exergetic Efficiency

The exergetic efficiency, also known as second law efficiency, is a suitable parameter for determining the performance of a thermal system. Refrigeration systems must be compared using exergetic efficiencies rather than values of coefficient of performance. This is because a system with high COP may have more exergy losses as compared to a system with low COP. Thus comparison on the basis of COP values does not give a true measure of a real performance of any system.

While discussing the exergetic efficiency, it is important to get familiarized with the fuel, product and loss (F-P-L) definitions. The product *is the desired result produced by the system* while the fuel *is the utilization of all the resources to generate the products*

[41]. The term fuel should not be confused with the real fuels like methane, natural gas etc.

$$\dot{X}_p = \dot{X}_F - \dot{X}_D - \dot{X}_L \quad (5.9)$$

Where,

$\dot{X}_p$  = exergy rate of products

$\dot{X}_F$  = exergy rate of fuel

$\dot{X}_D$  = rate of exergy destruction

$\dot{X}_L$  = rate of exergy loss

Therefore the exergetic efficiency can be expressed as

$$\varepsilon = \frac{\dot{X}_P}{\dot{X}_F} \quad (5.10)$$

## 5.2 Mathematical formulation of HSAR Cycle

The exergy balance equations are developed for each component of HSAR cycle. The exergy losses are calculated for each system component. The components with high exergy losses need to be reduced to enhance the overall performance of the system. The same assumptions as discussed in chapter 3 are used in the exergy analysis of HSAR cycle except the evaporator temperature which is assumed to be fixed at -5 °C.  $T_o$ , which is the reference temperature, is assumed as the ambient temperature. A detailed exergy analysis for each component of HSAR cycle is discussed below.



### 5.2.1 Generator- Double Rectification Column-Dehlegmator assembly

The two columns (exhausting and rectifying columns) along with the generator and dephlegmator units are analyzed together and thus the exergy analysis for the double rectifying column and the dephlegmator unit are not performed separately.

The inlet and outlet exergy transfer rates and rate of exergy loss for the generator-double rectification column-dephlegmator assembly are respectively:

$$\dot{X}_{g,i} = \dot{m}_3 (x_3 h_3 - T_0 (x_3 s_3)) + \dot{m}_{14} (x_{14} h_{14} - T_0 (x_{14} s_{14})) \quad (5.11)$$

$$\dot{X}_{g,o} = \dot{m}_{13} (x_{13} h_{13} - T_0 (x_{13} s_{13})) + \dot{m}_4 (x_4 h_4 - T_0 (x_4 s_4)) \quad (5.12)$$

$$\dot{X}_{g,L} = \dot{X}_{g,i} - \dot{X}_{g,o} + \dot{Q}_g (1 - T_o / T_g) - \dot{Q}_d (1 - T_o / T_d) \quad (5.13)$$

### 5.2.2 Condenser

At an instant of time, the following equations were developed for condenser:

$$\dot{X}_{c,i} = \dot{m}_7 (x_7 h_7 - T_0 (x_7 s_7)) \quad (5.14)$$

$$\dot{X}_{c,o} = \dot{m}_8 (x_8 h_8 - T_0 (x_8 s_8)) \quad (5.15)$$

$$\dot{X}_{c,L} = \dot{X}_{c,i} - \dot{X}_{c,o} - \dot{Q}_c (1 - T_o / T_c) \quad (5.16)$$

### 5.2.3 Evaporator

The evaporator exergy inlet and outlet transfer and loss rates during daytime are respectively:

$$\dot{X}_{e,i,day} = [\dot{m}_{10} (x_{10} h_{10} - T_0 (x_{10} s_{10}))]_{day} \quad (5.17)$$

$$\dot{X}_{e,o,day} = [\dot{m}_{11} (x_{11} h_{11} - T_0 (x_{11} s_{11}))]_{day} \quad (5.18)$$

$$\dot{X}_{e.L,day} = \dot{X}_{e.i,day} - \dot{X}_{e.o,day} + \dot{Q}_{e,day} \left(1 - T_{o,day} / T_e\right) \quad (5.19)$$

The same equations (5.17), (5.18) and (5.19) but with different values of mass flow rates, enthalpies, entropies, reference/ambient temperature and thermal power are used to determine the exergy loss of the evaporator during the nighttime.

#### 5.2.4 Absorber

The inlet and outlet exergy transfer and loss rates for absorber during daytime are respectively:

$$\dot{X}_{a.i,day} = [\dot{m}_{12} (x_{12}h_{12} - T_0(x_{12}s_{12})) + \dot{m}_6 (x_6h_6 - T_0(x_6s_6))]_{day} \quad (5.20)$$

$$\dot{X}_{a.o,day} = [\dot{m}_1 (x_1h_1 - T_0(x_1s_1))]_{day} \quad (5.21)$$

$$\dot{X}_{a.L,day} = \dot{X}_{a.i,day} - \dot{X}_{a.o,day} - \dot{Q}_{a,day} \left(1 - T_{o,day} / T_{a,day}\right) \quad (5.22)$$

The same equations (5.20), (5.21) and (5.22) but with different values of mass flow rates, enthalpies, entropies, reference/ambient temperature and thermal power are used to determine the exergy loss of the absorber during the nighttime.

#### 5.2.5 Liquid-Liquid Heat Exchanger/Solution Heat Exchanger (LLHX/SHX)

The inlet and outlet exergy transfer and loss rates for LLHX are respectively:

$$\dot{X}_{SHX.i} = \dot{m}_2 (x_2h_2 - T_0(x_2s_2)) + \dot{m}_4 (x_4h_4 - T_0(x_4s_4)) \quad (5.23)$$

$$\dot{X}_{SHX.o} = \dot{m}_5 (x_5h_5 - T_0(x_5s_5)) + \dot{m}_3 (x_3h_3 - T_0(x_3s_3)) \quad (5.24)$$

$$\dot{X}_{SHX.L} = \dot{X}_{SHX.i} - \dot{X}_{SHX.o} \quad (5.25)$$

## 5.2.6 Vapor-Liquid Heat Exchanger/Refrigerant Heat Exchanger (VLHX/RHX)

The inlet and outlet exergy transfer and loss rates for VLHX/RHX are respectively:

$$\dot{X}_{RHX.i} = \dot{m}_8 (x_8 h_8 - T_0 (x_8 s_8)) + \dot{m}_{11} (x_{11} h_{11} - T_0 (x_{11} s_{11})) \quad (5.26)$$

$$\dot{X}_{RHX.o} = \dot{m}_9 (x_9 h_9 - T_0 (x_9 s_9)) + \dot{m}_{12} (x_{12} h_{12} - T_0 (x_{12} s_{12})) \quad (5.27)$$

$$\dot{X}_{RHX.L} = \dot{X}_{RHX.i} - \dot{X}_{RHX.o} \quad (5.28)$$

## 5.2.7 COP, ECOP, Circulation Ratio (f) and Exergy Loss Ratio

The results of HSAR cycle and the HSAR cycle were compared on the basis of the following parameters: COP, ECOP, circulation ratio ( $f$ ) and the exergy loss ratio ( $y_{L,k}$ ) [41] and written as:

$$COP = (\dot{Q}_{e,day} + \dot{Q}_{AST}) / \dot{Q}_g \quad (5.29)$$

$$ECOP = -[\dot{Q}_{e,day} (1 - T_o/T_e)] / [\dot{Q}_g (1 - T_o/T_g)] \quad (5.30)$$

$$f = \dot{m}_{1*} / \dot{m}_7 \quad (5.31)$$

$$y_L = \dot{X}_{L,k} / \dot{X}_{L,tot} \quad (5.32)$$

# CHAPTER 6

## EXERGO-ECONOMIC EVALUATION OF HYBRID STORAGE ABSORPTION REFRIGERATION (HSAR) SYSTEM

### 6.1 Economic Evaluation

The economic analysis of any thermal system is very important in its successful installation and operation. The economic analysis of HSAR cycle involves the cost estimation of its each component. The estimated cost break down obtained in this section will be used to perform the exergo-economic evaluation of HSAR cycle.

The total capital investment (TCI) for each component of HSAR cycle is estimated from the economic data presented by Roberto et al. [40] using the following relation:

$$C_y = C_w \left( \frac{A_y}{A_w} \right)^\alpha \quad (6.1)$$

Where

$C_y$  = unknown cost of y item

$C_w$  = known cost of w item

$A_y$  = Area of y item

$A_w$  = Area of w item

$\alpha$  = Scaling component

TCI for HSAR cycle only refers to the purchased equipment cost. The installation cost, piping cost, cost of instrumentation and controls, land cost, cost of service facilities and engineering and supervision costs are all neglected for the sake of simplicity. Flat plate solar collector field has the highest cost in HSAR cycle followed by the absorber and generator costs. Refrigerant heat exchanger (RHX) has the least cost among all the components considered in the economic analysis of HSAR cycle.

**Table 6-1 Cost estimation of HSAR cycle**

<b>Components</b>	<b>Cost (USD)</b>
Flat Plate Solar Collectors (FSC)	16260
Generator	5390.6
Evaporator	4613.8
Condenser	3245.4
Absorber	7659.6
Solution Heat Exchanger (SHX)	1890.6
Refrigerant Heat Exchanger (RHX)	318.3
Pump	505.7
<b>Total</b>	<b>39,884</b>

The flow path of HSAR cycle is shown in Figure 6-1. This cycle has been explained in detail in Chapter 3. As the costs of dephlegmator and rectifier could not be obtained, therefore these components are neglected in the exergo-economic analysis of HSAR cycle. The evaporator assembly is composed of an evaporator, condenser and an absorber heat exchanger as shown by the box in Figure 6-1. These components are confined into a single assembly to simplify the analysis and to meet the criterion of F-P-L definition which is discussed in the next section.

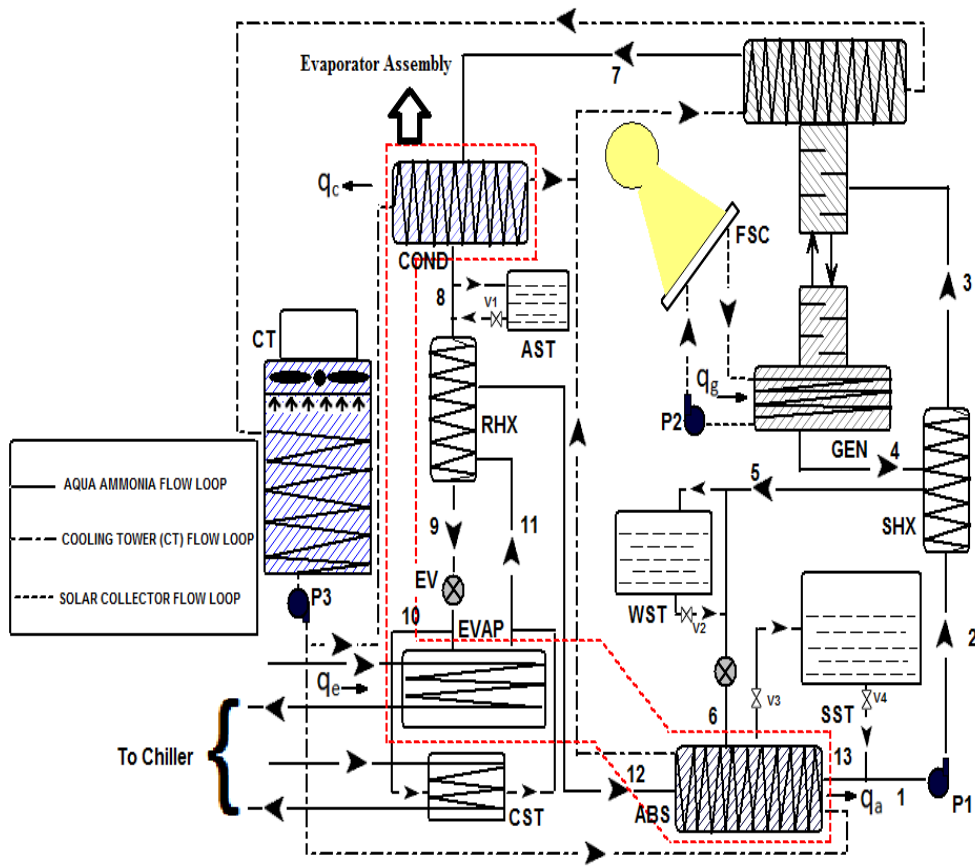


Figure 6-1 Flow path of refrigerant, weak solution and strong solution in HSAR cycle

## 6.2 Assumptions

The exergo-economic evaluation of HSAR cycle is based on the following assumptions:

1. The evaporator, condenser and the absorber are combined together in a single unit. i.e., evaporator assembly, as shown in Figure 6-1.
2. Concentrated solution ( $x_1=x_2=x_3$ ) is referred to as rich in ammonia and weak solution ( $x_4=x_5=x_6$ ) is referred to as weak in ammonia.
3. Almost pure refrigerant of  $x = 0.999$  ammonia concentration is assumed at the exit of the dephlegmator [21].
4. No energy loss is assumed between the solar collectors and the generator. i.e.,  
$$\dot{Q}_{\text{gen}} = \dot{Q}_{\text{SC}}$$
5. HSAR cycle is developed for 5 kW cooling capacity per day (120 kWh/day) at a constant cooling temperature of -5 °C.
6. For steady-state analysis, based on the 0.4% design conditions for Dhahran, the ambient summer temperature is assumed equal to the dry bulb temperature ( $T_{\text{amb}} = T_{\text{drybulb}} = 44.2$  °C) and the maximum coincident wet bulb temperature ( $T_{\text{wetbulb}}$ ) is 23.1 °C [56].
7. The condenser/absorber temperature is assumed 5 °C higher than the wet bulb temperature. i.e.,  $T_{\text{abs}} = T_{\text{cond}} = T_{\text{wetbulb}} + 5$  °C [1].
8. The reference temperature used in the exergy equations is assumed equal to the ambient temperature. i.e.,  $T_o = T_{\text{amb}}$ .
9. The net size of the storage tanks is increased if more cooling load is shared by the AST than by the CST overnight. On the other hand, the exergetic performance of



the system is dropped (due to high exergy losses) if more cooling load is shared by the CST than by the AST overnight. Therefore, the cooling load is assumed equally shared between the CST and AST overnight.

### **6.3 Exergy analysis of HSAR Cycle based on Fuel, Product and Loss (F-P-L) streams**

Fuel, product and loss streams for HSAR cycle are shown in Table 6-2. The exergy of heat ( $\dot{X}_{q,gen}$ ) is considered as a fuel in generator as it is used to produce the refrigerant from an aqua-ammonia mixture. There is no exergy loss in the generator; instead, it has exergy destruction. The exergy losses are only associated with the condenser and absorber in the HSAR cycle because these components reject heat directly to the environment. The exergy stream in evaporator, condenser and absorber is considered as the fuel in evaporator assembly. The cooling effect of the evaporator ( $\dot{X}_{q,evap}$ ) is selected as the required product of evaporator assembly while the exergy due to heat of condenser and the absorber is the exergy loss.

In refrigerant heat exchanger (RHX), the exergy stream of refrigerant vapors is the fuel while the exergy stream of the liquid refrigerant is defined as the required product. Similarly in SHX, the exergy stream of weak solution is the fuel whereas the exergy stream of strong solution is the product. The power input to the pump is considered as the fuel and the exergy stream of the strong solution is considered as the product. If an overall HSAR cycle is evaluated without considering the component by component detail, pump work and the generator exergy due to heat are designated as the fuel and the cooling effect of the evaporator is selected as the product. The overall exergy loss is the total exergy due to heat of condenser and absorber. In the rest of the components, the

irreversibilities are not perceived as exergy losses rather they are only considered as exergy of destruction.

**Table 6-2 Fuel-Product-Loss streams for HSAR cycle**

Components	Fuel	Product	Loss
Generator	$\dot{X}_{q,gen}$	$\dot{X}_7 + \dot{X}_4 - \dot{X}_3$	-
Evaporator Assembly	$\dot{X}_{12} + \dot{X}_6 - \dot{X}_{13} +$ $\dot{X}_7 - \dot{X}_8 + \dot{X}_{10} -$ $\dot{X}_{11}$	$\dot{X}_{q,evap}$	$\dot{X}_{q,con} + \dot{X}_{q,abs}$
RHX	$\dot{X}_{11} - \dot{X}_{12}$	$\dot{X}_9 - \dot{X}_8$	-
SHX	$\dot{X}_4 - \dot{X}_5$	$\dot{X}_3 - \dot{X}_2$	-
Pump	$\dot{W}_{pump}$	$\dot{X}_2 - \dot{X}_1$	-
Overall System	$\dot{X}_{q,gen} + \dot{W}_{pump}$	$\dot{X}_{q,evap}$	$\dot{X}_{q,con} + \dot{X}_{q,abs}$

After defining the F-P-L streams for HSAR cycle, the exergetic efficiency, exergy destruction ratios and exergy loss ratio for each component of the HSAR cycle are determined individually.

Exergy destruction ratio is defined as the ratio of the rate of exergy destruction ( $\dot{X}_D$ ) to the total exergy rate of fuel ( $\dot{X}_{F,tot}$ ) [41].

$$y_D = \frac{\dot{X}_D}{\dot{X}_{F,tot}} \quad (6.2)$$

Instead of total exergy rate of fuel, the rate of exergy destruction can also be compared to the total exergy destruction rate [41], i.e.,

$$y_D^* = \frac{\dot{X}_D}{\dot{X}_{D,tot}} \quad (6.3)$$

The exergy loss ratio is defined as the ratio of the exergy loss rate to the total exergy fuel rate.

$$y_L = \frac{\dot{X}_L}{\dot{X}_{F,tot}} \quad (6.4)$$

Since the generator has high entropy generation due to the heat transferred by solar collectors, it has the highest value of exergy destruction ratio among the components of HSAR cycle as shown in Table 7-6. The exergy destruction ratio in solution heat exchanger (SHX) and evaporator assembly is almost half to that of the generator. The exergy loss ratio is zero in all the components except for evaporator assembly because the evaporator assembly includes the absorber and condenser units which dissipate heat directly to the environment. Both pump and the RHX have very low percentage of exergy destruction ratio.

## 6.4 Exergy Costing

Exergy gives the qualitative measure of any thermal system. The exergy analysis measures the irreversibilities in a system and quantifies the actual amount of energy available to the system. In exergy costing, costs are associated with the exergy stream of each component of thermal system [41]. The following equations govern the exergy costing of the k component of the thermal system:

$$\sum_e \dot{C}_{e,k} + \dot{C}_{w,k} = \sum_i \dot{C}_{i,k} + \dot{Z}_k + \dot{C}_{q,k} \quad (6.5)$$

$$\dot{C}_i = c_i \dot{X}_i \quad (6.6)$$

$$\dot{C}_e = c_e \dot{X}_e \quad (6.7)$$

Where  $\dot{C}_{e,k}$  is the cost rate of exergy stream at exit,  $\dot{C}_{i,k}$  is the cost rate of exergy stream at inlet,  $\dot{C}_{w,k}$  and  $\dot{C}_{q,k}$  are the cost rates associated to the power and heat transfer respectively.  $c_i$  and  $c_e$  represent the average cost per unit of exergy and measured in dollars per gigajoule (\$/GJ). The cost rate is measured in dollars per unit time (\$/t) [41].  $\dot{Z}_k$  is the sum of the cost rates of capital investment and operation and maintenance (O&M) as shown in the following relation:

$$\dot{Z} = \dot{Z}_{CI} + \dot{Z}_{OM} \quad (6.8)$$

$\dot{Z}_{OM}$  is neglected in HSAR cycle as it does not involve any moving components except the pump. Hence the above equation is reduced to:

$$\dot{Z} = \dot{Z}_{CI} \quad (6.9)$$

The cost rates associated with the capital investment ( $\dot{Z}$ ) of each component of HSAR cycle is shown in the following table.

**Table 6-3 Cost rates of Capital Investment of HSAR cycle components [40]**

Components	$\dot{Z}$ (\$/yr)
Flat plat Solar Collectors (FSC)	649.6
Generator	214.12
Evaporator	184.48
Condenser	129.61
Absorber	306.21
Solution Heat Exchanger (SHX)	75.37
Refrigerant Heat Exchanger (RHX)	12.61
Pump	20.22

The exergy costing for each component of HSAR cycle is discussed below:

#### 6.4.1 Generator

The cost rate of exergy streams for generator assembly as shown in eq. (6.10) is governed by eq. (6.5).  $\dot{Z}_{gen}$  in eq. (6.10) is known and is obtained from Table 6-3. As no heat loss is assumed between the generator and solar collector, the heat required at generator is equal to the heat supplied by solar collector. Greater the heat required at

generator, greater will be the area of solar collectors. Therefore the cost rate associated with the exergy stream of heat of generator ( $\dot{C}_{gen}$ ) is equal to the cost rate of capital investment of solar collectors.

$$\dot{C}_7 + \dot{C}_4 - \dot{C}_3 = \dot{C}_{q,gen} + \dot{Z}_{gen} \quad (6.10)$$

$$c_7 \dot{X}_7 + c_4 \dot{X}_4 - c_3 \dot{X}_3 = c_{q,gen} \dot{X}_{q,gen} + \dot{Z}_{gen} \quad (6.11)$$

$$\dot{Z}_{FSC} = c_{q,gen} \dot{X}_{q,gen} \quad (6.12)$$

$\dot{X}_7, \dot{X}_4, \dot{X}_3, \dot{X}_{q,gen}$  are known values as obtained in Chapter 5.  $c_{q,gen}$  is obtained from eq. (6.12). Therefore  $c_7, c_4$  and  $c_3$  are the three unknowns and hence two auxiliary equations are required which are given as follows:

$$c_7 = c_8 \quad (6.13)$$

$$c_4 = c_5 \quad (6.14)$$

## 6.4.2 Condenser

The cost rate of exergy streams for condenser is shown by the following equations:

$$\dot{C}_8 = \dot{C}_7 + \dot{Z}_{con} - \dot{C}_{con,loss} \quad (6.15)$$

$$c_8 \dot{X}_8 = c_7 \dot{X}_7 + \dot{Z}_{con} - c_{F,EA} \dot{X}_{con,loss} \quad (6.16)$$

$\dot{Z}_{con}$  is obtained from Table 6-3 and  $\dot{E}_7$  and  $\dot{E}_8$  were calculated in Chapter 5.  $c_{F,EA}$  is the cost per exergy unit of fuel for evaporator assembly which will be discussed in the next section. We have one equation and two unknowns ( $c_8$  and  $c_7$ ). Hence an auxiliary equation is required which is given as:

$$c_7 = c_8 \quad (6.17)$$

### 6.4.3 Evaporator

The exergy costing of evaporator is governed by the relations as shown below.

$\dot{X}_{11}$ ,  $\dot{X}_{10}$ ,  $\dot{X}_{q,evap}$  and  $\dot{Z}_{evap}$  are known and  $c_{11}$ ,  $c_{10}$  and  $c_{q, evap}$  are unknowns.

$$\dot{C}_{11} = \dot{C}_{10} + \dot{C}_{q,evap} + \dot{Z}_{evap} \quad (6.18)$$

$$c_{11} \dot{X}_{11} = c_{10} \dot{X}_{10} + c_{q,evap} \dot{X}_{q,evap} + \dot{Z}_{evap} \quad (6.19)$$

Hence there are three unknowns and one equation. Hence two more auxiliary equations are required to solve exergy costing equations for evaporator which are shown below:

$$c_9 = c_{10} \quad (6.20)$$

$$c_{10} = c_{11} \quad (6.21)$$

### 6.4.4 Absorber

Absorber has two inlet exergy streams and one outlet exergy stream.  $c_{F,EA}$ ,  $\dot{Z}_{abs}$  and inlet and outlet exergy streams are known.

$$\dot{C}_{13} = \dot{C}_{12} + \dot{C}_6 + \dot{Z}_{abs} - \dot{C}_{abs,loss} \quad (6.22)$$

$$c_{13} \dot{X}_{13} = c_{12} \dot{X}_{12} + c_6 \dot{X}_6 + \dot{Z}_{abs} - c_{F,EA} \dot{X}_{abs,loss} \quad (6.23)$$

$c_{19}$ ,  $c_{12}$  and  $c_6$  are the three unknowns, so two more auxiliary equations are required which are shown below:

$$c_6 = c_5 \quad (6.24)$$

$$c_{12} = c_{11} \quad (6.25)$$

### 6.4.5 Refrigerant Heat Exchanger (RHX)

$\dot{C}_8$  and  $\dot{C}_{11}$  are cost rates of inlet exergy stream while  $\dot{C}_9$  and  $\dot{C}_{12}$  are the cost rates of outlet exergy stream.  $\dot{Z}_{RHX}$ ,  $c_{11}$ ,  $c_{12}$ ,  $c_8$  and all exergy streams ( $\dot{E}$ ) are known. There is one unknown ( $c_9$ ) and one equation. Therefore auxiliary equation is not required in the exergy costing of RHX.

$$\dot{C}_9 + \dot{C}_{12} = \dot{C}_8 + \dot{C}_{11} + \dot{Z}_{RHX} \quad (6.26)$$

$$c_9 \dot{X}_9 + c_{12} \dot{X}_{12} = c_8 \dot{X}_8 + c_{11} \dot{X}_{11} + \dot{Z}_{RHX} \quad (6.27)$$

### 6.4.6 Solution Heat Exchanger (SHX)

The cost rate of exergy streams for SHX is shown in the following equation:

$$\dot{C}_3 + \dot{C}_5 = \dot{C}_2 + \dot{C}_4 + \dot{Z}_{SHX} \quad (6.28)$$

$$c_3 \dot{X}_3 + c_5 \dot{X}_5 = c_2 \dot{X}_2 + c_4 \dot{X}_4 + \dot{Z}_{SHX} \quad (6.29)$$

$c_3$ ,  $c_4$ ,  $\dot{Z}_{SHX}$  and all the exergy streams are known while  $c_5$  and  $c_2$  are unknowns. There are two unknowns and one equation due to which one more auxiliary equation is required.

$$c_4 = c_5 \quad (6.30)$$

### 6.4.7 Pump

The equations of cost rate and cost per exergy unit for pump are given as:

$$\dot{C}_2 = \dot{C}_1 + \dot{Z}_{pump} \quad (6.31)$$

$$c_2 \dot{X}_2 = c_1 \dot{X}_1 + \dot{Z}_{pump} \quad (6.32)$$

$c_1$  and  $c_2$  are the two unknowns. Hence an additional auxiliary equation is given as follows:

$$c_1 = c_{13} \quad (6.33)$$



The exergo-economic data obtained by solving the exergy costing relations for each component of HSAR cycle is presented in Table 6-4. The table summarizes the cost rates, cost per exergy unit and cost per unit mass along with other variables for the flow path of HSAR cycle.

**Table 6-4 Exergo-economic data for HSAR cycle**

Flow order	Temperature (°C)	Pressure (bar)	NH <sub>3</sub> conc. (%)	Mass flow rates $\dot{m}$ (g/s)	Exergy $\dot{X}$ (kW)	Cost rate $\dot{C}$ (\$/day)	Cost/exergy $c$ (\$/GJ)	Cost/mass $c^*$ (€/kg)
1	25.92	3.52	52.2	27.67	55.07	127.5	26.8	5.33
2	25.92	10.9	52.2	27.67	55.1	127.6	26.79	5.33
3	65.4	10.9	52.2	27.67	55.17	129.6	27.2	5.42
4	120	10.9	24.59	17.45	36.04	123.2	39.56	8.17
5	44.73	10.9	24.59	17.45	35.37	120.9	39.56	8.01
6	44.73	3.52	24.59	17.45	27.29	93.28	39.56	6.18
7	56.06	10.9	99.9	10.22	21.75	4.09	2.178	0.46
8	28	10.9	99.9	10.22	15.68	2.95	2.178	0.33
9	19.53	10.9	99.9	7.23	15.69	2.92	2.155	0.46
10	-4.87	3.52	99.9	7.23	15.65	2.91	2.155	0.46
11	-5	3.52	99.9	7.23	14.3	2.66	2.155	0.42
12	11.5	3.52	99.9	7.23	14.26	2.65	2.155	0.42
1'	28	3.52	50.8	20.7	41.18	95.37	26.8	5.33

## 6.5 Non-Exergy costs of storage tanks

One ammonia storage tank, two aqua-ammonia storage tanks and one cold storage tank in HSAR cycle do not contribute in the exergy costing. But these storage tanks have high costs due to which they cannot be neglected and hence considered as non-exergy costs. Both ammonia and aqua-ammonia storage tanks have very high costs in the market

due to thick walls made of stainless steel. The non-exergy costs associated with these storage tanks is added to the exergy rate of the stream as shown by the following relation [41]:

$$\dot{C}_{k,tot} = \dot{C}_k + \dot{C}_k^{NE} \quad (6.34)$$

The non-exergy cost of ammonia storage tank is added to exergy stream 8, weak solution tank is added to exergy stream 5 and the strong solution tank is added to exergy stream 13 as shown by the following equations:

$$\dot{C}_{8,tot} = \dot{C}_8 + \dot{Z}_{AST}^{NE} \quad (6.35)$$

$$\dot{C}_{5,tot} = \dot{C}_5 + \dot{Z}_{WST}^{NE} \quad (6.36)$$

$$\dot{C}_{13,tot} = \dot{C}_{13} + \dot{Z}_{SST}^{NE} \quad (6.37)$$

Where  $\dot{Z}_{AST}$ ,  $\dot{Z}_{WST}$  and  $\dot{Z}_{SST}$  is the capital investment of ammonia storage tank (AST), weak solution tank (WST) and strong solution tank (SST).

## 6.6 Exergo-economic evaluation of HSAR cycle

The general relation based on fuel-product-loss definition for exergo-economic analysis is shown as follows:

$$\dot{C}_{P,k} = \dot{C}_{F,k} - \dot{C}_{L,k} + \dot{Z}_k \quad (6.38)$$

The cost rate of exergy destruction ( $\dot{C}_{D,k}$ ) does not appear explicitly in equation (6.38) used for exergy costing. These costs are referred to as *hidden costs* but are exceptionally important in the exergo-economic evaluation of HSAR cycle [41]. The cost

rates of fuel and product for each component of HSAR cycle are obtained in exactly the same manner as the exergy of fuel and product were obtained using the flow streams as shown in Table 6-2.

The mathematical formulation of exergo-economic evaluation for each component of HSAR cycle is discussed below:

### 6.6.1 Generator

The cost rates of exergy stream of the fuel and product and cost rate of capital expenditure for generator are governed by the following relation:

$$\dot{C}_{P,gen} = \dot{C}_{F,gen} + \dot{Z}_{gen} \quad (6.39)$$

The cost per exergy unit of the fuel and product for generator is calculated as:

$$c_{F,gen} = \frac{\dot{C}_{F,gen}}{\dot{X}_{F,gen}} \quad (6.40)$$

$$c_{P,gen} = \frac{\dot{C}_{P,gen}}{\dot{X}_{P,gen}} \quad (6.41)$$

Exergy destruction in generator is mainly due to the entropy generation. Cost rate of exergy destruction for generator is given as:

$$\dot{C}_{D,gen} = c_{F,gen} \dot{X}_{D,gen} \quad (6.42)$$

### 6.6.2 Evaporator Assembly

The cost rates and cost per exergy unit of the fuel and product for evaporator assembly are defined as:

$$\dot{C}_{P,ea} = \dot{C}_{F,ea} - \dot{C}_{L,ea} + \dot{Z}_{ea} \quad (6.43)$$

$$c_{F,ea} = \frac{\dot{C}_{F,ea}}{\dot{X}_{F,ea}} \quad (6.44)$$

$$c_{P,ea} = \frac{\dot{C}_{P,ea}}{\dot{X}_{P,ea}} \quad (6.45)$$

In the evaporator assembly, exergy losses occur in condenser and the absorber due to the heat dissipation to the environment. The cost rates of exergy losses and exergy destruction for evaporator assembly are as follows:

$$\dot{C}_{L,ea} = c_{F,ea} \dot{X}_{L,ea} \quad (6.46)$$

$$\dot{C}_{D,ea} = c_{F,ea} \dot{X}_{D,ea} \quad (6.47)$$

The cost rate of capital investment in evaporator assembly is the sum of cost rates for evaporator, condenser and absorber.

$$\dot{Z}_{ea} = \dot{Z}_{evap} + \dot{Z}_{con} + \dot{Z}_{abs} \quad (6.48)$$

### 6.6.3 Refrigerant Heat Exchanger (RHX)

The cost rates, cost per unit exergy and cost rate of exergy destruction for RHX are governed by the following equations:

$$\dot{C}_{P,RHX} = \dot{C}_{F,RHX} + \dot{Z}_{RHX} \quad (6.49)$$

$$c_{F,RHX} = \frac{\dot{C}_{F,RHX}}{\dot{X}_{F,RHX}} \quad (6.50)$$

$$c_{P,RHX} = \frac{\dot{C}_{P,RHX}}{\dot{X}_{P,RHX}} \quad (6.51)$$

$$\dot{C}_{D,RHX} = c_{F,RHX} \dot{X}_{D,RHX} \quad (6.52)$$

#### 6.6.4 Solution Heat Exchanger (SHX)

The cost rates, cost per unit exergy and cost rate of exergy destruction for SHX are governed by the following equations:

$$\dot{C}_{P,SHX} = \dot{C}_{F,SHX} + \dot{Z}_{SHX} \quad (6.53)$$

$$c_{F,SHX} = \frac{\dot{C}_{F,SHX}}{\dot{X}_{F,SHX}} \quad (6.54)$$

$$c_{P,SHX} = \frac{\dot{C}_{P,SHX}}{\dot{X}_{P,SHX}} \quad (6.55)$$

$$\dot{C}_{D,SHX} = c_{F,SHX} \dot{X}_{D,SHX} \quad (6.56)$$

#### 6.6.5 Pump

The cost rates, cost per unit exergy and cost rate of exergy destruction for pump is governed by the following equations:

$$\dot{C}_{P,pump} = \dot{C}_{F,pump} + \dot{Z}_{pump} \quad (6.57)$$

$$c_{F,pump} = \frac{\dot{C}_{F,pump}}{\dot{X}_{F,pump}} \quad (6.58)$$

$$c_{P,pump} = \frac{\dot{C}_{P,pump}}{\dot{X}_{P,pump}} \quad (6.59)$$

$$\dot{C}_{D,pump} = c_{F,pump} \dot{X}_{D,pump} \quad (6.60)$$

## 6.7 Exergo-economic variables

The following variables, also referred to thermo-economic variables, are extremely important in the exergo-economic analysis of HSAR cycle:

- a) The average unit cost of fuel  $c_{F,k}$
- b) The average unit cost of product  $c_{P,k}$
- c) The cost rate of exergy destruction  $\dot{C}_{D,k}$
- d) The relative cost difference  $r_k$
- e) The exergoeconomic factor  $f_k$

The relative cost difference ( $r_k$ ) shows the relative increase in the average cost per exergy unit between the fuel and the product [41]. Mathematically, it is shown as:

$$r_k = \frac{c_{P,k} - c_{F,k}}{c_{F,k}} \quad (6.61)$$

The relative cost difference should be minimized to optimize the HSAR cycle. This can be achieved by either decreasing the average cost of the product or by decreasing the difference between the average cost of the product and the average cost of the fuel.

Another important variable is the exergoeconomic factor ( $f_k$ ) which is given as:

$$f_k = \frac{\dot{Z}_k}{\dot{Z}_k + \dot{C}_{L,k} + \dot{C}_{D,k}} \quad (6.62)$$

Exergoeconomic factor shows the impact of costs related to capital investment  $\dot{Z}_k$  to the cost rate of exergy destruction and exergy losses. A high value of exergoeconomic

factor for any component suggests that the cost of capital investment should be reduced even at the expense of exergetic efficiency and a low value of exergoeconomic factor reveals that the exergetic efficiency of the component should be increased even at the expense of the cost of the capital investment.



## CHAPTER 7

### RESULTS AND DISCUSSION

#### 7.1 Steady State Thermodynamic Analysis

The paper presents the results of energy and exergy analysis of hybrid storage absorption refrigeration (HSAR) cycle with that of a refrigerant storage absorption refrigeration (RSAR) cycle and a cold storage absorption refrigeration (CSAR) cycle. All the three storage systems provide refrigeration 24-hours a day. In HSAR cycle, the nighttime refrigeration load (5kW) is equally shared (assumption 4) between the CST and the AST (2.5 kW each). The total size of the required storage tanks is therefore reduced to 62 % the total size of storage tanks required in refrigerant-storage absorption refrigeration (RSAR) cycle, as shown in Table 7-1.

**Table 7-1– Comparison of size of storage tanks for different storage designs**

Storage Tank	Pressure (bar)	Temperature (°C)	NH <sub>3</sub> mass concentration, x	$\rho$ (kg/m <sup>3</sup> )	Size for	Size for	Size for
					5 kW cooling power in HSAR Cycle (m <sup>3</sup> )	5 kW cooling power in RSAR Cycle (m <sup>3</sup> )	5 kW cooling power in CSAR Cycle (m <sup>3</sup> )
<b>CST</b>	1.01	-5	-	917.4	0.35	-	0.70
<b>AST</b>	17.69	43.86	0.996	573.2	0.17	0.34	-
<b>WST</b>	17.69	60	0.342	789.9	0.63	1.26	-
<b>SST</b>	3.53	45	0.404	846.7	0.70	1.40	-
<b>Total</b>					1.85	3.00	0.70

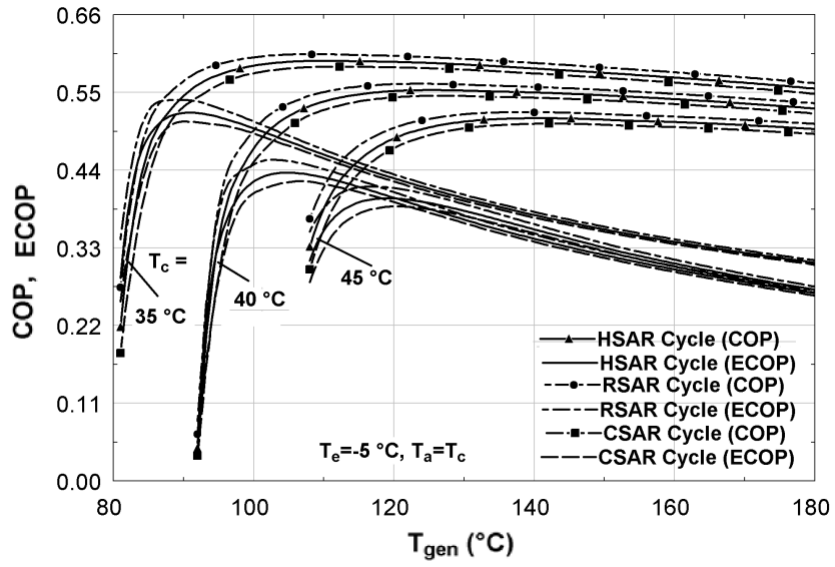
Thermal powers and the corresponding thermal energies for different components of HSAR cycle, RSAR cycle and CSAR cycle for the average summer ambient conditions of Dhahran are shown in Table 7-2. The generator has the maximum thermal energy among all the components for three storage cycles. Since the absorber does not operate during the night in CSAR cycle, the absorber energy is maximum during the day in CSAR cycle as compared to the respective energies of absorber for HSAR cycle and the RSAR cycle. More ammonia is absorbed in the absorber during the daytime in HSAR cycle than the amount of ammonia absorbed in RSAR cycle (as the ammonia is used both for refrigeration in evaporator and ice production in CST in HSAR cycle during the day whereas ammonia is only used for refrigeration during the day in RSAR cycle), therefore the absorber energy is more in HSAR cycle during the daytime than the absorber energy in RSAR cycle.

Since the parameters used to determine the condenser energy (ammonia concentration;  $x$ , condenser temperature;  $T_{cond}$  and the quality of ammonia at the condenser exit (saturated liquid)) are same for all the three cycles, the condenser energy remains the same for all the three storage cycles. The three storage systems are compared for fixed cooling capacity, i.e., 5kW, with the daily cooling energy of  $5kW \times 24h = 120$  kWh and the cooling load during the daytime equal to  $120kWh/12h = 10$  kW. In HSAR cycle, out of 10 kW of cooling load during the daytime, 5 kW is used in refrigeration, 2.5 kW is used to produce ice and 2.5 kW is the cooling load to be shared by ammonia in AST during the nighttime. In CSAR cycle, 5 kW is used in refrigeration during the daytime and 5 kW is used to produce ice for nighttime refrigeration. In RSAR cycle, 5 kW is used in refrigeration during the daytime and 5kW is the cooling load to be

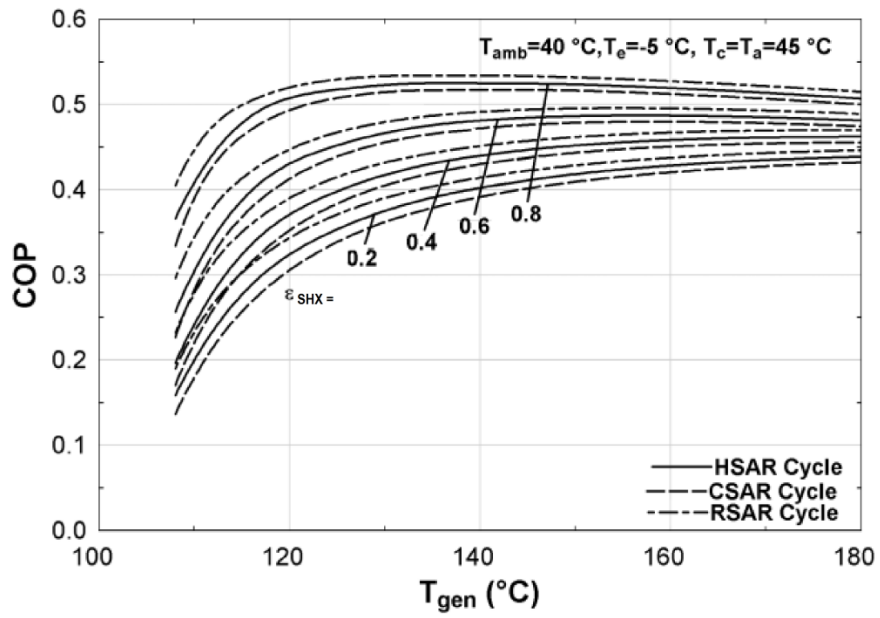
delivered by ammonia stored in AST during the nighttime. Over the 24 hours of the day, the net value of energy gained by the system (summation of positive values in kWh) should be equal to the net value of energy lost by the system (summation of negative values in kWh).

**Table 7-2 –Comparison of thermodynamic energy analysis of HSAR Cycle, RSAR Cycle and CSAR Cycle**

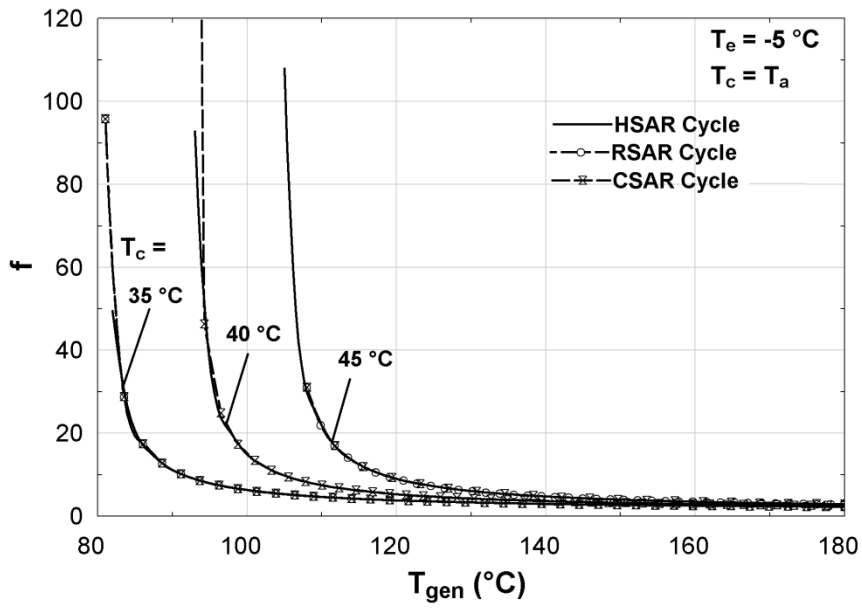
Components	Daytime Working hours	Daytime Power (kW)/Energy (kWh)			Nighttime Working hours	Nighttime Power (kW)/Energy (kWh)		
		HSAR	RSAR	CSAR		HSAR	RSAR	CSAR
<b>Generator</b>	12	+20.51/+246.12	+19.89/+238 .68	+21.11/+253.3 2	-	-	-	-
<b>Absorber</b>	12	-14.24/-170.88	-9.302/- 111.62	-19.31/-231.72	12	-4.51/-54.12	-8.905/- 106.86	-
<b>Condenser</b>	12	-10.2/-122.4	-10.2/-122.4	-10.2/-122.4	-	-	-	-
<b>Evaporator</b>	12	+7.5/+90.00	+5/+60	+10/+120	12	+2.50/+30.00	+5/+60	-
<b>Dephlegmator</b>	12	-1.606/-19.27	-1.513/- 18.156	-1.682/-20.184	-	-	-	-
<b>Pump</b>	12	+0.1218/+1.46	+0.1153/+1. 3836	+0.123/+1.476	-	-	-	-
<b>Total Energy (kWh)</b>		+25.03	+47.88	+0.492		-24.12	-46.86	-



(a)



(b)



(c)

**Figure 7-1 (a) COP and ECOP versus  $T_{gen}$  at different condenser temperatures (b) COP versus generator temperature for different values of SHX effectiveness ( $\epsilon_{SHX}$ ) (c) Circulation ratio ( $f$ ) versus generator temperature ( $T_{gen}$ ) at different condenser temperatures**

## 7.2 Unsteady Thermodynamic Analysis

The unsteady results are plotted for the selected five consecutive days of summer (June 15-19, 2011) and winter (December 21-25, 2011) for Dhahran region. The time along x-axis is shown in a 24-hour format in all the unsteady plots. The variation of the instantaneous  $COP_{day}$  and the condenser pressure ( $P_{cond} = P_{high}$ ) with the instantaneous ambient temperature and solar intensity for summer (June 15 –June 19) is shown in Figure 7-2. The ambient temperature during the daytime shows a progressive increase from June 15 to June 19. The instantaneous  $COP_{day}$  decreases with the increase in solar intensity and ambient temperature in the morning and reaches its minimum value near to the time of noon. Then it starts to increase with the decrease in solar intensity and ambient temperature till the end of effective sunlight hours. Such a behavior of the instantaneous  $COP_{day}$  is anticipated since the cooling load is constant while the instantaneous (hourly)  $Q_g$  is increasing and then decreasing with time. The instantaneous  $COP_{day}$  value at the end of the day is lower than the instantaneous  $COP_{day}$  value at the start of the day due to lower energy of generator ( $Q_g$ ) in the morning than in the afternoon. The  $COP_{day}$  has a peak value ( $=0.44$ ) on 15<sup>th</sup> June, which received the maximum peak solar radiation ( $1015 \text{ W/m}^2$ ) and has the minimum peak ambient temperature among the representative days of summer 2011.

Figure 7-2 shows also the variation with time of the weak solution concentration (at exit of generator,  $x_4 = x_5 = x_{16} = x_{17} = x_6 = x_{ws}$ ) for representative days of summer (2011). As the generator temperature increases with the increase in solar intensity and ambient temperature, more ammonia evaporates from the aqua-ammonia solution in the

generator and hence the concentration decreases inside and at exit of the generator ( $x_{ws}$ ) as shown in Figure 7-2.

Though the trend of the instantaneous  $COP_{day}$  for the representative days of winter is similar as that of summer, the instantaneous  $COP_{day}$  in winter is higher than that in summer as given in Figure 7-3. The given overall cooling output of the system ( $Q_{ref,d} + Q_{CST} + Q_{AST}$ ) during the effective sunlight hours in winter is assumed to be the same as in summer as shown in Table 4-1. Since  $COP_{day} = (Q_{ref,d} + Q_{CST} + Q_{AST})/Q_g$ , the higher  $COP_{day}$  in winter is due to the lower energy of generator ( $Q_g$ ) while the overall output in the numerator remains constant. Moreover, in winter, the condenser pressure is lower than in summer due to the lower ambient temperature. The low (evaporator) pressure of the cycle remains fixed throughout the year as this low pressure depends on the fixed evaporator conditions at its exit (i.e.,  $T_{evap} = T_{11} = T_{11'} = T_{11''} = -5\text{ }^\circ\text{C}$ , ammonia mass concentration = 0.996 and saturated ammonia vapor at the exit of evaporator). So the enthalpy difference between state 4 ( $h_4$ ), which lies on the high (condenser) pressure line, and the pole of the generator ( $h_{pg}$ ), which lies below the low pressure line, becomes less in winter than in summer. As this difference equals the ratio of the required generator energy ( $Q_g$ ) to the mass of weak solution at generator exit ( $m_4$ ) as shown by equation (7),  $Q_g/m_4$  becomes also less in winter than in summer, which leads to the higher values of  $COP_{day}$  in winter than in summer.

The condenser pressure ( $P_{cond} = P_{high}$ ) is the highest pressure in HSAR cycle and it varies with ambient temperature. The instantaneous value of condenser pressure is lowest at the beginning of the day but as time elapses the ambient temperature rises and causes the condenser pressure to raise as well. The peak condenser pressure occurs at the



peak ambient temperature for each day. The difference between summer and winter peak condenser pressure is about 6 bars. Among the five consecutive days of summer, June 17, 18 and 19 show the highest peak values of condenser pressure. In winter, Dec 25 shows the highest peak value of condenser pressure.

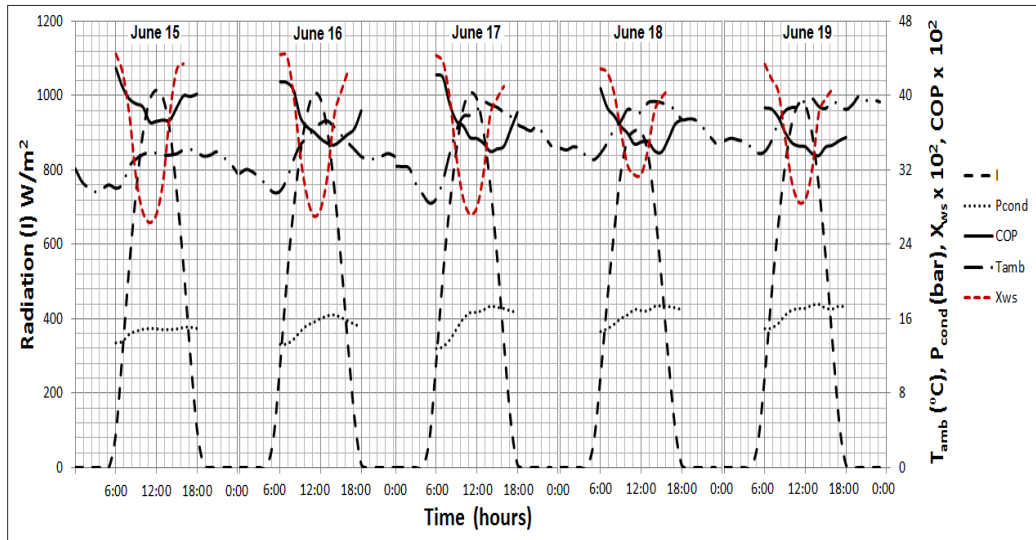


**Figure 7-2** Plots of instantaneous solar radiation, ambient temperature, condenser pressure, weak solution concentration at exit of generator ( $x_{ws} = x_4$ ) and  $COP_{day}$  versus time for summer

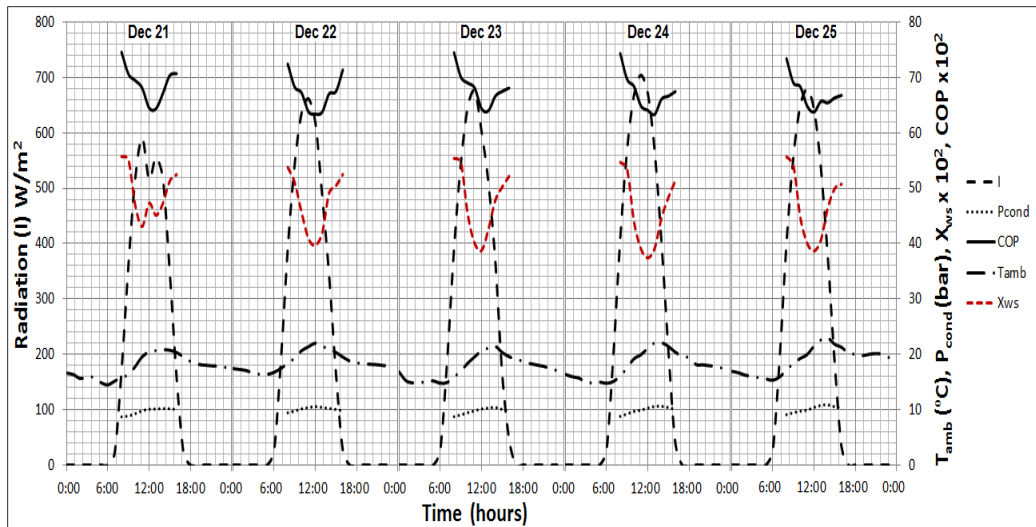


**Figure 7-3** Plots of instantaneous solar radiation ( $I$ ), ambient temperature ( $T_{amb}$ ), condenser pressure ( $P_{cond}$ ), weak solution concentration at generator exit ( $x_{ws}$ ) and  $COP_{day}$  versus time for winter

As shown in Table 7-3, the average daily  $COP_{day}$  for representative days of summer is about 55% of the average daily  $COP_{day}$  in winter. The maximum average daily COP was achieved in summer on June 15 and in winter on Dec 21/Dec 23. The difference between the maximum and minimum average daily COP for representative days is 0.03 for summer and 0.01 for winter. The average daily  $COP_{night}$  for representative summer nights is about 85% of the average daily  $COP_{night}$  for representative winter nights. For the representative winter days, the average daily COP during the night ( $COP_{avg, night}$ ) is nearly 50% of the average daily COP during daytime, i.e. during effective sunlight hours ( $COP_{avg, day}$ ). On the other hand, for representative summer days, the average daily COP during the night ( $COP_{avg, night}$ ) is nearly 78% of the average daily COP during effective sunlight hours ( $COP_{avg, day}$ ).

**Table 7-3- Average daily and night COP of HSAR Cycle for representative days of summer and winter**

Day	$COP_{avg, day}$		$COP_{avg, night}$	
	Summer	Winter	Summer	Winter
<b>Jun 15/ Dec 21</b>	0.39	0.68	0.304	0.347
<b>Jun 16/Dec 22</b>	0.37	0.67	0.285	0.337
<b>Jun 17/ Dec 23</b>	0.37	0.68	0.288	0.341
<b>Jun18/ Dec 24</b>	0.36	0.67	0.287	0.336
<b>Jun 19/ Dec 25</b>	0.36	0.67	0.279	0.337
<b>Overall Average</b>	0.370	0.674	0.2886	0.3396

For the given continuous 5 kW cooling load, the hourly energy plots (in MJ) for the four major components of HSAR cycle (generator, condenser, absorber and evaporator) during the representative days of summer and winter are shown in Figure 7-4

and Figure 7-5, respectively. The required hourly thermal solar energy input to the generator ( $Q_g$ ) for both summer and winter show an opposite trend to that of the COP and that the generator has the highest energy values among all components. The generator hourly solar thermal energy input varies during effective sun hours in compliance with the variation in solar intensity and ambient temperature. The increase in the generator energy with the time (between the start of effective sunlight hours till the noon) manifests itself on the h-x diagram of Figure 3-2 as an increase in the enthalpy difference ( $h_4 - h_{pg}$ ) due to the increase in condenser pressure with the progressive rise in ambient temperature. The daily average generator energy in summer is 94 MJ compared to the 79 MJ in winter. The energy of the condenser does not show any prominent change because it depends on the ambient temperature which shows a variation of only 5-6 °C throughout the day.

The absorber and evaporator operate 24 hours a day and their energy plots show a similar trend for all the consecutive days of summer and winter. The heat energy of the absorber drops by about 35/50 MJ in winter/summer during the night as compared to the day. For representative days of summer, the evaporator cooling energy is 27 MJ ( $Q_{e,day} = Q_{ref,d} + Q_{CST} = 7.5$  kWh) during the effective sunlight hours of day and 9 MJ ( $Q_{e,night} = 2.5$  kWh) during the nighttime cooling hours. For representative days of winter, the evaporator cooling energy is 36 MJ ( $Q_{e,day} = Q_{ref,d} + Q_{CST} = 10$  kWh) during the effective sunlight hours of day and 9 MJ ( $Q_{e,night} = 2.5$  kWh) during the nighttime cooling hours. Since the effective sunlight hours are reduced to 8 hours in winter as compared to the 12 hours in summer, the evaporator cooling energy is increased from 27 MJ in summer to 36 MJ in winter during the effective sunlight hours of the day.

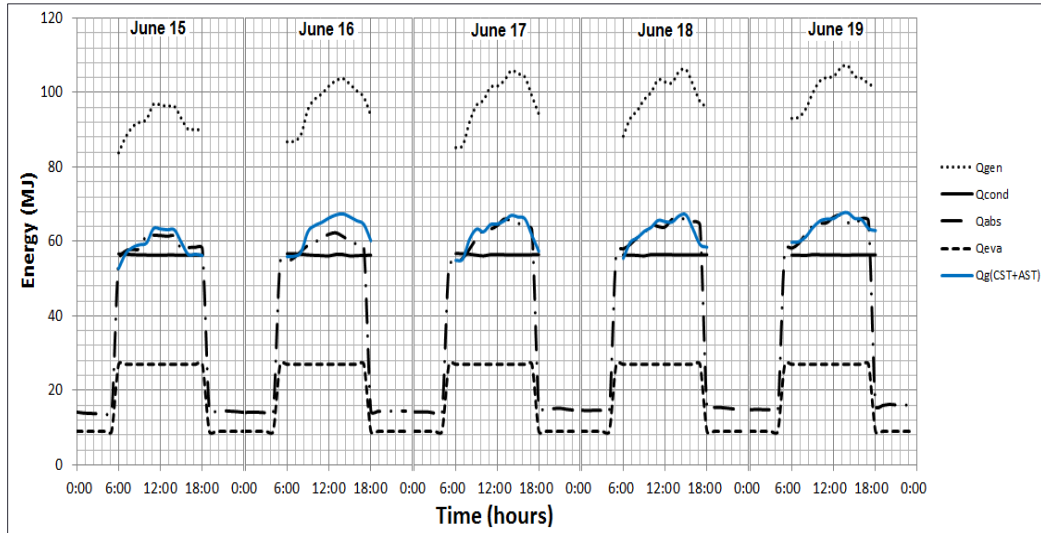


**Figure 7-4 Plot of hourly energy versus time for HSAR components for representative days of summer**

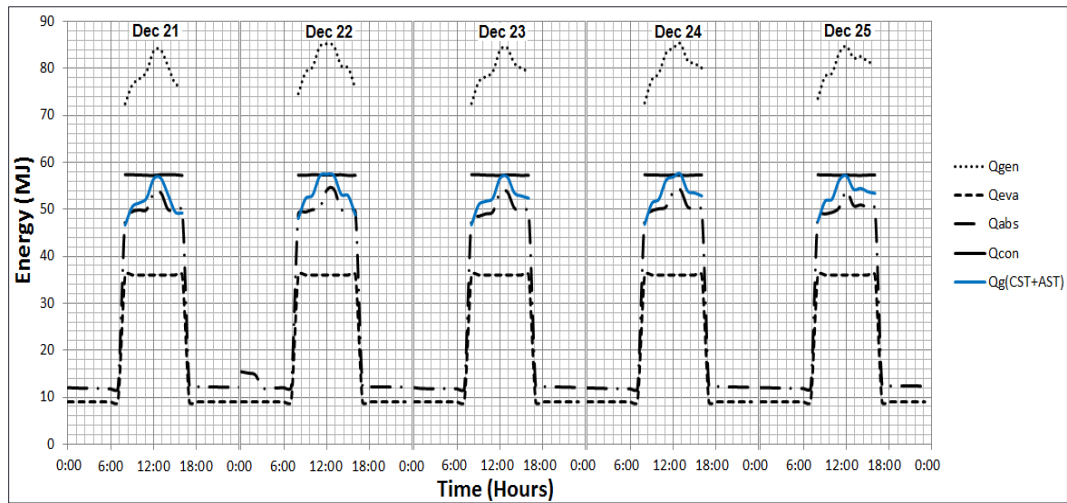


**Figure 7-5 Plot of hourly energy versus time for HSAR components for representative days of winter**

The required solar collector field area for the given continuous cooling power (5 kW) is determined using the method proposed by Duffie and Beckman [45]. With the actual hours of the day (from sunrise to sunset) and the instantaneous solar intensity ( $I$ ) for both summer and winter, the monthly average hourly solar radiation ( $I_T$ ) for Dhahran region was obtained [25]. With the assumed collector efficiency of  $\eta = 42\%$  (assumption 5) and the obtained monthly average hourly solar energy ( $I_T$ ), the monthly average hourly solar energy gain per unit area of the collector was obtained ( $q_c = \eta \times I_T$ ) for both summer and winter. Assuming no energy loss between the generator and the collector and using the computed monthly average required generator hourly solar energy gain ( $Q_g$ ) for summer and winter the required solar collector field area ( $A_c = Q_g/q_c$ ) is obtained for summer and winter.

Table 7-4 shows the required area of the flat plate solar collector field per kW of cooling power for different refrigeration cycles for summer and winter in Dhahran. CSAR cycle is the same as HSAR cycle with the only difference of absence of ammonia and aqua-ammonia storage tanks in CSAR cycle. Similarly, RSAR cycle is the same as HSAR cycle with the only difference of absence of a ice (cold) storage tank in RSAR cycle. The area of solar collector field per kW of cooling power is maximum for CSAR cycle and minimum for RSAR cycle. This is because CSAR cycle requires the highest heat input to the generator to suffice the cooling load during the day and to produce the ice for nighttime refrigeration. On the other hand, RSAR cycle requires the lowest value of heat input to the generator to accommodate the cooling load during the day and to produce surplus ammonia for nighttime refrigeration. Thus the required solar collector

field area for HSAR cycle is less than that of a CSAR cycle but more than that required for RSAR cycle.

**Table 7-4 Required solar collector field area per kW of cooling power for different cycles**

Refrigeration Cycle	$A_c$ for Summer ( $m^2/kW$ )	$A_c$ for Winter ( $m^2/kW$ )	$T_{\text{evaporator}}$ ( $^{\circ}C$ )	Solar Collector Type
<b>HSAR</b>	$A_c = 13.84$	$A_c = 15.26$	-5	Selective coated flat plate  $\eta = 0.42$
	$A_{c1} = 5.19$	$A_{c1} = 5.04$		
	$A_{c2} = 8.65$	$A_{c2} = 10.22$		
<b>CSAR</b>	15.01	15.8	-5	Same as HSAR
<b>RSAR</b>	12.75	14.8	-5	Same as HSAR

The ambient temperature, solar intensity and hence both the available monthly average hourly solar energy ( $I_T$ ) and the energy gain per unit area ( $q_c = \eta \times I_T$ ) are less in winter than in summer. Hence the required solar collector field area ( $A_c = Q_g/q_c$ ) per kilowatt of cooling power is found to be more in winter than in summer as shown in Table 3. The part of the solar collector field area in HSAR cycle ( $A_{c1}$ ) that is used for daytime refrigeration (during the effective sunlight hours) only (without storage) is only 37.5% of the total collector field area ( $A_c$ ) in summer and 33.02% in winter. This shows that more than 60% of the total solar collector field area is used for the storage purposes (for nighttime refrigeration) in both summer and winter.

For the given constant 5 kW cooling power during day and night, the conditions and the density of the substances stored and the size of the storage tanks used in HSAR

cycle are presented in Table 7-5. Ammonia storage tank (AST) is the smallest in size (volume) among all the storage tanks because it stores liquid ammonia under high pressure and hence stores the least masses (97.2kg/120.3kg in summer/winter) compared to the storage masses of ice (323.7 kg/433.6 kg in summer/winter), weak solution (502kg/236.6kg in summer/winter) and strong solution (599.2kg/356.9kg in summer/winter). The higher mass of ice in CST compared to that of ammonia liquid in AST makes the CST volume almost double in size that of the AST. The mass of ice required to share the nighttime cooling load is almost three times the mass of ammonia stored in AST. The ambient temperature is higher in summer and the concentration of the strong solution formed in the absorber is less as compared to the winter. Therefore, the mass and volume of WST required for night absorption in the absorber is also more in summer than in winter. The SST is the largest in size among all the storage tanks.

**Table 7-5 Size of storage tanks used in HSAR cycle**

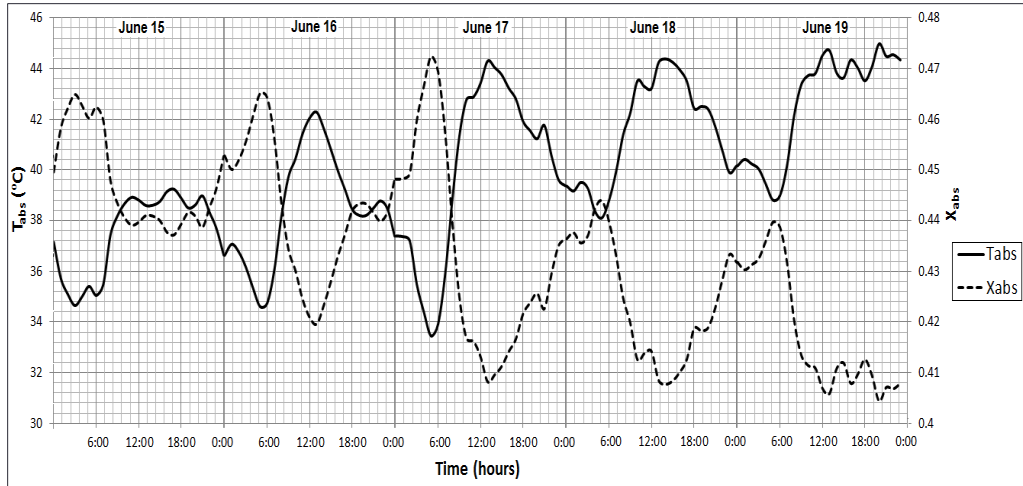
Storage Tank	Pressure (bar)	Temperature (°C)	NH <sub>3</sub> mass concentration, x	ρ (kg/m <sup>3</sup> )	Size for 5 kW cooling power (m <sup>3</sup> )
	Summer/ Winter	Summer/ Winter	Summer/ Winter	Summer/ Winter	Summer/Winter
<b>CST</b>	1.01/1.01	-5/-5	-	917.4/917.4	0.35/0.47
<b>AST</b>	17.69/9.34	43.86/21.7 3	0.996/0.996	573.2/607.5	0.17/0.19
<b>WST</b>	17.69/9.34	60/38	0.342/0.458	789.9/825.8	0.63/0.28
<b>SST</b>	3.53/3.53	45/23	0.404/0.543	846.7/811.6	0.70/0.47



Figure 7-6 shows the instantaneous absorber temperature and aqua-ammonia strong solution concentration at exit of the absorber (i.e., at inlet to generator,  $x_{\text{abs}} = x_3 = x_1 = x_{1*} = x_2 = x_{\text{ss}}$ ) for representative days of summer. These plots are for both day and night as the absorber in HSAR cycle works 24 hours a day. The aqua-ammonia concentration ( $x_{\text{abs}} = x_{\text{ss}}$ ) at the exit of the absorber depends on the ambient temperature. Lower ambient temperature implies more absorption inside the absorber and hence higher concentration for the strong solution formed. Therefore, concentration of aqua-ammonia solution at exit of absorber is generally higher during night than during daytime as shown in Figure 7-6. The weak solution concentration ( $x_{\text{ws}}$ , presented in Figure 7-2) shows more tangible variation during the daytime than the strong solution concentration ( $x_{\text{ss}}$ ) because the latter depends essentially on the variation of ambient temperature with time which is less tangible than the variation of generator temperature with time that affects  $x_{\text{ws}}$ .

For summer representative days, Figure 7-7 shows the variation during daytime of the generator temperature (weak solution temperature at generator exit,  $T_{\text{gen}} = T_4$ ), mass of produced ammonia vapor ( $m_7$ ) at exit of the dephlegmator and mass of weak aqua-ammonia solution at exit of generator ( $m_4$ ). The generator temperature depends on the intensity of solar radiation and ambient temperature (hence it has a similar unsteady behavior like them and the peak generator temperature can be observed at noon in Figure 7-7). The mass  $m_4$  depends on the generator temperature and ambient conditions; as explained before, both  $Q_g$  and  $Q_g/m_4$  becomes more in hotter days. Moreover, concentration of the strong solution formed in absorber decreases with ambient temperature, less absorption takes place inside the absorber and hence more  $m_4$  is consumed inside the absorber. Therefore,  $m_4$  increases with ambient temperature from

June 15 to June 19. Similarly, the mass of produced ammonia vapor ( $m_7$ ) increases with generator temperature ( $T_{\text{gen}} = T_4$ ) and hence it has a similar variation with time as  $T_{\text{gen}}$ ;  $m_7$  reaches its maximum almost at noon and then decreases with the decrease in generator temperature.



**Figure 7-6 Plots of absorber temperature ( $T_{abs}$ ) and strong solution (aqua-ammonia) concentration ( $X_{abs}$ ) inside absorber for representative days of summer**

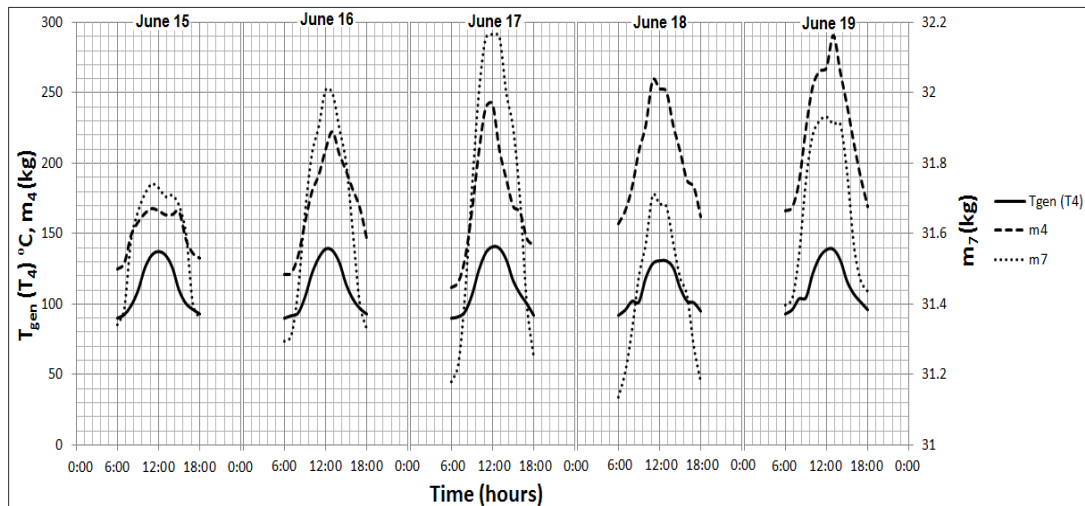


**Figure 7-7 Generator temperature ( $T_4$ ), mass of ammonia vapor at exit of dephlagmator ( $m_7$ ) and mass of weak solution at exit of generator ( $m_4$ ) versus time for representative days of summer**

### 7.3 Exergy Analysis

With the rise in condenser/absorber temperature from 35 °C to 45 °C, the values of generator exergy loss ratio decrease for all the three storage systems as shown in Figure 7-8. RSAR cycle and HSAR cycle show a similar trend whereas the CSAR cycle shows a trend similar to that of the basic absorption cycle without any storage tank (shown in the validation part). The HSAR cycle shows the highest evaporator exergy loss ratio followed by the CSAR cycle and the RSAR cycle (Figure 7-9). The exergy loss ratio plots for evaporator show an abrupt change within a narrow temperature range of generator just after the cut-off temperature [60]. With the further rise in generator temperature, the evaporator exergy loss ratio decreases gradually. Evaporator shows the highest values of exergy loss ratio among the chiller components. The peak value of exergy loss ratio in evaporator ranges between 0.53-0.65 in HSAR cycle, 0.48-0.6 in CSAR cycle and 0.45-0.58 in RSAR cycle as shown in Figure 7-9.

The absorber exergy loss ratio is maximum for CSAR cycle followed by the HSAR cycle and the RSAR cycle. The absorber exergy loss ratio increases with the rise in generator temperature as shown in Figure 7-10 (a). The absorber exergy losses increase for all the three storage chillers with the increase in condenser/absorber temperature from 35 °C to 45 °C (Figure 7-10(a)). Since  $T_c = T_a = T_{amb} + 5$  °C, the rise in condenser/absorber temperature increases the difference between the exergy at absorber inlet and the exergy at absorber outlet which leads to the increase in absorber exergy losses. The condenser exergy loss ratio increases sharply following the cut-off temperature [26], reaches the peak point and then decreases with the decrease in generator temperature. Condenser has low exergy losses (1% - 2% of the total exergy losses of the chiller) for all the three storage systems. The condenser exergy losses also increase with the rise in

condenser/absorber temperature (Figure 7-10(b)). The peak value of condenser exergy loss ratio in RSAR cycle is about 14.28% more the exergy loss ratio in HSAR cycle and 16.66% more the exergy loss ratio in CSAR cycle.

The exergy losses in solution heat exchanger (SHX) are 15% - 30 % of the total exergy losses in all the three storage cycles. The SHX exergy losses for CSAR cycle are maximum near the cut-off temperature [60] but at high generator temperatures, the exergy losses for CSAR cycle become minimum among the three storage systems. Since the difference between the net inlet exergy and the net outlet exergy decreases with the rise in generator temperature, the exergy loss ratio in SHX also decreases (Figure 7-11(a)). The RHX peak exergy losses are about 1.1% - 1.25% of the total exergy losses in CSAR cycle, 0.78% - 0.98% in HSAR cycle and 0.63% - 0.8% in RSAR cycle (Figure 7-11(b)).

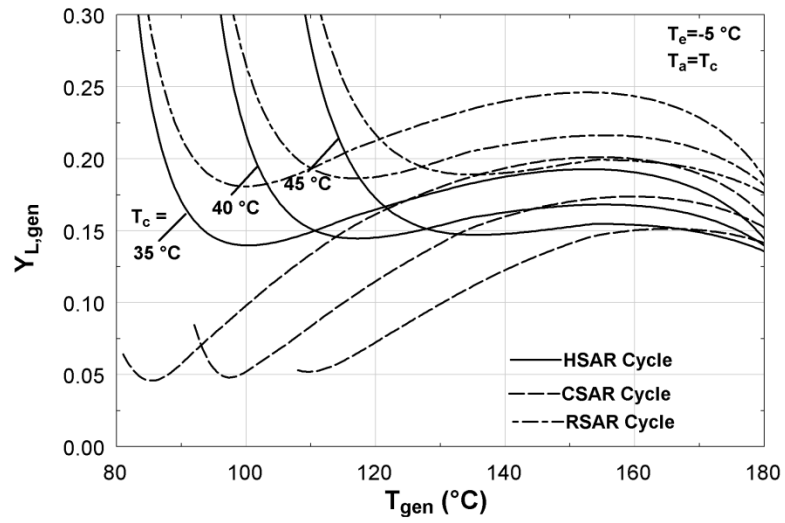


**Figure 7-8 Generator exergy loss ratio versus generator temperature at different condenser temperatures.**

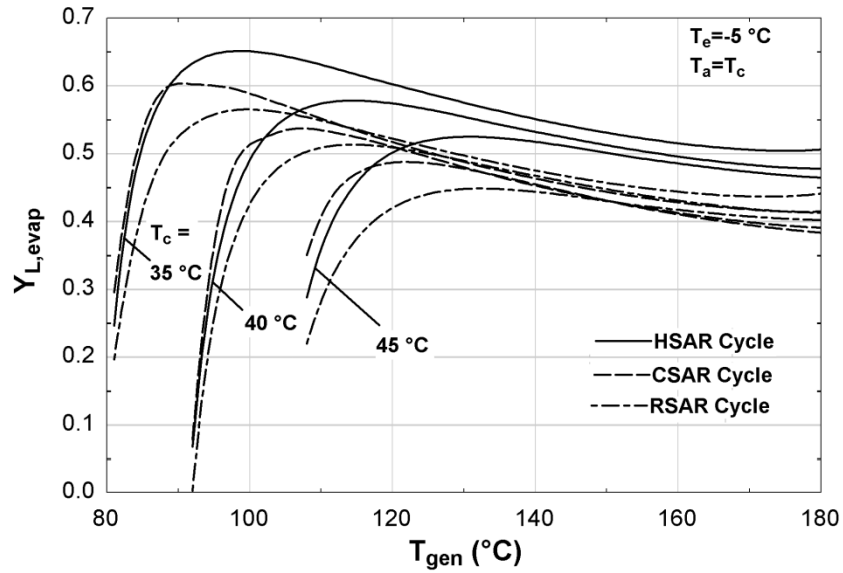
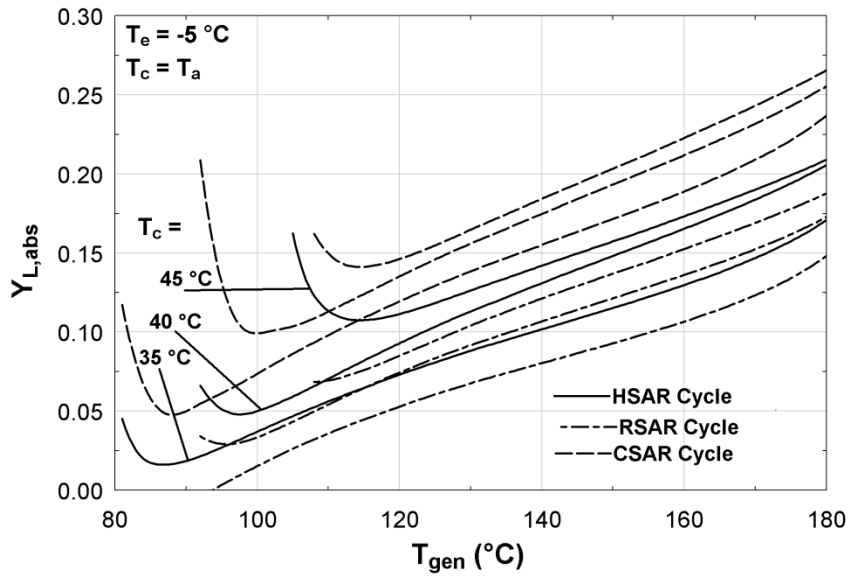
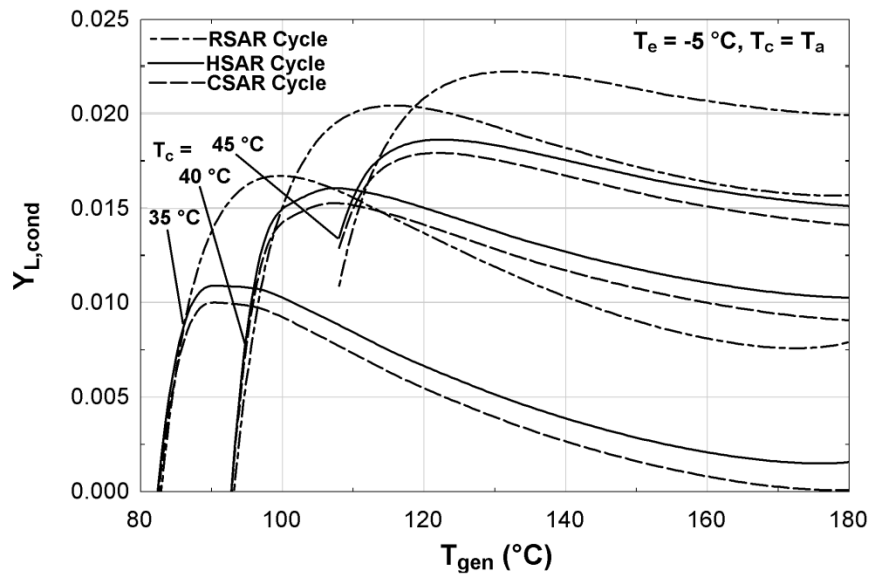


**Figure 7-9 Evaporator exergy loss ratio versus generator temperature at different condenser temperatures.**



(a)



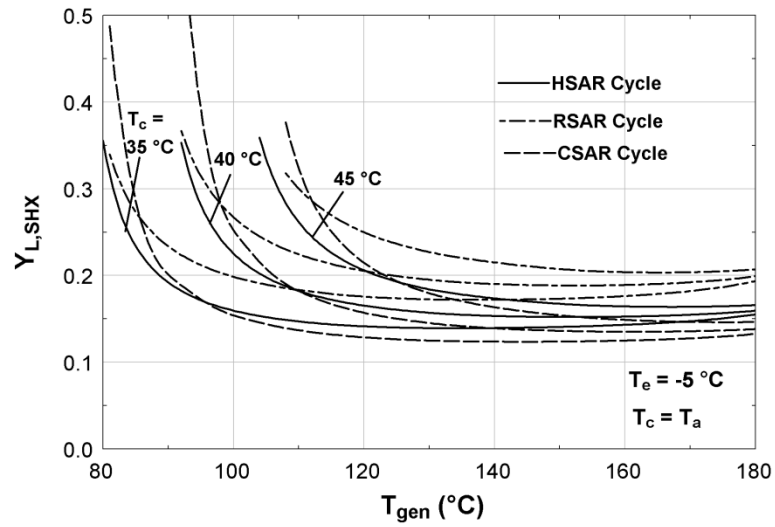
(b)

**Figure 7-10 (a) Absorber exergy loss ratio versus generator temperature at different condenser temperatures (b) Condenser exergy loss ratio versus generator temperature at different condenser temperatures**

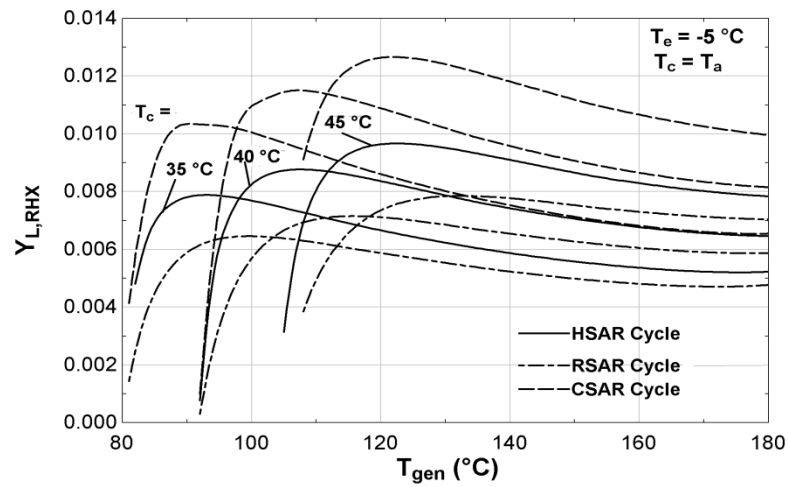
The pump exergy losses are lowest (0.06% of the total exergy losses) among the components in all the three storage chillers (Figure 7-12). At high generator temperatures ( $>165\text{ }^{\circ}\text{C}$ ), the difference in pump exergy loss ratio becomes negligible for various condenser/absorber temperatures ( $35\text{ }^{\circ}\text{C}$ ,  $40\text{ }^{\circ}\text{C}$ ,  $45\text{ }^{\circ}\text{C}$ ).

RSAR cycle has the lowest values of total exergy loss ratio among the three storage systems. The total exergy loss ratio is highest in HSAR cycle at generator temperature  $20\text{-}30\text{ }^{\circ}\text{C}$  above the cut-off temperature [60]. At higher generator temperatures (beyond  $20\text{-}30\text{ }^{\circ}\text{C}$  above the cut-off temperature), the total exergy loss ratio becomes maximum for CSAR cycle. At  $T_c=T_a=45\text{ }^{\circ}\text{C}$  and  $T_{\text{gen}} = 120\text{ }^{\circ}\text{C}$  (assumption 3), the total exergy loss ratio in HSAR cycle is 20.4% and in CSAR cycle is 15.21% more than the total exergy loss ratio in RSAR cycle.





(a)



(b)

**Figure 7-11 (a) SHX exergy loss ratio versus generator temperature at different condenser temperatures (b) RHX exergy loss ratio versus generator temperature at different condenser temperatures**

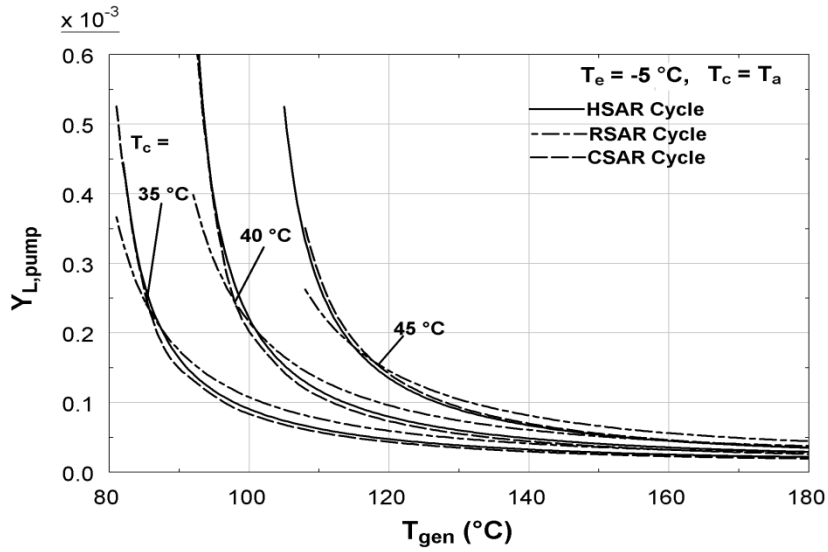


**Figure 7-12 Exergy loss ratio of pump ( $y_{L,pump}$ ) versus generator temperature at different condenser temperatures**

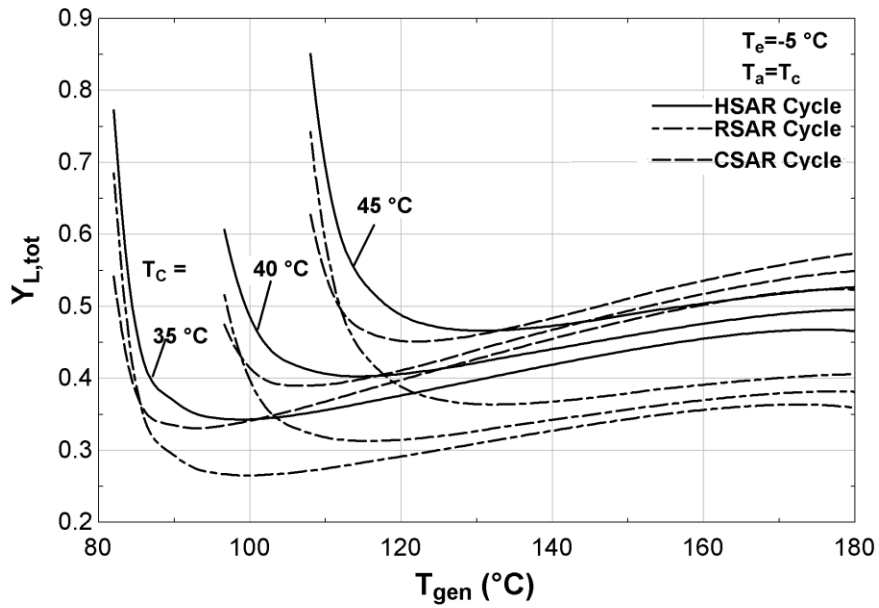


**Figure 7-13 Total exergy loss ratio ( $y_{L,tot}$ ) versus generator temperature at different condenser temperatures**

## 7.4 Exergo-Economic Evaluation

Exergo-economic analysis for HSAR cycle is performed using the exergo-economic variables. The objective function of the exergo-economic evaluation is to determine the components with high costs associated to irreversibilities (exergy destruction and exergy loss). The costs associated with irreversibilities are wasted without any additional gain in system's performance. These costs can be reduced to increase the performance of the system but usually at the expense of Capital Investment. So a tradeoff needs to be made between the costs of irreversibilities and the costs associated to the Capital Investment to achieve the optimal cost and performance of HSAR cycle.

The cost rate of capital investment ( $\dot{Z}$ ) for flat plate solar collectors is very high as compared to any of the components of HSAR cycle as shown in Figure 7-14. Among the chiller components, absorber has the maximum cost rate of capital investment and is almost the double of the cost rate of condenser. The cost rate of generator and evaporator is around 60%-65% of the cost rate of absorber. Refrigerant heat exchanger and the pump have the least values of cost rates in HSAR cycle.

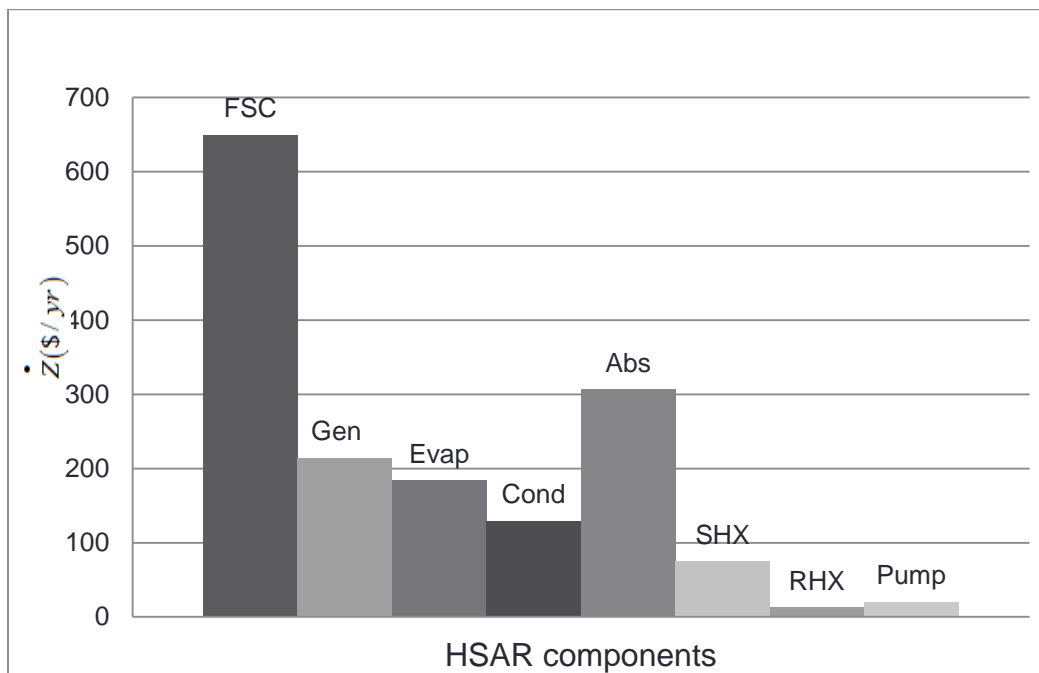


**Figure 7-14 Cost rates associated to Capital Investment for HSAR components**

Since the generator has high entropy generation due to the heat transferred by solar collectors, it has the highest value of exergy destruction ratio among the components of HSAR cycle as shown in Table 7-6. The exergy destruction ratio in solution heat exchanger (SHX) and evaporator assembly is almost half to that of the generator. The exergy loss ratio is zero in all the components except for evaporator assembly since the evaporator assembly includes the absorber and condenser units which dissipate heat directly to the environment. Both pump and the RHX have very low percentage of exergy destruction ratio.

The exergetic efficiency for each component of HSAR cycle is shown in Table 7-6. Pump has the highest exergetic efficiency equal to 86.66%. The exergetic efficiency of the generator is 68.76% which can be further improved by modifying the generator design provided the net capital investment is not substantially affected. A relatively low exergetic efficiency of the evaporator assembly is due to the exergy losses in condenser and absorber and the exergy destruction in evaporator. Solution Heat Exchanger (SHX) has the lowest exergetic efficiency among the system components (10%) due to high value of exergy rate of the fuel compared to exergy rate of the product.

Table 7-7 shows the sum of cost rates for exergy destruction, exergy loss and capital investment ( $\dot{C}_D + \dot{C}_L + \dot{Z}$ ) of HSAR cycle components.  $\dot{C}_D + \dot{C}_L + \dot{Z}$  is an important exergo-economic variable used to identify the components which contribute a large percentage of the total system cost. The variable  $\dot{C}_D + \dot{C}_L + \dot{Z}$  has a maximum value for evaporator assembly among all the system components. Exergo-economic factor ( $f$ ) equal to 61.4% for evaporator assembly (shown in Table 7-7) indicates that the cost of evaporator assembly is predominantly shared by the initial capital investment.

This indicates that the cost due to exergy destruction and exergy losses in evaporator assembly is relatively less compared to the cost of capital investment. Hence the design of the evaporator assembly should to be modified to reduce the initial capital investment even at the cost of exergy destruction and exergy losses.

Solution heat exchanger (SHX) has the second largest value of variable  $\dot{C}_D + \dot{C}_L + \dot{Z}$ . A low percentage (15.95%) of exergo-economic factor ( $f$ ) indicates that the large proportion of the cost of SHX is shared by the cost of exergy destruction than by the cost of initial capital investment. Hence the exergy destruction must be reduced in SHX even at the expense of initial capital investment. The improvement in design for any heat exchanger increases its cost but this increase in cost (capital investment) is acceptable for SHX due to low percentage of exergo-economic factor.

Solution heat exchanger (SHX) is followed by the generator in high value of variable  $\dot{C}_D + \dot{C}_L + \dot{Z}$ . Exergo-economic factor equal to 55.43% for generator suggests slightly more cost contributed by the capital investment compared to the cost contributed by exergy destruction. Thus the capital investment of generator may be reduced at the expense of the cost of exergy destruction. Both refrigerant heat exchanger (RHX) and the pump possess the lowest values of variable  $\dot{C}_D + \dot{C}_L + \dot{Z}$  and highest values of exergo-economic factor among the system components.

The relative cost difference ( $r$ ) value is maximum for evaporator assembly (133.89%) as shown in Table 7-7. This suggests that the average cost of product ( $c_P$ ) should be reduced which ultimately decreases the relative cost difference. The average cost of the product, which is the objective function of the exergo-economic evaluation, depends on the heat capacity and the temperature of the evaporator. Since generator also

has a high percentage (66%) of relative cost difference, the cost of product should be reduced. Refrigerant heat exchanger (RHX), solution heat exchanger (SHX) and the pump have relatively low percentage of relative cost difference.

**Table 7-6 Exergy analysis results for HSAR cycle**

<b>Components</b>	$\dot{X}_F$ (kW)	$\dot{X}_P$ (kW)	$\dot{X}_L$ (kW)	$\dot{X}_D$ (kW)	$y_D$ (%)	$y_D^*$ (%)	$y_L$ (%)	$\varepsilon$ (%)
<b>Generator</b>	3.81	2.62	0	1.19	28.60	46.85	0	68.76
<b>Evaporator Assembly</b>	2.36	1.23	0.39	0.74	17.78	29.13	9.37	52.11
<b>RHX</b>	0.038	0.016	0	0.022	0.52	0.86	0	42.10
<b>SHX</b>	0.67	0.067	0	0.60	14.42	23.62	0	10
<b>Pump</b>	0.030	0.026	0	0.0043	0.10	0.16	0	86.66
<b>Overall System</b>	4.16	1.23	0.39	2.54	61.05	100	9.37	29.56

**Table 7-7 Exergo-economic variables of HSAR cycle**

<b>Components</b>	$c_F$	$c_P$	$\dot{C}_L$	$\dot{C}_D$	$\dot{Z}$	$\dot{C}_D + \dot{C}_L + \dot{Z}$	$f$ (%)	$r$ (%)
	(\$/GJ)	(\$/GJ)	(\$/yr)	(\$/yr)	(\$/yr)	(\$/yr)		
<b>Generator</b>	4.62	7.67	0	172.1	214.12	386.22	55.43	66.01
<b>Evaporator assembly</b>	9.56	22.36	203.4	185.9	620.3	1009.6	61.4	133.89
<b>RHX</b>	2.04	2.44	0	0.58	12.61	13.19	95.6	19.60
<b>SHX</b>	108.6	110.9	0	396.9	75.37	472.27	15.95	2.11
<b>Pump</b>	60.27	76.41	0	2.95	20.22	23.17	87.26	26.77
<b>Overall System</b>	16.13	18.43	132.1	1626	1592.2	3350.3	47.52	14.25



The cut-off temperature [60] (minimum generator temperature needed to separate ammonia from aqua-ammonia binary mixture) is shifted to higher temperatures with the rise of condenser temperature as shown in Figure 7-15. As the condenser temperature is increased from 28 °C to 40 °C, the peak exergetic efficiency of the overall system drops from 72% to 34% as shown in Figure 7-15. Figure 7-16 shows the variation of the overall exergetic efficiency with the evaporator temperature at different condenser temperatures. Since HSAR cycle is only designed for refrigeration (not for air-conditioning), the range of evaporator temperature was selected from 0 °C to -40 °C (shown in Figure 7-16). Low temperature evaporator cooling can be achieved at low condenser temperature with better overall system performance compared to that achieved at high condenser temperature as shown in Figure 7-16. At  $T_{\text{cond}} = 28 \text{ °C}$  and  $T_{\text{evap}} = -25 \text{ °C}$ , the peak exergetic efficiency achieved is 45% while at  $T_{\text{cond}} = 40 \text{ °C}$  and  $T_{\text{evap}} = -10 \text{ °C}$ , the peak exergetic efficiency achieved is 32%. The peak exergetic efficiency of the overall system is improved from 48% to 72% as the effectiveness value of solution heat exchanger (SHX) increases from 0.2 to 0.8 as shown in Figure 7-17.

For 0.4% design conditions of Dhahran, the plots of total cost rate ( $\dot{C}_D + \dot{C}_L + \dot{Z}$ ) and the cost of the product of overall system ( $c_{p,os}$ ) is shown in Figure 7-18. The cost of the product of overall system achieves a minimum value at  $T_{\text{gen}} = 76 \text{ °C}$  whereas the total cost rate of the overall system shows a minimum value at  $T_{\text{gen}} = 84 \text{ °C}$ . Therefore, the minimum cost of the product which is the objective function of the exergo-economic optimization, can be achieved by maintaining the generator temperature in the range 75 °C – 85 °C for assumed operating conditions (assumption 6, 7) for Dhahran region.

A quasi-steady exergy and exergo-economic analysis were performed for a representative summer day (as this day received maximum solar radiation) of Dhahran region using the temperature and solar radiation data from Research Institute, KFUPM. Both exergetic efficiency and the exergo-economic factor decrease with the increase of ambient temperature and the solar intensity as shown in Figure 7-19. Since the cost of irreversibilities is less due to low exergy losses/exergy destruction in the morning/evening, the exergo-economic factor and the exergetic efficiency is relatively high compared to that in the noon. The exergetic efficiency is dropped from 35% in morning to 27 % in the noon time and the exergo-economic factor decreases from 76% in morning to 35% in the noon time.

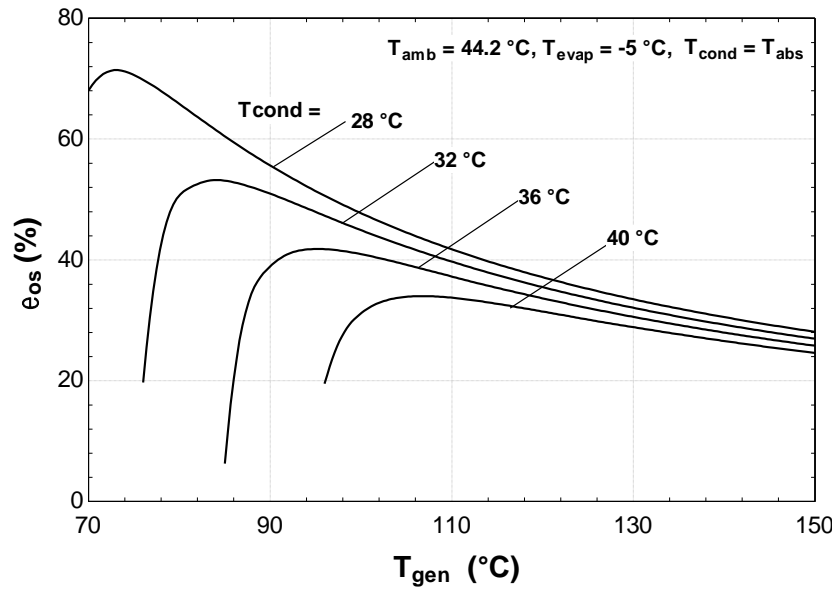


**Figure 7-15 Exergetic efficiency of overall system versus generator temperature at different condenser temperatures**

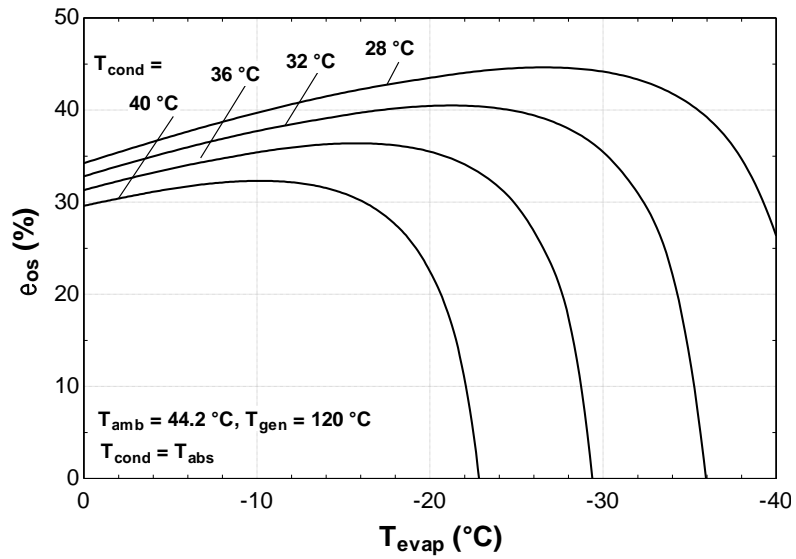


**Figure 7-16 Exergetic efficiency of overall system versus evaporator temperature at different condenser temperatures**

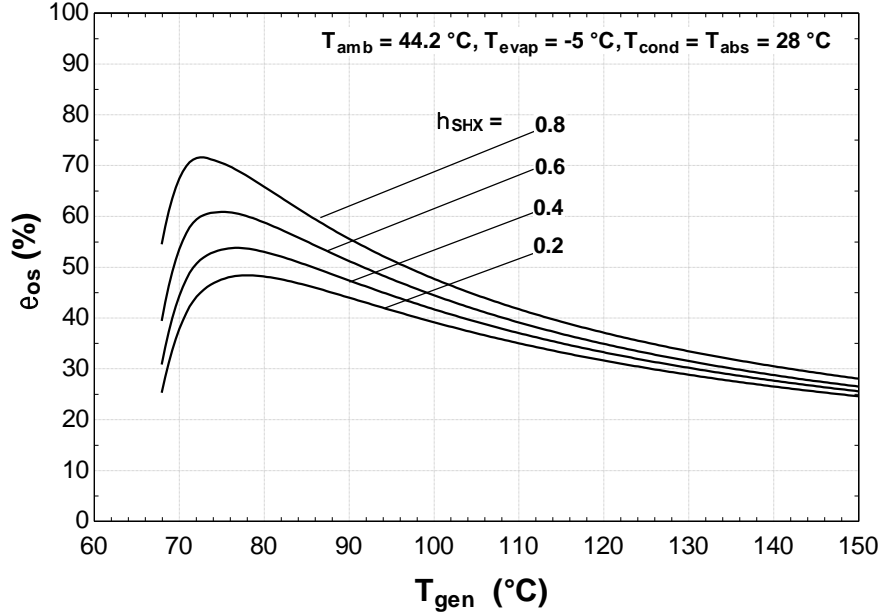


Figure 7-17 Exergetic efficiency of overall system versus generator temperature at different effectiveness values of solution heat exchanger (SHX)

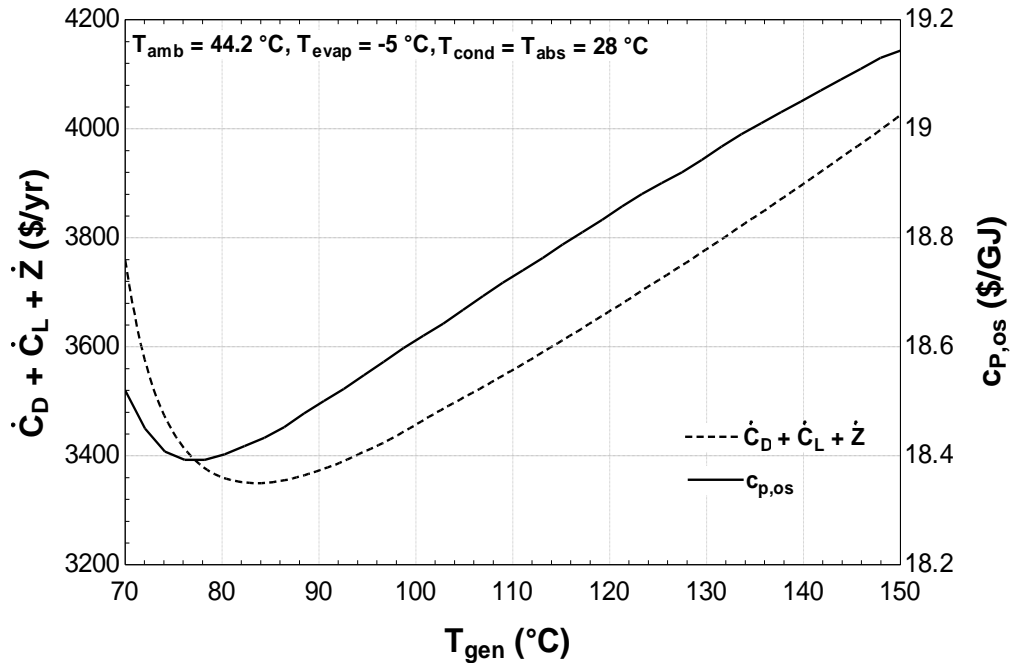
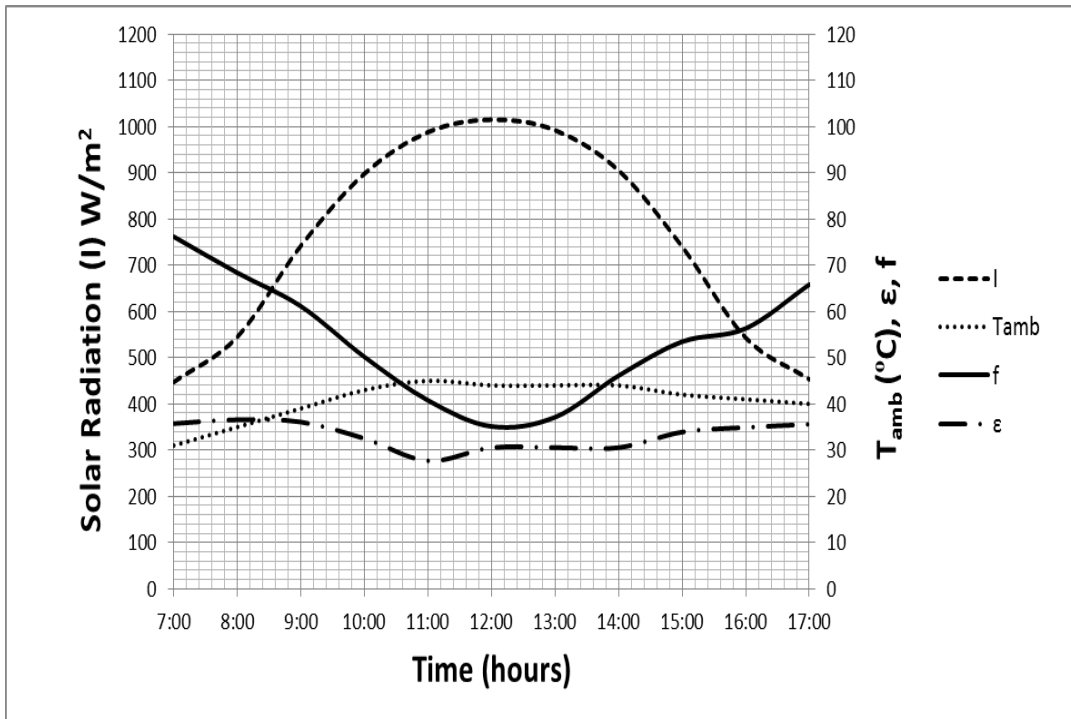


Figure 7-18 Plots of total cost rate ( $\dot{C}_D + \dot{C}_L + \dot{Z}$ ) and cost of the product ( $c_{p,os}$ ) of overall system versus generator temperature



**Figure 7-19 Plots of solar radiation ( $I$ ), ambient temperature ( $T_{amb}$ ), exergo-economic factor of overall system ( $f_{os}$ ) and the exergetic efficiency of overall system ( $\epsilon_{os}$ ) versus time (hours) for June 16, 2013.**

## CHAPTER 8

### VALIDATION

#### 8.1 Unsteady analysis

The unsteady software of HSAR cycle is validated against an available steady-state software [1] by feeding the unsteady software with hourly ambient temperatures, solar intensity, etc that are non-variable with time (average values) for same given input data and 5 kW cooling power for both summer and winter. Exactly, the same results were obtained from the two programs for generator heat rate, condenser heat rate, absorber heat rate and COP. The reverse was also done and the unsteady software was fed with the variable data with time and values of the obtained results for the COP and the heat rates of the system components (from unsteady analysis for the same 5 kW cooling power) were averaged for representative days of summer and winter and presented in Table 8-1. In Table 8-1, the corresponding results obtained from the steady-state software that was fed with the average ambient conditions for the representative days of both summer and winter are also presented and compared. The maximum percentage difference between the steady and unsteady model results was 3.67% for the absorber heat rate in winter.

**Table 8-1 Comparison between unsteady and steady software results of HSAR Cycle for same given input non-variable with time (average values) data and 5 kW cooling power**

	Unsteady Model	Steady State Model	Percentage difference (%)
	<i>Summer/ Winter</i>	<i>Summer/ Winter</i>	<i>Summer/ Winter</i>
Generator heat rate, kW	<b>26.11 /21.94</b>	<b>25.90/21.97</b>	<b>0.80/0.13</b>
Condenser heat rate, kW	<b>15.92/16.11</b>	<b>15.65/15.94</b>	<b>1.69/1.05</b>
Absorber heat rate, kW	<b>16.66 /13.88</b>	<b>16.45/13.37</b>	<b>1.26/3.67</b>
COP	<b>0.38/0.683</b>	<b>0.39/0.682</b>	<b>2.56/0.14</b>

The basic solar absorption chiller model (without storage tank) was also validated against the experimental results of a diffusion absorption cooling machine (DACM # 3) [46]. The following fixed/steady input parameters were used in the experimental setup of Jakob and Eicker [46]: evaporator cooling capacity = 0.7 kW, generator inlet temperature = 105 °C, evaporator cold brine in/out = 12/6 °C, condenser in/out = 31/34 °C and absorber in/out = 31/34 °C. As the input parameters were fixed/steady throughout the time period of the experiments, the heating/cooling capacities of the chiller components were also steady / fixed over the same time interval of the experiments. Therefore, a single (fixed/steady) value of heating/cooling capacities for each component of the DACM chiller was used for validation of the steady-state model of basic solar absorption chiller model (without any storage tank). The comparison shows the maximum percentage difference of 8.3 % in the generator heat capacity (Table 8-2).

**Table 8-2 Comparison of heat capacities and COP between basic solar absorption chiller model (without storage tank) and a DACM chiller # 3 [46]**

Parameters	Present Model, Basic Solar Absorption Chiller	DACM Chiller # 3 of Jakob & Eicker[21]	Percentage Difference (%)
Generator power ( $\dot{Q}_{gen}$ ), kW	3.3	3.6	8.3
Absorber power ( $\dot{Q}_{abs}$ ), kW	2.1	2.0	4.7
Condenser power ( $\dot{Q}_{con}$ ), kW	1.5	1.4	6.6
Dephlegmator power ( $\dot{Q}_{deph}$ ), kW	0.39	0.4	2.5
COP	0.21	0.21	0

The unsteady analysis of a basic solar absorption refrigeration cycle (without any storage tank) was also validated against the experimental work of Jakob and Eicker [54] on a solar powered diffusion absorption cooling machine (DACM chiller # 1) under the Stuttgart (Germany) ambient conditions (Figure 8-1). The input data for the present basic solar absorption chiller model are: evaporator cooling load = 1.3 kW, generator temperature = 150-170 °C, absorber/condenser temperatures = 45 °C, evaporator temperature = 5 °C. In Figure 8-1,  $\dot{Q}_{gen}$ ,  $\dot{Q}_{abs}$ ,  $\dot{Q}_{con}$  and COP are the generator, absorber and condenser thermal powers and the COP of the basic solar absorption chiller (without any storage tank). The heating capacities and the COP of the absorption chiller were plotted against time for 4 continuous hours (240-480 mins) [54]. The plots of heating capacities and COP with time show a similar trend for both the chillers and the plots of condenser heat capacity ( $\dot{Q}_{con}$ ) are superimposed at time = 300, 360 and 420 minutes.



The maximum percentage difference (9.16 %) was observed for generator heat capacity ( $\dot{Q}_{gen}$ ,  $\dot{Q}_{gen}^*$ ) at time = 420 minutes.

The unsteady analysis of basic solar absorption chiller model (without storage tanks) was also validated using the experimental results of Zetzsche et al. [55] as shown in Figure 8-2. The experimental setup [55] also includes an ice storage tank which was only charged when the normal operation of the chiller cycle was not needed. (e.g. on weekends) [55]. The basic solar absorption chiller model was validated using the same ambient conditions as in the experiments of [55]. Moreover, same time varying data as given in [55], such as the solar radiation ( $I^{**}$ ), ambient temperature ( $T_{amb}^{**}$ ), generator temperature ( $T_{gen}^{**}$ ) and generator heat flux/heat capacity ( $\dot{Q}_{gen}^{**}$ ) over the period of 8 hours (10 AM-6 PM), were used as input parameters. The plot of evaporator cooling capacity ( $\dot{Q}_{evap}$ ) with time was obtained as an output in the simulation model of basic solar absorption chiller. The plot of evaporator cooling capacity of a chiller model ( $\dot{Q}_{evap}$ ) is almost superimposed over the plot of the cooling capacity of experimental setup ( $\dot{Q}_{evap}^{**}$ ) with the maximum percentage difference of 6.25 % as shown in Figure 8-2.

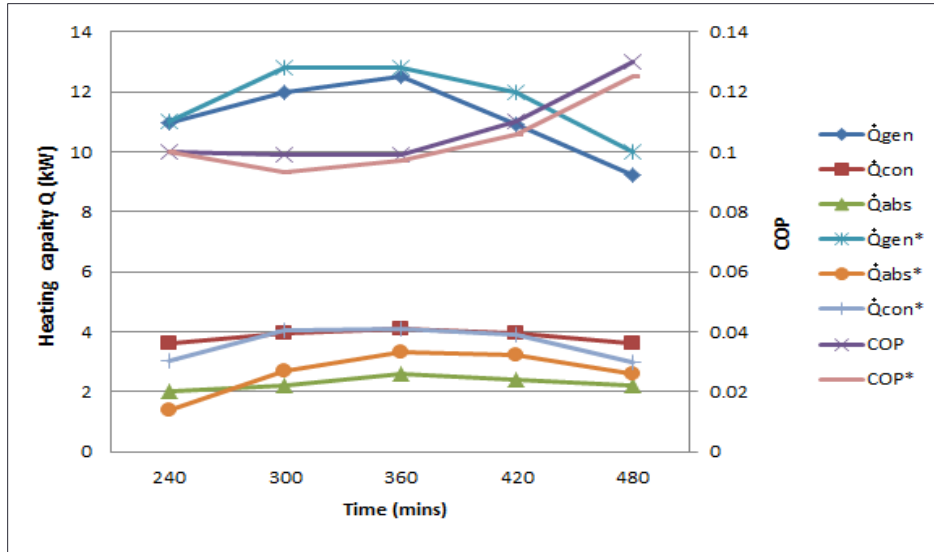


Figure 8-1 Plots of heating capacity and COP for basic solar absorption chiller model (without storage tanks) and a DACM chiller#1 (experimental setup) [54], the quantities with superscript \* are from the results of Jakob and Eicker, 2002

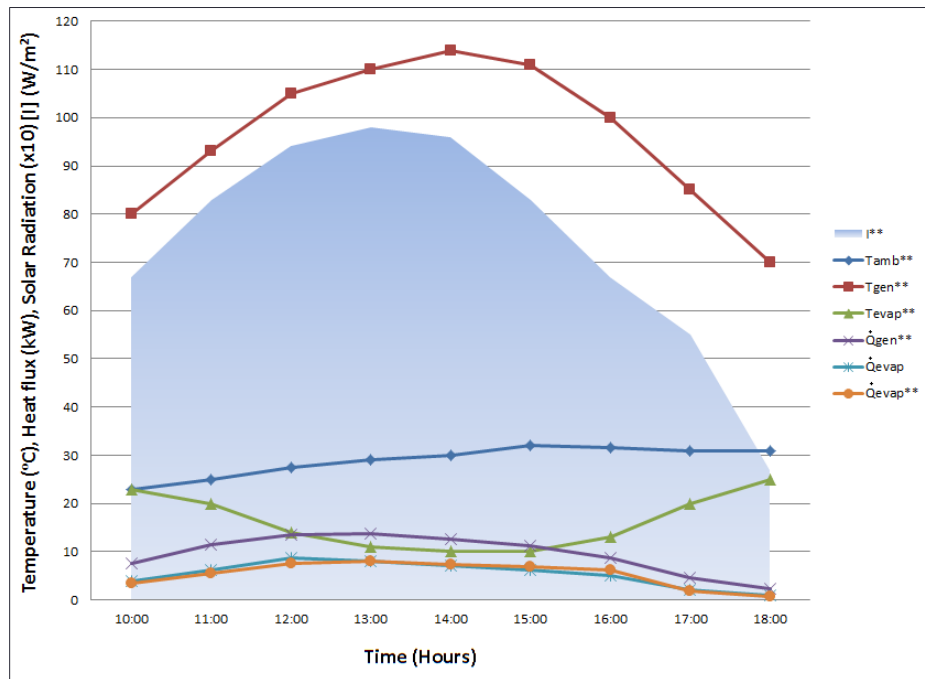
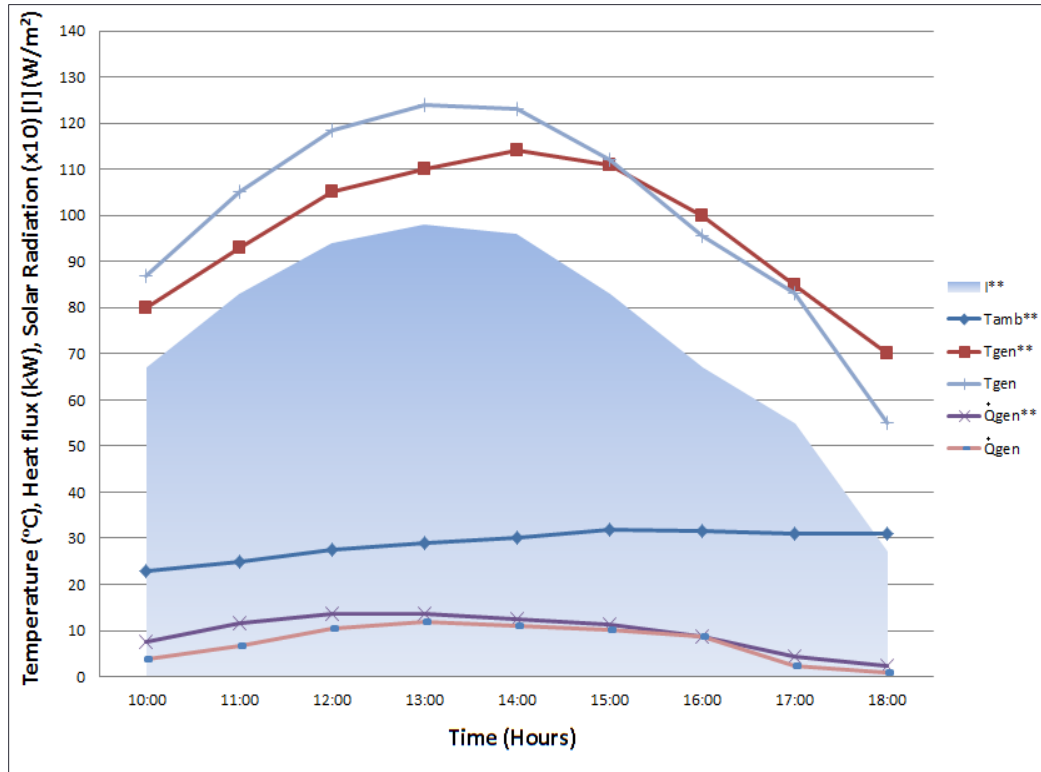


Figure 8-2 Plots of solar radiation, temperatures and heat fluxes for basic solar absorption chiller model (without storage tanks) and a small scale absorption chiller (experimental setup) [55], the quantities with superscript \*\* are obtained from Zetzsche et al. 2008

Figure 8-3 shows the comparison of the generator temperature and the generator heat flux/heat capacity between the basic solar absorption chiller model (without any storage tank) and the experimental setup of absorption chiller [55]. The solar intensity ( $I^{**}$ ) and the ambient temperature ( $T_{amb}^{**}$ ) were used as an input data [55] to obtain the plots of generator temperature ( $T_{gen}$ ) and generator heat capacity ( $\dot{Q}_{gen}$ ) with time.  $T_{gen}$  was determined using assumption 4 and equation (b) in section 4 and thus it shows some variation with  $T_{gen}^{**}$  but the overall trend of the two plots is the same.  $\dot{Q}_{gen}$  also shows a similar trend as  $\dot{Q}_{gen}^{**}$ . Once the unsteady analysis of the basic solar absorption cycle (without storage tanks) was validated, this cycle was extended with the addition of dual storage system to accommodate a continuous 24-hour refrigeration.



**Figure 8-3 Plots of solar radiation, temperatures and heat fluxes for basic solar absorption chiller model (without storage tanks) and a small scale absorption chiller (experimental setup) [55], the quantities with superscript \*\* are from the results of Zetzsche et al. 2008**

## 8.2 Energy and exergy analysis

The energy and exergy analysis of the basic solar absorption refrigeration (HSAR (without any storage tank)) cycle is validated using the comparative study of irreversibilities in an aqua-ammonia absorption refrigeration system conducted by Ataer and Gogus (1990) [21]. The validation of HSAR cycle was conducted using the same conditions as were used by Ataer and Gogus in their analysis:

Generator temperature ( $T_g$ ) = 50 – 130 °C; Evaporator temperature ( $T_e$ ) = -20 – 10 °C; Condenser temperature ( $T_c$ ) = 22 – 28 °C; Absorber temperature ( $T_a$ ) = 24 – 30 °C; refrigeration capacity = 1 kW.

The plots of coefficient of performance (COP) and exergetic coefficient of performance (ECOP) of HSAR cycle show a good compromise with the plots of aqua-ammonia absorption refrigeration system proposed by Ataer and Gogus (1990) (shown in Figure 8-4) [21]. The absorption chiller model analyzed by Ataer and Gogus [21] does not include any storage tank, therefore, it is an appropriate model for comparison with the HSAR cycle. The maximum percentage difference in COP is 1.63% at  $T_{gen} = 130$  °C, in ECOP is 2.43 % at  $T_{gen} = 80$  °C, in  $Y_{L,evap}$  is 6.45% at  $T_{gen} = 80$  °C, in  $Y_{L,abs}$  is 4.61% at  $T_{gen} = 90$  °C, in  $Y_{L,gen}$  is 6.36% at  $T_{gen} = 100$  °C and in  $Y_{L,SHX}$  is 10% at  $T_{gen} = 90$  °C . Once the BSAR model was validated, it was extended (using the storage tanks) as a hybrid storage absorption refrigeration (HSAR) model.

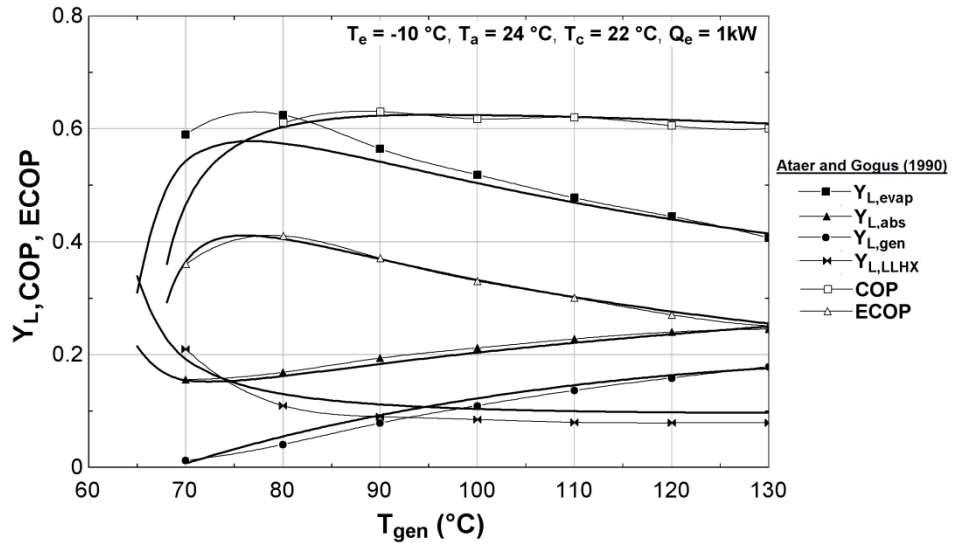


**Figure 8-4 – Plot of exergy loss ratio ( $y_L$ ), COP and ECOP versus generator temperature used for validation of basic solar absorption refrigeration (HSAR) system, the plots of HSAR system are shown by lines (—) without legend symbols**

## CHAPTER 9

### CONCLUSIONS AND RECOMMENDATIONS

The novel HSAR cycle was developed specifically for Dhahran region for average ambient conditions. Chapter 3 concludes that size of the storage tanks is reduced by 50% as compared to the refrigerant storage system and the cold storage system for same cooling capacity. Such a notable reduction in the size of storage tanks makes a system less bulky than the refrigerant storage system and saves the capital investment used to manufacture these storage tanks.

The unsteady analysis of HSAR cycle in chapter 4 shows the transient behavior of HSAR cycle for every one hour interval throughout the day. Due to lower ambient and hence cooling water temperatures in winter than summer the condenser pressure is reduced by 6 bars, which suggests less pump work is required in winter than in summer. For the given fixed 9 MJ cooling energy of evaporator during the nighttime, the heat energy values of HSAR components are also reduced in winter as compared to the summer. Despite the higher solar intensity in summer than in winter and the more effective sunlight hours during the day in summer than in winter, the following major results have been found for the given 24-hour a day fixed cooling load (of 5 kW) in both winter and summer. HSAR cycle has a better  $COP_{day}$  as well as  $COP_{night}$  in winter than in summer and the required solar collector field area per kilowatt of cooling capacity is more in winter (9.3%) than that required in summer. The part of solar collector field area used in storage is more (40% / 50% in summer / winter) than the part of it used in refrigeration.

In chapter 5, based on the comparison of energy and exergy analysis between the HSAR cycle and the HSAR cycle, the following can be concluded: the COP and circulation ratio of the HSAR cycle is the same as the HSAR cycle under all operating conditions; HSAR cycle has more exergy losses in all the components as compared to the exergy losses of the respective components in HSAR cycle; the difference in exergy losses between the HSAR cycle and the HSAR cycle is negligible near to the cut-off temperature; the evaporator has the maximum exergy losses (60% - 70% of the total exergy losses of HSAR cycle) followed by the generator and absorber exergy losses; since the HSAR cycle has more exergy losses (predominantly due to evaporator exergy losses) than HSAR cycle, the ECOP of HSAR cycle is less than the ECOP of the HSAR cycle; decreasing the evaporator temperature and increasing the condenser temperature increases the exergy losses of the evaporator. The evaporator temperature, condenser temperature and the generator temperature in HSAR cycle should be optimized to lower the exergy losses of the evaporator and other components which may bring the ECOP of the HSAR cycle closer to the ECOP of the HSAR cycle. The exergo-economic evaluation of HSAR cycle concludes that the pump and generator show the highest exergetic efficiencies among the system components. Low temperature cooling effect can be achieved at reduced condenser temperature with better system performance in HSAR cycle. The exergetic efficiency in HSAR cycle increases with the increase in effectiveness value of solution heat exchanger (SHX). Since the pump, RHX and evaporator assembly have high cost due to capital investment compared to the cost due to irreversibilities, the initial capital investment of these components should be reduced even at the expense of the costs of irreversibilities. Based on the quasi-steady



exergy/exergo-economic analysis of HSAR cycle, the exergetic efficiency and the exergo-economic factor reduce in the noon time as compared to that in the morning/evening. To make the system cost effective, the overall cost of the product must be reduced by optimizing the design variables of the system.

## REFERENCES

- [1] S. A. M. Said, M. A. I. El- Shaarawi, M. U. Siddiqui, "Alternate designs for a 24 – h operating solar powered absorption refrigeration technology," *Int. J. Refrigration.*, 2012.
- [2] M. A. El- Shaarawi, S. A. M. Said, M. U. Siddiqui, "New simplified correlations for aqua – ammonia intermittent solar powered absorption refrigeration systems," *Int. J. Air-Cond. Refrigeration*, vol. 20, pp. 125008/1 – 125008/13, 2012.
- [3] T. Brendel, M. Zetsche, H. M. Steinhagen, "Development of a small scale ammonia/water absorption chiller," *9th IIR Gustav Lorentzen Conference*, 2010.
- [4] J. Cerezo, M. Bourouis, M. Valles, A. Coronas, R. Best, "Experimental study of an ammonia–water bubble absorber using a plate heat exchanger for absorption refrigeration machines," *Appl. Thermal Eng.*, vol. 29, pp. 1005 – 1011, 2009.
- [5] J. Abdulateef, M. Alghoul, A. Zaharim, K. Sopian, "Experimental Investigation on Solar Absorption Refrigeration System in Malaysia," *Int. Conf. Renew. Energy Sources*, pp. 267 – 271, 2010.
- [6] J. Abdulateef, K. Sopian, M. A. Alghoul, M. Y. Sulaiman, A. Zaharim, I. Ahmad, "Solar Absorption Refrigeration System using New Working Fluid Pairs," *Int. Conf. Energy Environ.*, pp. 23 – 28, 2008.
- [7] L.A. Chidambaram, A.S. Ramana, G. Kamaraj, R. Velraj, "Review of solar cooling methods and thermal storage options," *Renew. Sustain. Energy Reviews*, vol.15, pp. 3220– 3228, 2011.
- [8] A. Koca, H. F. Oztop, T. Koyunc, Y. Varola, "Energy and exergy analysis of a latent heat storage system with phase change material for a solar collector," *Renew. Energy*, vol. 33, pp. 567 – 574, 2008.
- [9] M. Mokhtar, M. T. Ali, S. Bräuniger, A. Afshari, S. Sgouridis, P. Armstrong, M. Chiesa, "Systematic comprehensive techno-economic assessment of solar cooling technologies using location-specific climate data," *Applied Energy*, vol. 87, pp. 3766–3778, 2010.
- [10] P. Srihirin, S. Aphornratana, S. Chungpaibulpatana, "A review of absorption refrigeration Technologies," *Renew. Sustain. Energy Reviews*, vol. 5, pp. 343-372, 2001.
- [11] M. A. I. El-Shaarawi and R. A. Ramadan, "Effect of condenser temperature on the performance of intermittent solar refrigerators," *Energy Convers. Mgmt.*, vol. 27,

pp. 73 – 81, 1987.

- [12] A. Francisco, R. Illanes, J.L. Torres, M. Castillo, M. De Blas, E. Prieto, A. Garcí'a, "Development and testing of a prototype of low power water–ammonia absorption equipment for solar energy applications," *Renew. Energy*, vol. 25, pp. 537–544, 2002.
- [13] D. S. Kim, L. Wang, C. H. M. Machielsen, "Dynamic modeling of a small-scale NH<sub>3</sub>/H<sub>2</sub>O Absorption chiller," *Int. Conf. Refrigeration*, 2003.
- [14] S. Alizadeh, "Multi-pressure absorption cycles in solar refrigeration: A technical and economical study," *Solar Energy*, vol. 69, pp. 37–44, 2000.
- [15] M. Bayramoglu, A. T. Bulgan, "Sensitivity analysis of an Aqua Ammonia Absorption Refrigeration System," *Energy*, vol. 20, pp. 567 – 571, 1995.
- [16] S. G. Alvares, C. Trepp, "Simulation of a solar driven aqua ammonia absorption refrigeration system," *Int. Froid*, vol.10, 1987.
- [17] M.I. Karamangil, S. Coskun, O. Kaynakli, N. Yamankaradeniz, "A simulation study of performance evaluation of single-stage absorption refrigeration system using conventional working fluids and alternatives," *Renew. Sustain. Energy*, vol.14, pp. 1969 – 1978, 2010.
- [18] N.A. Darwish, S.H. Hashimi, A.S. Mansoori, "Performance analysis and evaluation of a commercial absorption–refrigeration water–ammonia (ARWA) system," *Int. J. Refrigeration*, vol. 31, pp. 1214 – 1223, 2008.
- [19] A. Sozen, "Effect of heat exchangers on performance of absorption refrigeration systems," *Energy Conv. Manag.*, vol.42, pp. 1699 – 1716, 2001.
- [20] K. S. Alqdah, "Performance and Evaluation of Aqua Ammonia Auto Air Conditioner System Using Exhaust Waste Energy," *Energy Procedia*, vol. 6, pp. 467–476, 2011.
- [21] O. E. Ataer, Y. Gogus, "Comparative study of irreversibilities in an aqua ammonia absorption refrigeration system," *Int. J. Refrigeration*, vol.14, 1991.
- [22] A. T. Bulgan, "Optimization of the thermodynamic model of aqua ammonia absorption refrigeration systems," *Energy Convers. Manag.*, vol. 36, pp. 135 – 143, 1995.
- [23] A. T. Bulgan, "Use of low temperature energy sources in Aqua-ammonia absorption Refrigeration Systems," *Energy Convers. Manag.*, vol. 38, pp. 1431-

1438, 1997.

- [24] R.D. Misra, P.K. Sahoo, A. Gupta, “Thermoeconomic evaluation and optimization of an aqua-ammonia vapour-absorption refrigeration system,” *Int. J. Refrigeration*, vol. 29, pp.47–59, 2006.
- [25] F. A. Al-Sulaiman and B. Ismail, “Estimation of monthly average daily and hourly solar radiation impinging on a sloped surface using the isotropic sky model for Dhahran, Saudi Arabia,” *Renew. Energy*, vol. 11, pp. 257–262, 1997.
- [26] W. Cai, M. Sen, S. Paolucci, “Dynamic modeling of an absorption refrigeration system using ionic liquids,” *ASME Int. Mech. Eng. Cong. Exposition*, 2007.
- [27] W. Cai, M. Sen, S. Paolucci, “Dynamic Simulation of an Ammonia water Absorption Refrigeration System,” *IECR*, vol.51, pp. 2070 – 2076, 2011.
- [28] D. Kong, J. Liu, L. Zhang, H. He, Z. Fang, “Thermodynamic and Experimental Analysis of an Ammonia-Water Absorption Chiller,” *Energy Power Eng.*, vol. 2, pp. 298 – 305, 2010.
- [29] M. Clerx, G. J. Trezek, “Performance of an aqua-ammonia absorption Solar refrigerator at sub-freezing Evaporator conditions,” *Solar Energy*, vol. 39, pp. 379–389, 1987.
- [30] D. Sun, “Thermodynamic design data and optimum Design maps for absorption refrigeration systems,” *Appl. Therm. Eng.*, vol. 17, pp. 211–221, 1997.
- [31] B. Zalba, J. Marin, L. F. Cabeza, H. Mehling, “Review on thermal energy storage with phase change: materials, heat transfer analysis and applications,” *Appl. Therm. Eng.*, vol.23, pp. 251–283, 2003.
- [32] D.S. Kim, C.A. I. Ferreira, “Solar refrigeration options – a state-of-the-art review,” *Int. J. Refrigeration*, vol. 31, pp. 3–15, 2008.
- [33] D. Boer, M. Medrano, M. Nogués, “Exergy and Structural Analysis of an Absorption Cooling Cycle and the Effect of Efficiency Parameters,” *Int. J. of Thermodynamics*, vol. 8, pp. 191–198, 2005.
- [34] M. A. Rosen, “A Concise Review of Exergy-Based Economic Methods,” *3rd IASME/WSEAS Int. Conf. on Energy Environ.*, pp. 23–25, 2008.
- [35] O. Kızılkın, A. Sencan, S. A. Kalogirou, “Thermoeconomic optimization of a LiBr absorption refrigeration system,” *Chem. Eng. Process.*, vol. 46, pp. 1376–1384, 2007.

- [36] M. D. d'Accadia, F. Rossi, "Thermoeconomic optimization of a refrigeration plant," *Int. J. Refrigeration*, vol. 21, pp. 42-54, 1998.
- [37] B. H. Gebreslassie, M. Medrano, D. Boer, "Exergy analysis of multi-effect water–LiBr absorption systems: From half to triple effect," *Renew. Energy*, vol.35, pp. 1773–1782, 2010.
- [38] B. H. Gebreslassie, M. Medrano, F. Mendes, D. Boer, "Optimum heat exchanger area estimation using coefficients of structural bonds: Application to an absorption chiller," *Int. J Refrigeration*, vol. 33, pp. 529 – 537, 2010.
- [39] B. H. Gebreslassie, G. G. Gosálbez, L. Jiménez, D. Boer, "Design of environmentally conscious absorption cooling systems via multi-objective optimization and life cycle assessment," *Appl. Energy*, vol. 86, pp. 1712–1722, 2009.
- [40] H. D. A. Varela, W. S. Gomez, O. C. Lopez, "Thermodynamic design of a solar refrigerator to preserve sea products," *ISES Solar World Congress*, vol.3, 1999.
- [41] Bejan, Tsatsaronis, Moran, *Thermal Design and Optimization*, John Wiley & Sons Inc., 1996.
- [42] Y. A. Cengel, M. A. Boles, *Thermodynamics: An Engineering Approach*, 5<sup>th</sup> edition, McGraw-Hill, 2006.
- [43] D. D. Rama, D. R. Durgaiyah, *Fluid Mechanics and Machinery*, New Age International, 2007.
- [44] R. M. Johnston, *Elements of Applied Thermodynamics*, 5<sup>th</sup> edition, Naval Institute Press, 1992.
- [45] Duffie, Beckman, *Solar Engineering of Thermal Sciences*, 2<sup>nd</sup> edition, John Wiley & Sons, 1991.
- [46] U. Jakob, U. Eicker, "Simulation and performance of diffusion absorption cooling machines for solar cooling," *9<sup>th</sup> World Renew. Energy Congress*, pp. 21-25, 2006.
- [47] Threlkeld, L. James, *Thermal Environmental Engineering*, 2<sup>nd</sup> edition, Prentice Hall, Inc., pp. 97-113, 1970.
- [48] K. P. Tyagi, "Cut-off temperatures of aqua-ammonia absorption refrigeration system," *Heat Rec. Sys.* vol. 8, pp. 371 – 373, 1988.
- [49] <http://carboncompact.co.za/learning-centre/>

- [50] F. P. Incropera, D. P. DeWitt, T. L. Bergman & A. S. Lavine, *Fundamentals of Heat and Mass Transfer*, 6th edition, John Wiley & Sons US, pp. 686–688, 2006.
- [51] C. Black, “Importance of thermophysical data in process simulation”, *Int. J. Thermophysics*, vol. 7(4), pp. 987-1002, 1986.
- [52] <http://en.wikipedia.org/wiki/Brine>
- [53] R. S. Lavanya, B. S. R. Murthy, “Design of solar water cooler using aqua-ammonia absorption refrigeration system”, *Int. J. Adv. Eng. Res. Stud.* vol. 2, pp. 20-24, 2013.
- [54] U. Jakob, U. Eicker, “Solar cooling with diffusion absorption principle,” *World Renew. Energy Cong.*, 2002.
- [55] M. Zetsche, T. Koller, H. M. Steinhausen, “Solar Cooling with an Ammonia/Water Absorption Chiller”, *Int. Cong. on heating, cooling and buildings*, 2008.
- [56] *ASHRAE Fundamentals Handbook*, ASHRAE Inc., 2013.
- [57] H. Z. Hassan, A. Mohamad, “A review on solar cold production through absorption technology,” *Renew. Sustain. Energy Reviews*, vol. 16(7), 2012.
- [58] N. K. Ghaddar, M. Shihab, F. Bdeir, “Modeling and simulation of solar absorption system performance in Beirut,” *Renew. Energy*, vol. 10(4), pp. 539–558, 1997.
- [59] K. Herold, R. Radermacher, S. A. Klein, *Absorption Chillers and Heat Pumps*, CRC Press, 1996.
- [60] Y. Shiran, A. Shitzer, D. Degani, “Computerized design and economic evaluation of an aqua-ammonia solar operated absorption system,” *Solar Energy*, vol. 29, pp. 43–54, 1982.

## VITAE

Name	Farooq Riaz Siddiqui
Nationality	Pakistani
Date of Birth	June 28, 1988
Email	farooqriazsiddiqui@hotmail.com
Address	P.O.BOX 5040, CORE-RE, RI, 31261, Dhahran, KSA
Academic Background	B.E. Mechanical Engineering (September 2011)  National University of Sciences and Technology  Rawalpindi, Pakistan

## Publications

- F. R. Siddiqui, M. A. I. El-Shaarawi, S. A. M. Said, “Exergo-economic analysis of a solar driven hybrid storage absorption refrigeration cycle,” *Journal of Energy Conversion and Management*, 80 (2014) 165-172. <http://dx.doi.org/10.1016/j.enconman.2014.01.029>
- M. A. I. El-Shaarawi, S. A. M. Said, F. R. Siddiqui, “Unsteady thermodynamic analysis for a solar driven dual storage absorption refrigeration cycle in Saudi Arabia,” submitted in *Journal of Solar Energy*.
- M. A. I. El-Shaarawi, S. A. M. Said, F. R. Siddiqui, “Energy and exergy analysis of a solar driven hybrid storage absorption refrigeration cycle,” submitted in *International Journal of Refrigeration*.

## Patent

- Hybrid Storage Absorption Refrigeration System, filed in U.S patent list.